TITLE

TITOLO

Monte-Carlo with variance reduction in and around near-critical configurations

AUTHORS

AUTORI

P. Console Camprini, K. W. Burn [1], and M. Brovchenko [2]

[1] former ENEA researcher

[2] IRSN (Institut de Radioprotection et de Sûreté Nucléaire)

CONTRIBUTIONS

CONTIBUTI

SUMMARY

SOMMARIO

We report on advances in the use of Monte-Carlo variance reduction in the source-iteration solution of the eigenvalue problem. The context is the modelling of neutron transport in and around reactor cores and criticality safety architectures. The application requiring variance reduction is the estimation of differential responses within and outside the core or fissile configuration. The ex-fissile configuration problems focus on the dose outside a PWR spent fuel cask and on a variety of radiation responses around a GEN III PWR core. Comparison is made with an empirical approach involving analog Monte-Carlo in the fissile zone and variance reduction outside. The in-core test looks at the neutron flux and the $^{96}Zr(n,\gamma)$ reaction rate at the lower surface of a control rod in two VERA Core Physics Benchmark problems. Comparison is made with analog Monte-Carlo. This paper provides support and technical background to a summary article that contains the principal results.

REV.	WRITTEN / REDAZIONE	CHECKED / CONVALIDA	APPROVED / APPROVAZIONE
0	P. Console Camprini	M. Tarantino	M. Tarantino
1	P. Console Camprini	M. Tarantino	M. Tarantino

LIST OF REVISIONS

Revision	Date	Scope of revision	Page
0	11/11/2021	First edition	73
1	26/01/2022	Graphical optimization of some plots and text editing and formatting.	71

TABLE OF CONTENTS

1. INTRODUCTION

This paper provides support and technical background to a summary, stand-alone article [1] that contains the principal results and discussion.

The latest series of developments of the Direct Statistical Approach (*DSA*), a method of semi-automatically generating variance reduction (*VR*) parameters in Monte-Carlo (*MC*), have been concerned with eigenvalue calculations [2-4]. The methodology employs a modified version of MCNP [5] as vehicle, the modifications written in "patch" form. For in-core problems the new approach provides results of a higher quality than analog or alternatively allows to calculate responses previously considered unfeasible. For ex-core problems, the new approach avoids decoupling and calculates the ex-core responses within the eigenvalue calculation.

The new approach relies on three key aspects:

- superhistories [6] have an important role in maintaining the stability of the fundamental mode [7,8].
- we include components of the fundamental mode among the responses of interest and perform a multi-response optimization [9].
- "fictitious source cells" ("*FS* cells"), already useful in some fixed source problems ([10], p. 740), also play a role in eigenvalue problems.

In the next section we discuss the above three items in more detail.

In §3 the test problems are described. Two ex-core test problems are firstly treated: the dose above the lid of a flooded fuel flask in §3.1 and the differential energy neutron flux at several positions around the core of a PWR GEN III in §3.2.

There are some indications from both these sets of test problems that the technique produces too few fission neutrons entering the "real-world" source cells from the *FS* cells. Focusing on the calculation of the fast neutron flux on a limited part of the lower pressure vessel (PV) in §3.2.4, two different workarounds are suggested in §3.2.5 and §3.2.6 to increase the number of fission neutrons. The approach in §3.2.6 substantially improves the quality of the results compared with those in §3.2.4. In §3.2.8 the same approach is applied to the calculation of a range of responses in the PV well and in the basemat at the bottom of the well, already addressed in §3.2.1 with unpromising results. The results are improved. In §3.3, three in-core problems are treated based on the VERA benchmark, with the penetration getting successively higher, going from §3.3.1 through §3.3.2 to §3.3.3.

After each test problem set, a summary is made in §3.1.5, §3.2.9 and §3.3.4 outlining the main conclusions that can be drawn.

Finally, in §3.4 in the three sets of test problems we attempt to quantify the correlations between the samples (or steps) that were previously assumed independent.

§4 contains concluding remarks.

2. METHODOLOGY

We started from the *VR* techniques that we had developed for fixed source problems [9]. There are three important features, one new (superhistories) and two already existing that are crucial to the eigenvalue version.

2.1 SUPERHISTORIES

The solution by Monte-Carlo of the source-iteration (or power iteration) technique for solving the eigenvalue problem [11] involves a constant renormalization of the fission source [6,12]. Such normalization introduces biases [ibid.]. One way of mitigating the biases introduced by the normalizations is to delay the point at which the normalization is made. That is, rather than to normalize after each fission generation (as is done in the standard procedure), instead to normalize after n fission generations. These longer fission chains are called superhistories [6]. Their employment has the additional advantage of reducing the bias on the error estimates, which are usually made between normalization points.

At the normalization point any desired distortion of the ensemble of fission points is immediately negated. In this way there is very little time or space to move the particles towards important phase space regions (either through population control or through biasing) before the next fission at which the desired distortion of the neutron population is cancelled.

So as to delay normalization and allow the distorted population to achieve its desired effect, we introduced superhistories. Typically a superhistory of 10 fission generations seemed adequate. (It should furthermore be mentioned that *VR* was allowed to be played differently according to the fission generation within the superhistory [2].) As illustration, we depict in Fig. 1 (taken from [2]) a superhistory of 1 then 4 fission generations with a local detector.

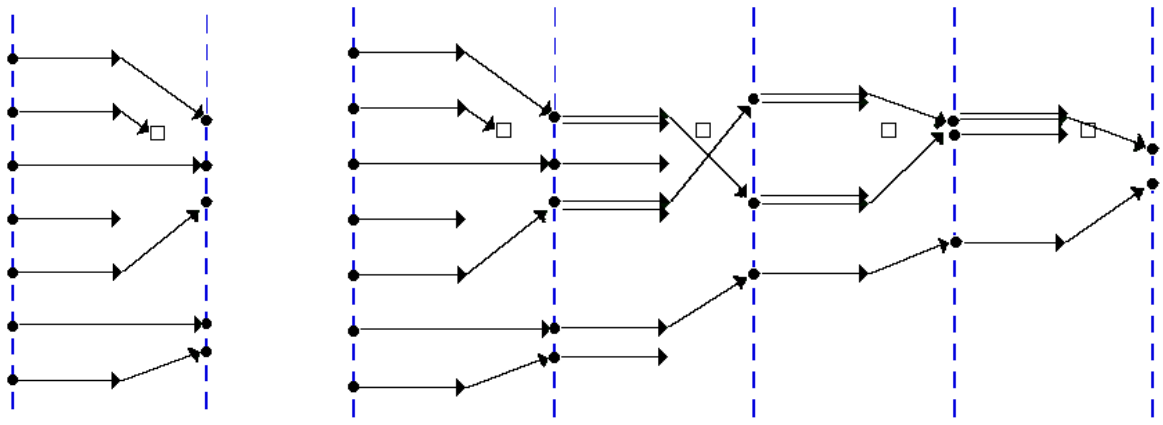

Figure 1: Illustration of a superhistory containing 1 fission generation (left) and 4 fission generations (right) with variance reduction and 1 local response

This looked to work for in-core problems. Instead for ex-core problems, at first superhistories were not thought to be useful [2-4]. Subsequently as *VR* is employed in the fissile zone, we realized that superhistories play an important role in holding the fundamental mode steady [7,8] so that they should actually be employed for problems with either ex- or in-core responses.

2.2 LOCAL AND GLOBAL RESPONSES

We name the response(s) that we are interested in calculating, “local” (because they often occupy a localized volume in phase space). Then rather than optimize to the responses-of-interest and assume that the fundamental mode is automatically held steady by contributing to the responses through future fission generations, we add components of the fundamental mode distribution, that we call “global responses”, to the responses-of-interest. In this way we hope to hold the fundamental mode as steady as possible, compatibly with the necessary distortion of the population so as to improve the calculation of the local response(s).

2.3 FICTITIOUS SOURCE CELLS

In fixed source problems so as to provide some compensation for a lack of, or an inappropriate, source biasing, we introduced the splitting or Russian rouletting (RR) of source particles immediately after they are born. (An example was dose estimations from γ activation sources.) Although this technique is not as efficient as well-executed source biasing – if the particle is split at its point of birth, correlations are introduced which are not present with source biasing – it is quite robust. [We may mention that this refers to “weight-independent splitting/RR” ([13] and citations therein). If the splitting/RR depends on the weight (such as in [14] or the well-known “weight window” [15]), then splitting or RR is implicitly executed immediately a particle is born.] As will shortly be illustrated, with weight-independent splitting/RR, *FS* cells also allow the desirable feature of all particles in a particular phase space cell having the same weight, no matter which phase space cell they were born in and no matter which path they took between the source and the cell in question.

In Fig. 2 we illustrate a configuration of phase space cells (i,j) in a fissile zone with 7 spatial cells, i, and 4 energy groups, j. (Spatial cells 1 – 4 contain fissile material whilst spatial cells 5 – 7 do not.) Splitting or RR between phase space cells with importances *F*(i,j) is governed by the rules given in [13] or [16] (which are the same rules as those employed in MCNP [5] or other codes).

There are shown two paths for a neutron born in phase-space cell (1,1) to reach phase-space cell (4,1): scattering down through spatial cells 1, 2, 3 and 4 and undergoing fission in phase-space cell (4,4) (path A), or travelling from spatial cell 1 to 4 maintaining its energy (path B). In a fixed source sub-critical mode with weight-independent splitting/RR and for any set of phase-space cell importances *F*(i,j), neutrons from these two paths arriving in phase space cell (4,1) have the same weight [13,16]. Instead, if one of these paths started in a different phase space cell, for example cell (2,1) rather than (1,1), then neutrons from the two paths arriving in cell (4,1) would not necessarily have the same weight. This is inefficient: intuitively we wish neutrons in the same phase space cell to have the same weight.

If we employ the *MC*-based source-iteration approach (with or without superhistories), a neutron born from fission must have the same weight, wherever it is born. Path A in Fig. 2, after undergoing the n’th fission of the superhistory in cell (4,4) may suffer splitting or RR, depending on its weight as it entered fission and on the current best estimate of keff. Such splitting or RR does not depend on *F*(4,4) or *F*(4,1) and the weight of the subsequent fission neutron(s) is not the same as the weight of the neutron in path B that maintains its energy.

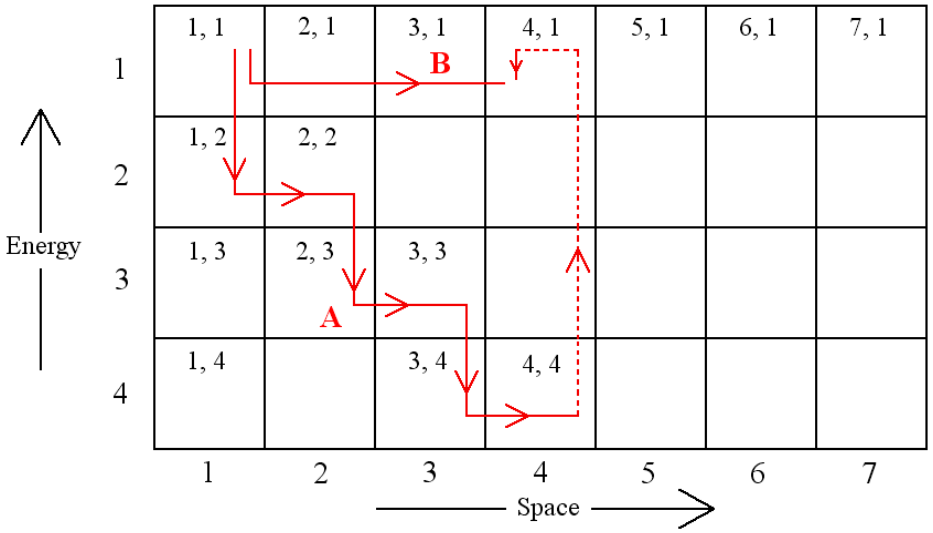

Figure 2: Depiction of a configuration of phase space cells (i, j) in a fissile zone

When the *DSA* is applied to source iteration [2-4,7,8], fission neutrons are treated as source neutrons and the *DSA* operates only in the short interval between fission events. Introducing superhistories allows intra-superhistory fissions to be treated with the normal *DSA* splitting/RR rules [16] that ensure the same weight of fission neutrons as other neutrons entering a cell. Thus, with a superhistory length of 10 fission generations, 9 intra-superhistory fissions follow the normal *DSA* splitting/RR rules and only at the 10^{th} are these rules broken and renormalization occurs.

We now introduce *FS* cells in Fig. 3. The *FS* cells are represented by the top part in grey. The row in black represents a one-way path to the real-world, in white. The *VR* importances *F*(i,j) are assigned both to the real-world phase space cells as well as to the fictitious phase space source cells. In the latter case we call the importances *E*(i,j). After being born in *FS* cell (i,j), the fission neutron is immediately subject to splitting or RR before passing to the real world cell (i,j) according to the ratio *F*(i,j)/*E*(i,j) [16].

Considering *MC* source-iteration with or without superhistories, we see that some importance values *E*(1,1) and *E*(4,1) lead to neutrons in real-world cell (4,1) having the same weight, independent of the path from *FS* cell (1,1) [and independent of the importance values *F*(i,j)]. It is easy to see that such sets must have the same importances *E*(i,j) in all the fictitious source cells. Thus only constraining the importances of the *FS* cells *E*(i,j), for any set of real-world cell importances *F*(i,j) we have again the desirable feature of neutrons in each phase space cell having the same weight, independently of where they were born and independently of which normalization generation (superhistory) they are in. (That is, this feature obtains both for neutrons born in different cells within the same superhistory and neutrons born in different cells in different superhistories.)

Among all possible solutions are the above-mentioned ones that ensure that neutrons in a particular phase space cell all have the same weight. However, the optimum solution is not necessarily one of these sets as indeed many sample problems have shown. This is probably because the sampling also forms part of the optimization, and improved sampling might trump the feature of neutrons in the same phase space cell having the same weight.

It is clear that introducing *FS* cells with superhistories (of 10 fission generations for example) should not give the same gain as without, as we are looking at improving the source sampling once every 10 fission generations rather than every generation.

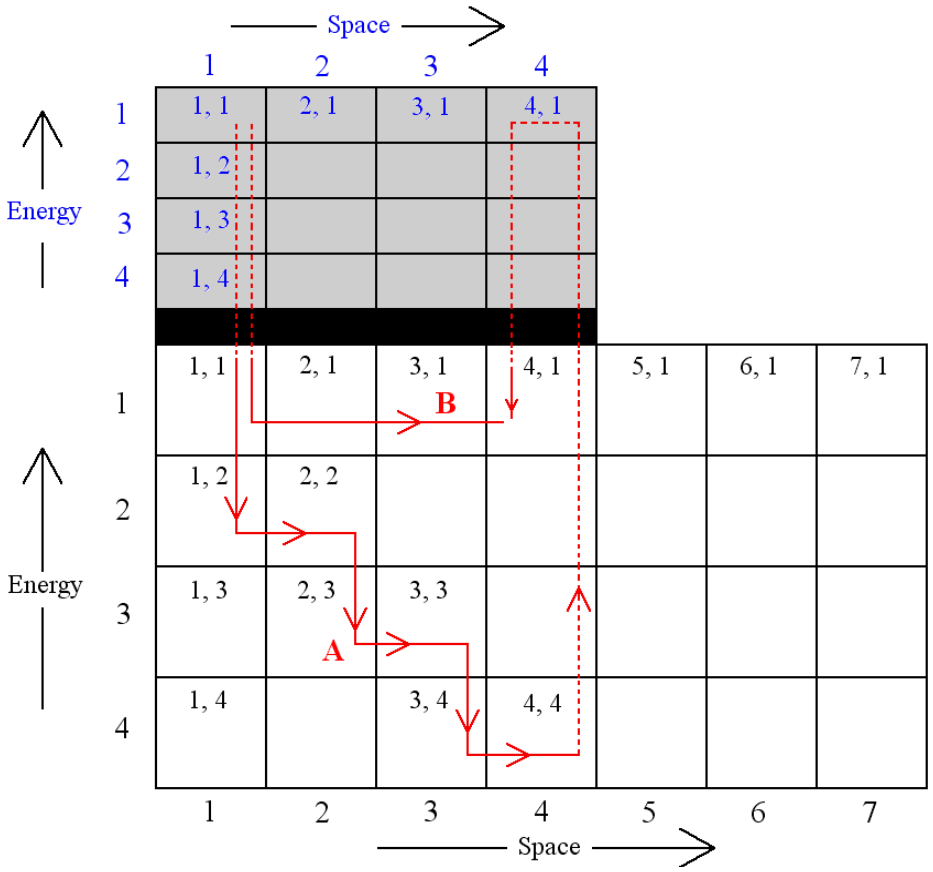

Figure 3: Depiction of a configuration of phase space cells in a fissile zone with FS cells

3. TEST PROBLEMS

The *DSA* optimizes the phase space cell importances with respect to a compound response figure-of-merit FOM_c. Here we modify slightly the definition of FOM_c by multiplying the value defined previously (see for example [9]) by the number of responses. This is implicit in all that follows. (Instead, when we only consider a single response, we employ the normal nomenclature, *FOM*.) Thus

$$FOM_c = M.[\sum_{i=1}^{M}(fsd_i)^2 \, . \, T]^{-1} \quad (1)$$

where M is the number of responses, fsd_i is the fractional standard deviation of response *i*, and *T* is the CPU time.

In each problem we assume that we have available a sufficiently large set of fission sites representing the fundamental mode of the problem that has been generated by a separate analog calculation and is the starting point of the calculations.

For the test problems in §3.2 and §3.3, only supporting results are shown here. Final results are given in [1].

3.1 EX-FISSILE CONFIGURATION: FIVE BURNT FUEL ASSEMBLIES IN FLOODED FLASK

We chose the most reactive fuel assembly from the GEN III PWR equilibrium core of §3.2 and placed five such assemblies in a flooded fuel flask. The resulting value of k_{eff} was 0.963. The local tally-of-interest was the neutron dose within radius 25 cm above the steel lid of the cask (thickness 45 cm). Dividing the fissile zone into 12 axial and 2 radial segments (< and > 25 cm), produced 24 global tallies of the fission source (ν x fission rate). A third radial segment was added in the flask wall outside the cavity. Axially 1 segment was added for the lower plenum and base of the flask and 3 axial segments were added in the upper plenum and lid. Thus, the total number of axial segments was 16 making a total of 16 x 3 = 48 spatial segments. In Fig. 4 is shown a radial section of the fissile zone and in Fig. 5 an axial section of the whole flask. In Fig. 4 we see the radial division in the four outer fuel assemblies around 2/3 towards the outside on the centre line of each outer assembly.

We employed 7 energy groups with upper limits 10 eV, 10 keV, 70 keV, 500 keV, 2 MeV, 5 MeV and 20 MeV. Thus, there were 24 x 7 = 168 phase space cells in the fuel and a total of 336 phase space cells.

We generated optimum *VR* parameters in these phase space cells for various circumstances (superhistory lengths, presence or not of *FS* cells). Then for each set of optimum parameters we ran calculations of variable numbers of fission generations and looked at both the local response and the 24 global responses. In the presented figures, all error bars are ±2 standard deviations and, unless otherwise stated, all errors are calculated between source neutron histories (or starting superhistory neutrons for the case of more than 1 fission generation in a superhistory).

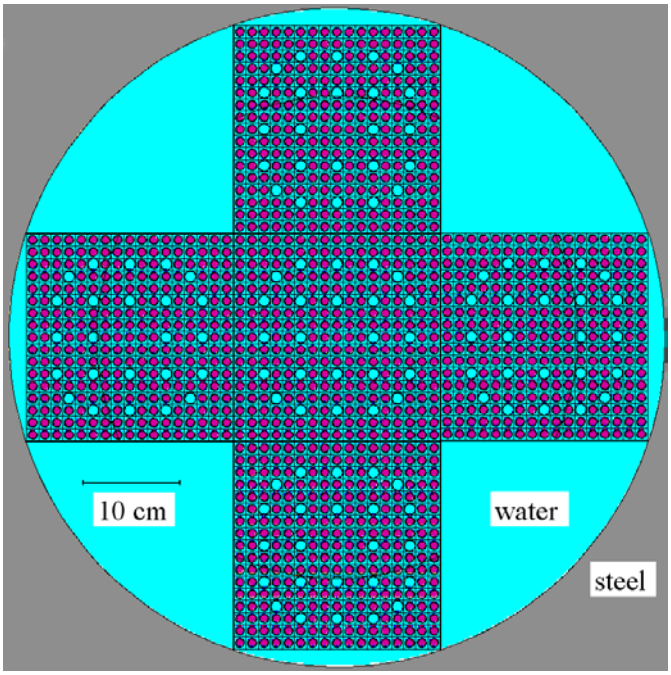

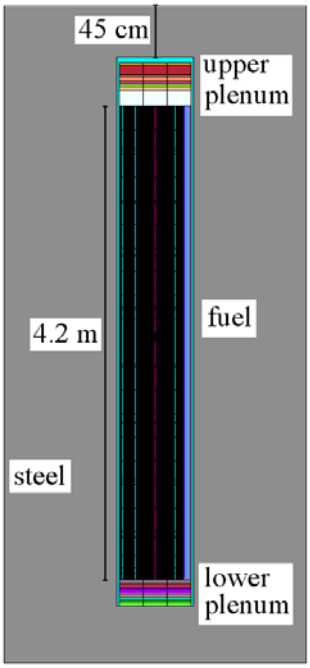

Figure 4. Flooded fuel flask: radial section of the fissile zone ***Figure 5. Flooded fuel flask: axial section***

3.1.1 Flooded Fuel Flask: examination of the length of the superhistory

We firstly verified the results with superhistory lengths of 1 and 10 fission generations, without *FS* cells. In Figs. 6 and 7 are shown the variation of respectively the dose above the lid and the fission source in the inner (< 25 cm radius), upper 10 cm height of the fissile zone, against the number of fission generations for a generation size of 2×10^5 fission neutrons. The number of fission generations runs from 10 to 30000 ($\log_{10}$ scale) for both 1 and 10 fission generations per superhistory. Although as we have subcriticality the total number of starting fission neutrons is slightly less for the superhistory=10 case, the computer times of the respective superhistory=1 and superhistory=10 cases turned out similar because of the two different sets of *VR* parameters employed. Also shown as an independent data point on the right-hand side in Fig. 6 and as a dashed line in Fig. 7 is the result from a separate analog run (that is, analog *VR* both in- and ex-fuel assemblies) with a generation size of 2×10^6, a superhistory of 1 fission generation and 2200 superhistories.

As is well known the errors are biased, especially when a superhistory consists of one fission generation [6]. Instead, the errors for the superhistory of 10 generations should be more realistic than those of 1. In the analog case for the fission source tally (dashed line in Fig.7) they are too small to be visible and, although certainly underestimated, should allow a reasonable idea of the correct result.

In Figs. 6 and 7 the variations of the dose and fission source are similar as it is that part of the fission zone that is providing most of the local response. Bearing in mind that the abscissa is $\log_{10}$ scale, we attach much greater weight to the longer calculations and therefore the results with superhistory length of 10 look superior to those with 1.

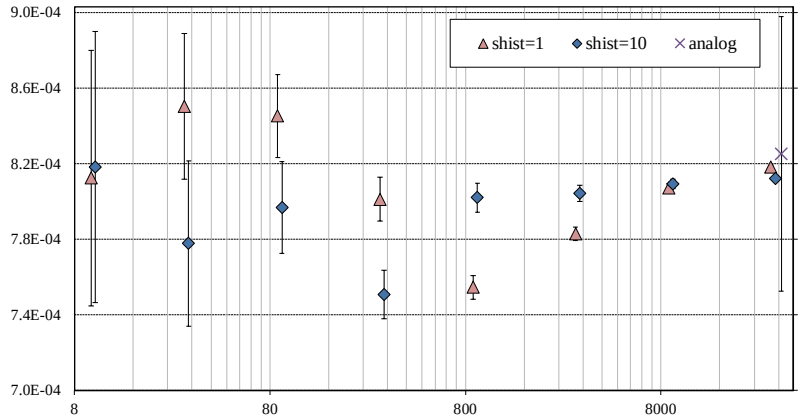

Figure 6. Flooded fuel flask: dose above lid (arbitrary units) against the number of fission generations for superhistories of 1 and 10 generations without FS cells

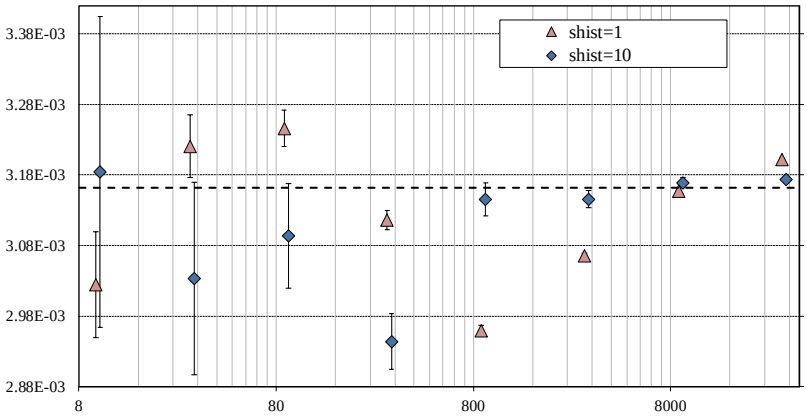

Figure 7. Flooded fuel flask: fission source in upper 10 cm and inner 25 cm against the number of fission generations for superhistories of 1 and 10 generations without FS cells

We generated comparisons of the fission sources similar to Fig. 7 for all 24 global responses. Here we summarize the results by summing over all the 24 global responses the squares of the fractional deviations from the results of the separate analog run. (The uncertainties of the results are ignored here.) The results are shown in Fig. 8 where we see a definite superiority of the superhistory 10 results.

Notwithstanding the fact that the errors are biased, especially in the case of a superhistory length of 1, it is interesting to look at the compound figure-of-merits (FOM_c). Fig. 9 shows the evolution of the FOM_c's of all 25 responses and all 24 fission zone responses, with the number of fission generations for the cases of 1 and 10 fission generations per superhistory. Fig. 10 is like Fig. 9 but shows the dose response only and the fission source in the inner, upper 10 cm of the fission zone.

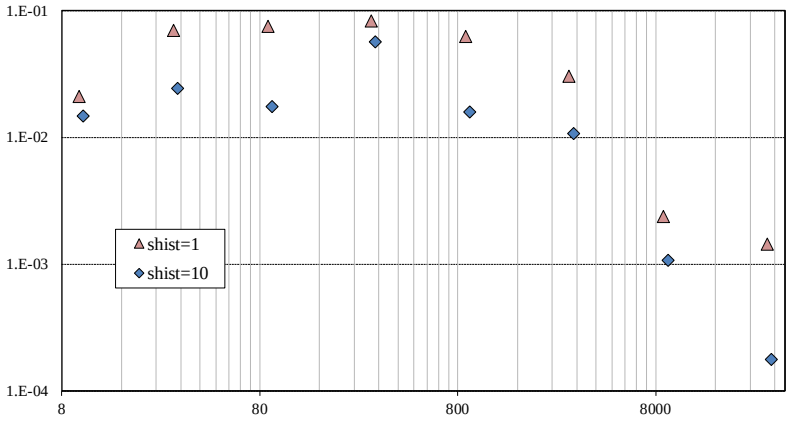

Figure 8. Flooded fuel flask: sums of the squares of the fractional deviations from analog of the 24 global tallies of the fission source against the number of fission generations for superhistories of 1 and 10 generations without FS cells

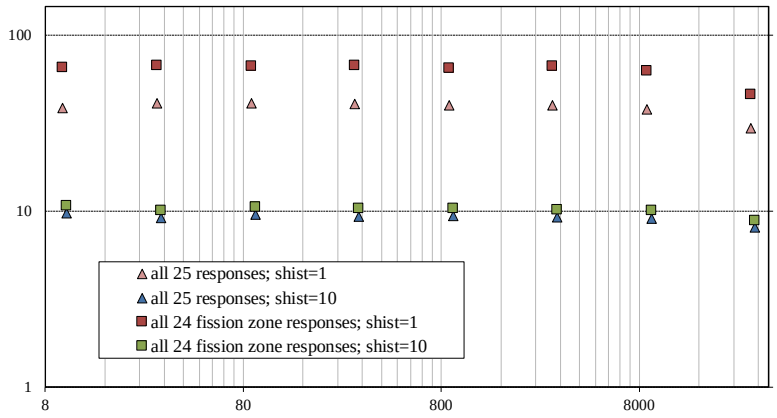

Figure 9. Flooded fuel flask: FOM_c's of all 25 responses and all 24 fission zone responses against the number of fission generations for superhistories of 1 and 10 generations without FS cells

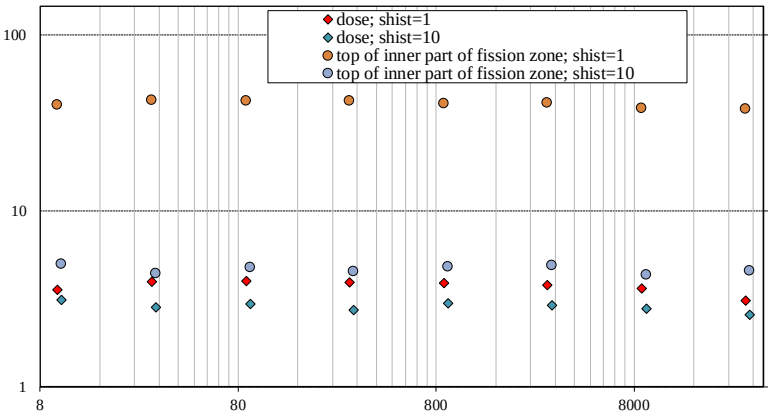

Figure 10. Flooded fuel flask: FOM's of dose response and fission source in upper 10 cm and inner 25 cm against the number of fission generations for superhistories of 1 and 10 generations without FS cells

In Figs. 9 and 10 we see that the FOM_c's for a superhistory of 1 fission generation are apparently a factor of 3.7 – 9.3 better than those for a superhistory of 10 fission generations apart from those of the dose which are a factor of 1.1 – 1.4 better. As can be seen from Figs. 6 and 7, the errors are underestimated, grossly so in the case of 1 generation per superhistory. The inverse applies to the FOM_c's. In the case of the dose response this under (error) / over (*FOM*) estimate should be less marked although still present.

Instead, as we know from Fig. 8 and from the results in [7], the results for a superhistory of 1 fission generation should actually be poorer than those for a superhistory of 10 fission generations. The reason for this is the limited interval for the optimization of the splitting/RR technique within the standard source-iteration scheme as discussed in §2.1 and §2.3. A result of this only partial optimization is an unbalanced and apparent collective behaviour described in [2,8] as analogous to sloshing.

In Fig. 9 we remark on the reduction of the FOM_c for 9000 and 30000 fission generations for all the cases. This is due to rounding errors on the fractional standard deviation which are given to 4 decimal places – for the longer runs the error only appears at the 4th decimal place.

Finally, we mention that the analog calculation whose result for the dose above the lid is shown in Fig. 6 (with a fractional standard deviation (*fsd*) of 4.40%) took 5.2×10^5 mins of CPU time and thus the *FOM* for the dose result was 9.9×10^{-4} (compare the values of around 3 in Fig. 10).

3.1.2 Flooded Fuel Flask: examination of fictitious source cells

We then looked at the effect of including fictitious source cells. Figs. 11 and 12 show the variation of the dose above the lid against the number of fission generations for superhistory lengths of 1 and 10 fission generations respectively, for the cases with and without *FS* cells.

Following the MCNP nomenclature [5] we employ *NSRCK* as the number of starting fission neutrons per superhistory. For both superhistory lengths, the cases without *FS* cells had a *NSRCK* value of 2×10^5 fission neutrons and required around a factor of 1.4 – 1.6 more calculational effort as measured by CPU time than the cases with *FS* cells with a *NSRCK* value of 2.3×10^6 fission neutrons. This was because the optimum *VR* parameters tended to execute RR between the fictitious and the real-world source cells over a large part of the length of the assemblies, with splitting executed only in the top axial cell in the highest (and lowest) energy groups. For the superhistory length of 10, out of 168 phase space cells in the fuel, RR was executed between the fictitious and the real-world source cells in 165 and splitting in 3. The maximum splitting parameter was 3 and the minimum RR survival probability was 0.0139: a range of over 200.

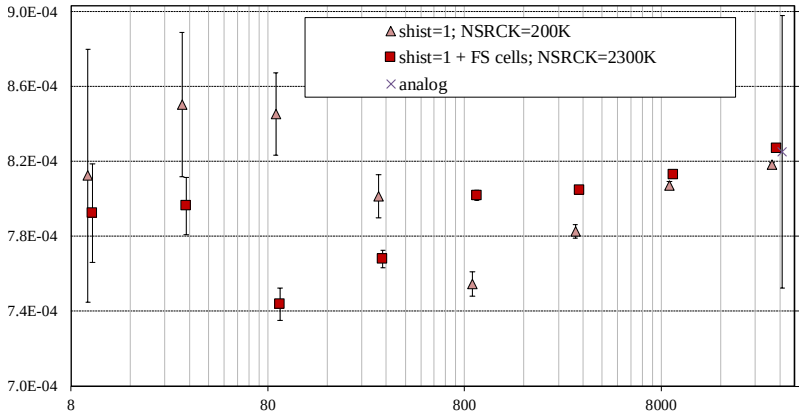

Figure 11. Flooded fuel flask: dose above lid (arbitrary units) against the number of fission generations for 1 generation per superhistory for the cases with and without FS cells

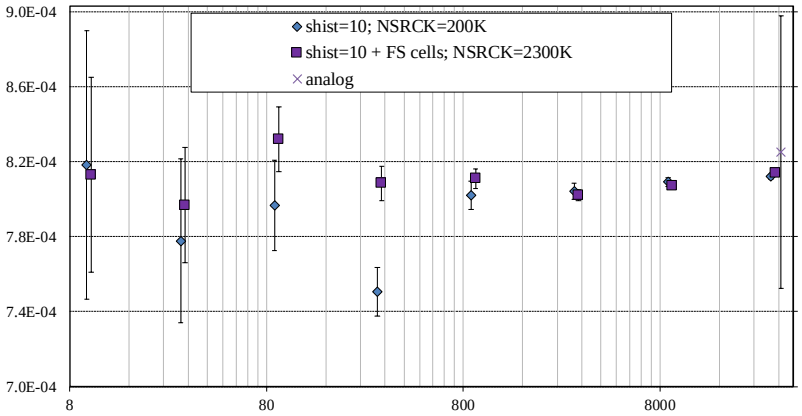

Figure 12. Flooded fuel flask: dose above lid (arbitrary units) against the number of fission generations for 10 generations per superhistory for the cases with and without FS cells

We see in Figs. 11 and 12 a definite improvement after including *FS* cells for 1 fission generation per superhistory with possibly a more marginal improvement for 10 fission generations per superhistory. In an analogous fashion to what was done in §3.1.1 we summarize the results for the fission source tallies by summing the squares of the fractional deviations from the analog values for each of the 24 global responses. The results are shown in Figs. 13 and 14. From Figs. 13 and 14 it again looks as if *FS* cells provide a greater improvement for 1 fission generation per superhistory compared with 10.

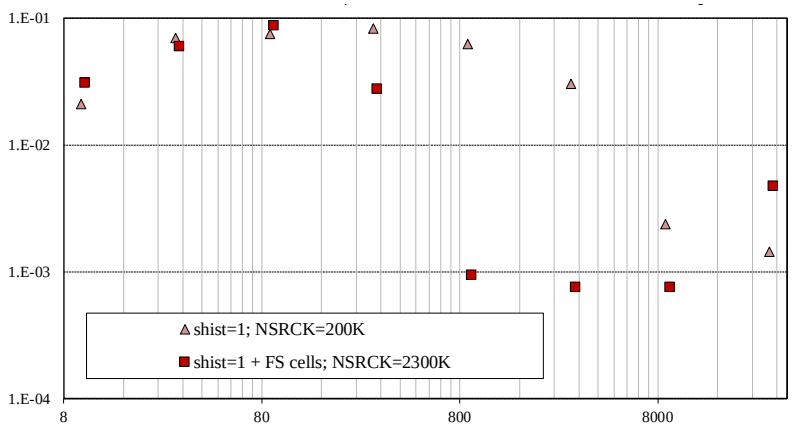

Figure 13. Flooded fuel flask: sums of the squares of the fractional deviations from analog of the 24 global tallies of the fission source against the number of fission generations for 1 generation per superhistory for the cases with and without FS cells

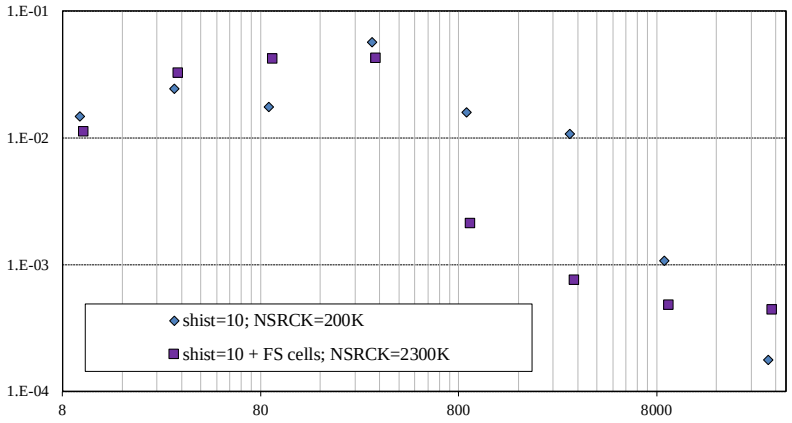

Figure 14. Flooded fuel flask: sums of the squares of the fractional deviations from analog of the 24 global tallies of the fission source against the number of fission generations for 10 generations per superhistory for the cases with and without FS cells

Following §3.1.1 we look at the evolution of the FOM_c's. Fig. 15 shows the evolution of the FOM_c's of all 25 responses and all 24 fission zone responses, with the number of fission generations for the cases of 1 fission generation per superhistory with and without *FS* cells. Fig. 16 is like Fig. 15 but shows the dose response above the lid and the fission source in the inner, upper 10 cm of the fission zone. Figs. 17 and 18 are analogous to Figs. 15 and 16 but are for a superhistory of 10 fission generations. (Note in Fig. 17 the blue triangles are underneath the green squares.)

In Figs. 15-18 we see that the FOM_c with *FS* cells is always better than without, for any of the responses or combination thereof that was considered and for both 1 and 10 fission generations per superhistory. Although the FOM_c's are overestimates, we are comparing results within superhistories of 1 or 10 generations and therefore we expect the comparisons to be reasonably sound. Finally, as already discussed the fluctuation in the FOM_c at 30000 fission generations (and sometimes at 10000) is due to rounding errors in the *fsd*.

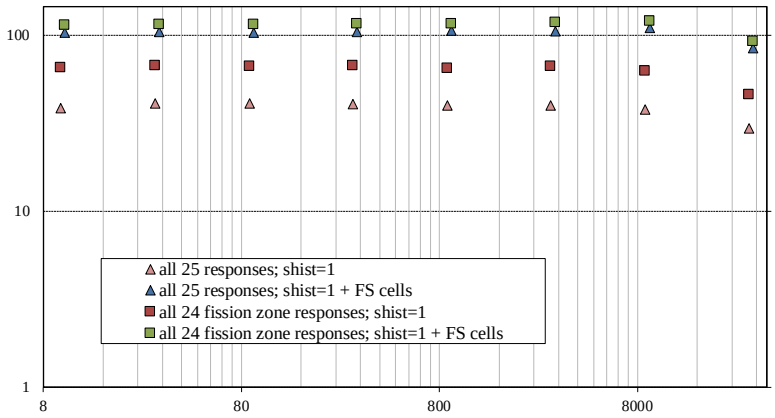

Figure 15. Flooded fuel flask: FOM$_c$'s of all 25 responses and all 24 fission zone responses against the number of fission generations for a superhistory of 1 generation with and without FS cells

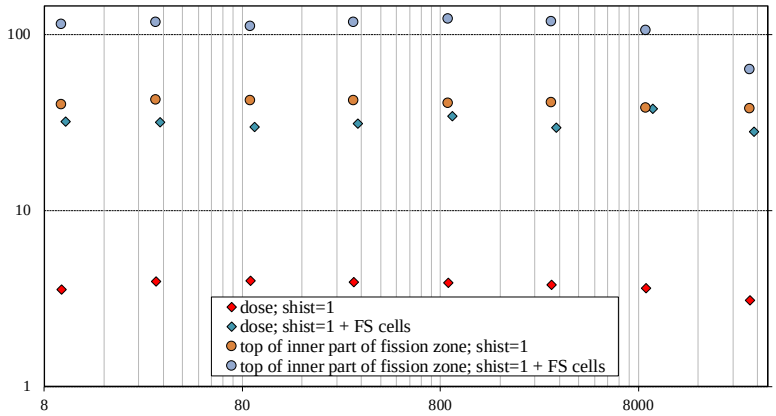

Figure 16. Flooded fuel flask: FOM's of dose response and fission zone responses in upper 10 cm and inner 25 cm against the number of fission generations for a superhistory of 1 generation with and without FS cells

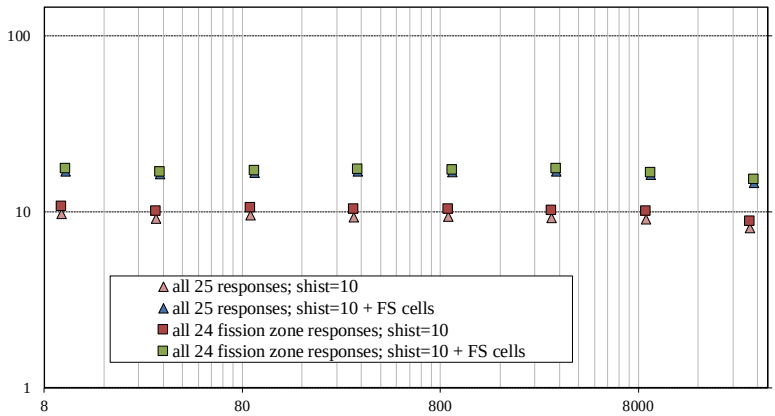

Figure 17. Flooded fuel flask: FOM$_c$'s of all 25 responses and all 24 fission zone responses against the number of fission generations for a superhistory of 10 generations with and without FS cells

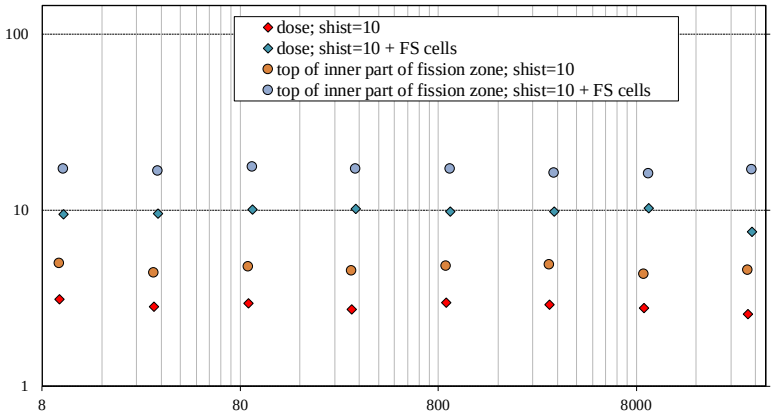

Figure 18. Flooded fuel flask: FOM's of dose response and fission zone responses in upper 10 cm and inner 25 cm against the number of fission generations for a superhistory of 10 generations with and without FS cells

3.1.3 Flooded Fuel Flask: constraining the *VR* in the fissile zone to be analog

We now examine an empirical approach – employing *VR* parameters generated with 1 fission generation per superhistory (and including *FS* cells) outside the fissile zone while at the same time constraining the *VR* within the fissile zone to be analog (that is, putting the importances in both the real-world and fictitious source cells unity). Figs. 19 and 20 are analogous to Figs. 12 and 14 but compare the results for a superhistory of 10 fission generations with *FS* cells, with a superhistory of 1 fission generation with analog *VR* in the fissile zone. Note that as in §3.1.2, to achieve a similar calculational effort in the two calculations it was necessary to run with a generation size *NSRCK* in the former case (superhistory 10) that was more than an order of magnitude greater than with the latter case (superhistory 1), that is, 2.3×10^6 against 9.2×10^4. It then turned out that the calculational effort was very similar in the two cases.

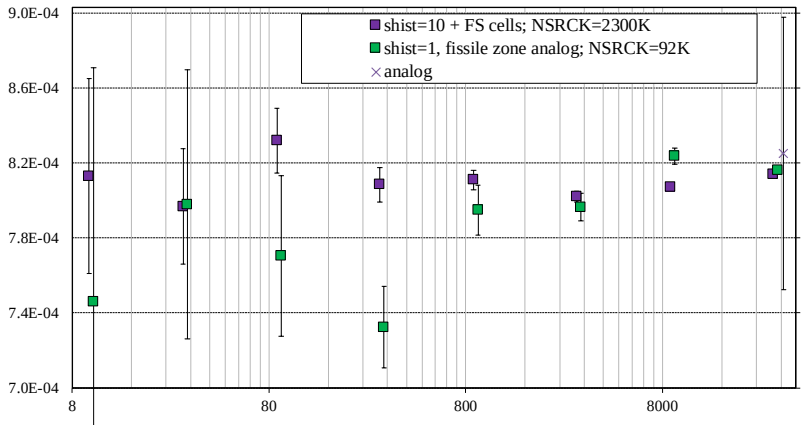

Figure 19. Flooded fuel flask: dose above lid (arbitrary units) against the number of fission generations for a superhistory of 10 generations with FS cells and a superhistory of 1 generation with analog VR in the fissile zone

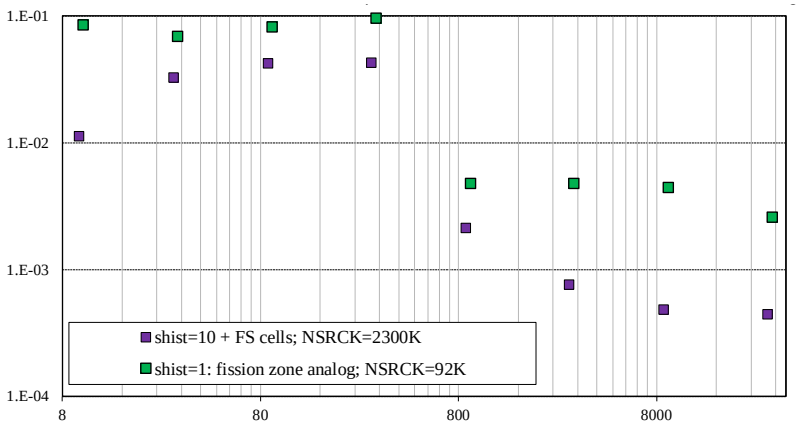

Figure 20. Flooded fuel flask: sums of the squares of the fractional deviations from analog of the 24 global tallies of the fission source against the number of fission generations for a superhistory of 10 generations with FS cells and a superhistory of 1 generation with analog VR in the fissile zone

We see in Fig. 19 that for the dose the shist=10 case looks better than the empirical case. Surprisingly Fig. 20 implies that it is also better at holding the fundamental mode, at least in this example.

Fig. 21 shows the evolution of the FOM_c's for all 25 responses and all 24 fission zone responses, with the number of fission generations for the two cases (the blue triangles are beneath the green squares). Fig. 22 is like Fig. 21 but shows the dose response above the lid and the fission source in the inner, upper 10 cm of the fission zone.

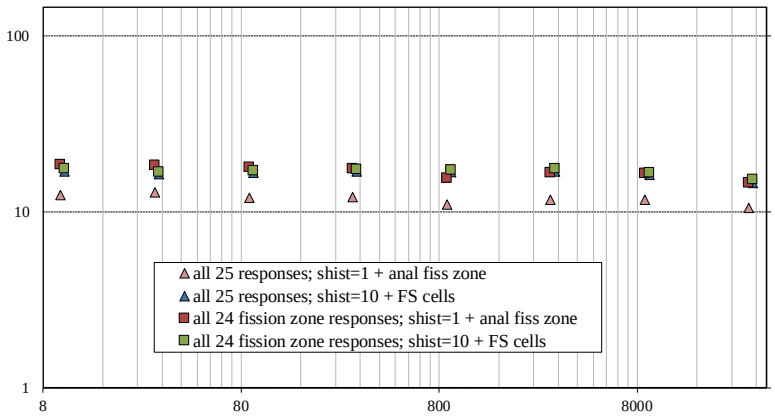

Figure 21. Flooded fuel flask: FOM_c's of all 25 responses and all 24 fission zone responses against the number of fission generations for a superhistory of 10 generations with FS cells and a superhistory of 1 generation with analog VR in the fissile zone

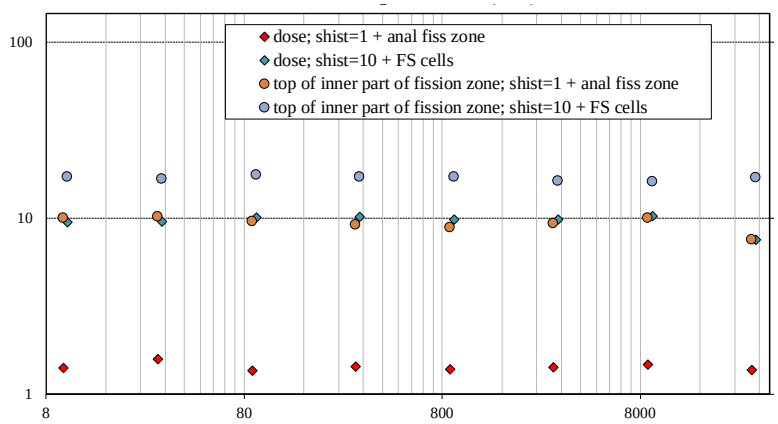

Figure 22. Flooded fuel flask: FOM's of dose response and fission zone responses in upper 10 cm against the number of fission generations for a superhistory of 10 generations with FS cells and a superhistory of 1 generation with analog VR in the fissile zone

In Fig. 21 we see that the FOM_c for the 24 fission zone responses with the superhistory of 1 fission generation and analog *VR* in the fission zone is very similar to that with the superhistory of 10 fission generations and *FS* cells. Instead, when the external dose response is included, the shist=10 case is slightly superior. In Fig. 22 we see that the *FOM* of the dose response with the superhistory of 10 fission generations and *FS* cells is very roughly 6 – 7 times better than that with the superhistory of 1 fission generation and analog *VR* in the fission zone. The gain is less (around 1.5 – 2) for the *FOM*'s of the fission rate in the top of the fission zone. Note that although the estimation of the error of the dose response should be less biased than that of any of the 24 fission sources, it is still an underestimate. Furthermore, such underestimate may be greater for a superhistory of 1 fission generation than 10.

3.1.4 Flooded Fuel Flask: constraining the *VR* in the fissile zone to be analog: changing the way the error is estimated

So far, all errors have been calculated between starting superhistories. As already discussed, such error estimates are biased as are therefore the FOM_c's. Furthermore, the error and FOM_c estimates are inconsistent for superhistories of 10 fission generations compared with superhistories of 1 generation and thus comparison of the respective FOM_c's is not comparing like with like. We verify this for the investigation in §3.1.3 where the *VR* in the fission zone is constrained to be analog.

As the optimization procedure that generated the *VR* parameters is based on the assumption of independence of the superhistories, it is instructive to firstly examine the values generated by the procedure, whose last two steps are shown in Table I.

Table I. Flooded fuel flask: last two steps of the iterative procedure to arrive at the optimum VR parameters, for the case of the superhistory of 10 fission generations with fictitious source cells

step	Generating the 2nd moment and time functions (superhistory of 10 fission generations)						
	Direct Estimate						
	CTM min	*CTRK* min	*NSRCK*(M)* *KCT*	Dose (*fsd*)	S^2	τ	*1/q*
penultimate	1470	957	2 * 12	7.33E-4 (0.0097)	4.92E+4	3.99E-5	0.510
last	2221	1399	2 * 15	7.71E-4 (0.0089)	3.41E+4	4.66E-5	0.629

step	Minimizing the quality function							
	At current VRP's			At « optimum » VRP's			q_{curr}/q_{opt}	q_{an}/q_{opt}
	S^2	τ	*1/q*	S^2	τ	*1/q*		
penultimate	4.07E+4	3.99E-5	0.617	2.97E+4	4.53E-5	0.744	1.21	776
last	2.92E+4	4.66E-5	0.734	2.03E+4	6.70E-5	0.736	1.00	732

In Table I, *NSRCK*, already defined, is the size of the superhistory, *KCT* is the total number of superhistories (equal to the number of "active" superhistories which accumulate tallies – we always impose *IKZ*, the number of superhistories to skip before accumulating tallies, as zero), *CTM* is the CPU time, *CTRK* is the actual Monte-Carlo tracking time (i.e. that does not include bookkeeping time), S^2 is the compound (i.e. for all the 25 responses) population 2nd moment, τ is the time per source particle, q is S^2 x τ (whose inverse, after taking into account the number of responses, is FOM_c), $1/q_{curr}$ is the *1/q* value at the current *VR* parameters and $1/q_{an}$ is the analog *1/q* value. The first seven columns of the 4th and 5th rows are direct statistical estimates, the last eight columns are *DSA* function values[1]. (Note that some of these variables – *NSRCK*, *KCT*, *CTM*, *IKZ* – are those employed by MCNP [5]. We use *KCT* as the total number of normalization cycles, or superhistories, that may or may not equal the total number of fission generations, depending on the number of fission generations per superhistory.) *CTM* and *CTRK* are measured on the ENEA CRESCO system – see acknowledgement. Typically, 96 CPU's were employed in the phase of generating the *VR* parameters and between 192 and 576 CPU's in the execution phase with the optimum *VR* parameters.

We ran 40 independent calculations for the two cases in §3.1.3 (a superhistory of 10 fission generations with *FS* cells and a superhistory of 1 fission generation with analog *VR* in the fissile zone), focusing on the dose, the fission response at the top, inner part of the fission zone and on all 24 fission neutron production tallies. Each of these 80 calculations started from the same fission source. We compared the results with statistics calculated between 40 independent runs of the two cases and with statistics calculated between superhistories. The results are in Table II. (Note that in Table II the size of each superhistory for the case: superhistory of 1 generation and analog *VR* in the fission zone, with statistics evaluated between superhistories, has been

[1] The *DSA* operates by generating coefficients of the 2nd moment and (CPU) time functions. If splitting/RR is independent of the weight of the incoming particle, such functions are separable [2,16,13]. If not, an approximation is applied to force the functions to be separable [14]. Once separable into a coefficient part and a part with a dependence on the splitting/RR parameters, a product is made of the 2nd moment and time functions which is minimized in a standard fashion to generate the optimum splitting/RR parameters. (The inverse of the product is proportional to *FOM*.)

increased from the previous 9.2×10^4 to 2.3×10^6.)

Table II. Flooded fuel flask: Comparison of the dose above the lid and the fission source in the top, inner, part of the fissile zone for a superhistory of 10 fission generations and FS cells and a superhistory of 1 fission generation with analog VR in the fission zone, with statistics between superhistories and between 40 independent calculations

statistics	Details of each single run	Dose above lid (unnormalized) (1 *fsd*)	*FOM*	*FOM* / *FOM* (shist=1; fiss. *VR* anal.)	Fission neutron tally in top inner part of assemblies (1 *fsd*)	*FOM*	*FOM* / *FOM* (shist=1; fiss. *VR* anal.)	FOM_c (24 fission neutron tallies)	FOM_c / FOM_c (shist=1; fiss. *VR* anal.)
between superhistories of a single run	shist=1 with analog *VR* in fissile zone (*NSRCK*=2.3M; *KCT*=30)	7.9385E-4 (0.0090)	1.58	1	3.1295E-3 (0.0036)	9.85	1	17.5	1
between superhistories of a single run	shist=10 with fictitious source cells (*NSRCK*=2.3M; *KCT*=30)	8.0846E-4 (0.0057)	10.2	6.4	3.1762E-3 (0.0044)	17.1	1.73	17.4	0.99
between 40 independent runs	shist=1 with analog *VR* in fissile zone (*NSRCK*=2.3M; *KCT*=1)	8.3175E-4 (0.0067)	2.13	1	3.2210E-3 (0.0032)	9.27	1	20.2	1
between 40 independent runs	shist=10 with fictitious source cells (*NSRCK*=2.3M; *KCT*=1)	8.0024E-4 (0.0044)	12.2	5.7	3.1619E-3 (0.0032)	23.4	2.52	17.8	0.88

In Table II we see that calculating the statistics between the independent runs corroborates the results with statistics calculated between superhistories and indeed the ratios turn out not to be underestimates. The factor of 6 improvement in the dose is confirmed. Furthermore, the results for the neutron production tally in the top, inner part of the fissile zone are in line with those in Fig. 22 and the compound figure-of-merit results for all 24 fission production tallies confirm the results in Fig. 21 – that the case of 10 fission neutrons per superhistory with *FS* cells does not damage greatly the fundamental mode. Although not reported in Table II, the FOM_c for all 25 responses (24 fission + dose) for the case shist=10 with *FS* cells and statistics between superhistories, was 16.8, consistent with the *1/q* value in Table I after removing the factor 25.

While the results in Table II are consistent with those in Figs. 21 and 22, which presented the evolution of results of a calculation at 8 points between 10 and 30000 fission generations, they are for a limited number of fission generations [precisely a total of 300 / 10 fission generations (statistics between superhistories / 40 independent runs) for superhistories of 10 fission generations and $1/10^{th}$ that number of fission generations for superhistories of 1 fission generation]. This may not be enough fission generations to encompass the statistical variation in the fundamental mode. We instead desire to build statistics between independent runs, each run consisting of many more than 300 fission generations.

To compare a sufficient number of independent calculations (>30 – 40) each with a sufficient number of fission generations (some thousands) was impractical due to time and machine constraints. Thus, it was decided to run a calculation over a relatively large number of fission generations, splitting it into a number of steps. The fundamental mode, written at the end of a step is used as source for the subsequent step. Each step is assumed independent.

[The greater the number of fission generations within each step, the greater the independence

between steps. (Furthermore, the size of each generation also affects the independence of each step.) As will be seen, some handle on the degree of independence of each step is achieved by plotting the cumulative moving averages (*CMA*'s) of the most important responses. In §3.4 a more quantitative evaluation of the assumption of independence of the steps is given. In this problem, 50 fission generations per step were first tried, but looked insufficient, whilst 500 looked satisfactory.]

In the two cases – superhistory of 10 fission generations + *FS* cells and superhistory of 1 fission generation + analog *VR* in the fission zone (which from now on for brevity we name the "*DSA* case" or "*DSA* approach" and the "analog case" or "analog approach" respectively), the same number of fission generations were run per step and the same number of steps. Furthermore the "*DSA* case" and the "analog case" employed identical ex-core *VR* parameters (those from the "*DSA* case"). (Note that this is in contrast to all previous runs with analog *VR* in the fission zone and a superhistory of 1 fission generation which employed ex-core *VR* parameters generated with a superhistory of 1 fission generation.) Finally, it was also desired that each case should take roughly the same amount of CPU time. Given the strong RR between the fictitious and the real-world source cells in the case superhistory of 10 fission generations, this meant that the fission generation size in the "analog case" had to be a lot less than in the "*DSA* case".

We chose a generation size of 9×10^6 for the "*DSA* case" (near the maximum allowed by our hardware). The above constraint gave a generation size of 3.5×10^5 for the "analog case". Each step consisted of 5 superhistories for the "*DSA* case" and 50 superhistories for the "analog case", thus 50 fission generations in both cases. The results after 60 steps are summarized in Table III.

Table III. Flooded fuel flask: Comparison of the dose above the lid and the fission source in the top, inner, part of the fissile zone for the "analog case" and "DSA case", statistics between 60 steps each of 50 fission generations

statistics	Details of each individual step	Dose above lid (unnormalized) (1 *fsd*)	*FOM*	*FOM* / *FOM* (shist=1; fiss. *VR* anal.)	Fission neutron tally in top inner part of assemblies (1 *fsd*)	*FOM*	*FOM* / *FOM* (shist=1; fiss. *VR* anal.)	FOM_c (24 fission neutron tallies)	FOM_c / FOM_c (shist=1; fiss. *VR* anal.)
between 60 steps	"analog case" (*NSRCK*=350K; *KCT*=50)	8.2262E-4 (0.0069)	0.176	1	3.2069E-3 (0.0059)	0.241	1	0.418	1
between 60 steps	"*DSA* case" (*NSRCK*=9M; *KCT*=5)	7.9536E-4 (0.0065)	0.203	1.15	3.1098E-3 (0.0065)	0.199	0.83	0.334	0.80

We see in Table III that in contrast to the previous results, the "*DSA* case" hardly improves the dose results (factor 1.15). On the other hand the quality of the fundamental mode degrades more than before (80%). We assume that the reduction in gain of the dose is due to the fundamental mode varying between generations, this effect being accentuated with *VR* parameters in the fission zone. In fact we note that the FOM_c values for the 24 fission responses are around a factor of 50 lower than those in Table II. We note also that the statistical error of the response in the upper, inner part of the fission zone is very similar to that of the dose above the lid, especially when *VR* is performed in the fission zone in the "*DSA* case".

It is instructive to examine the fluctuation of the dose above the lid together with the fission source in the upper 10 cm and inner 25 cm of the fission zone, during the calculation. Figs. 23 and 24 show *CMA*'s of these quantities plotted against the step number (from 1 to 60) for the "*DSA* case" and "analog case" respectively. We show the respective *FOM*'s of the dose and their ratio in Fig. 25. The final values after 60 steps are those given in Table III.

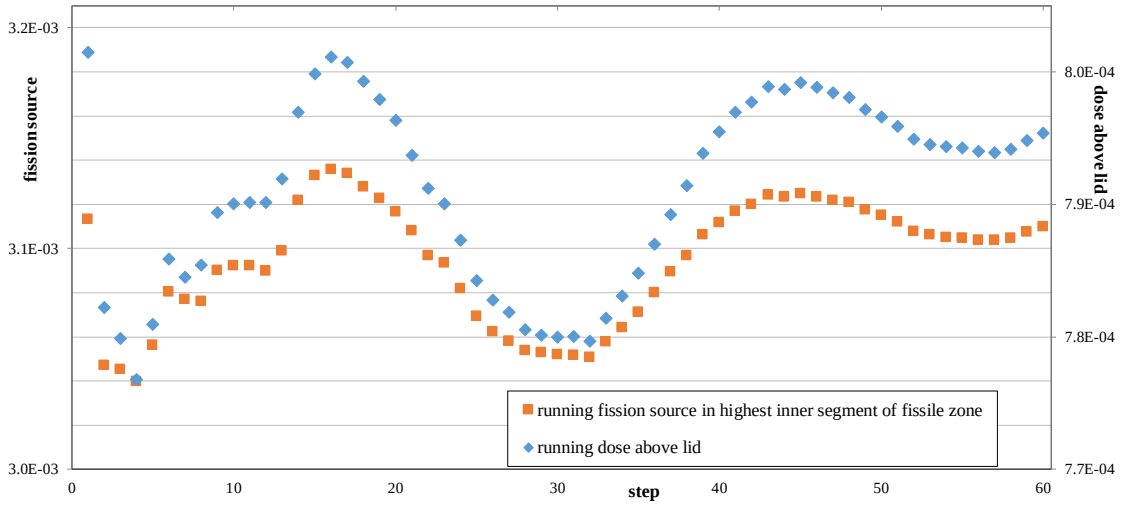

Figure 23. Flooded fuel flask: CMA's of dose above lid (arbitrary units) and fission source in upper 10 cm and inner 25 cm against number of steps (each of size 9×10^6 and length 5 superhistories = 50 fission generations) with "DSA approach"

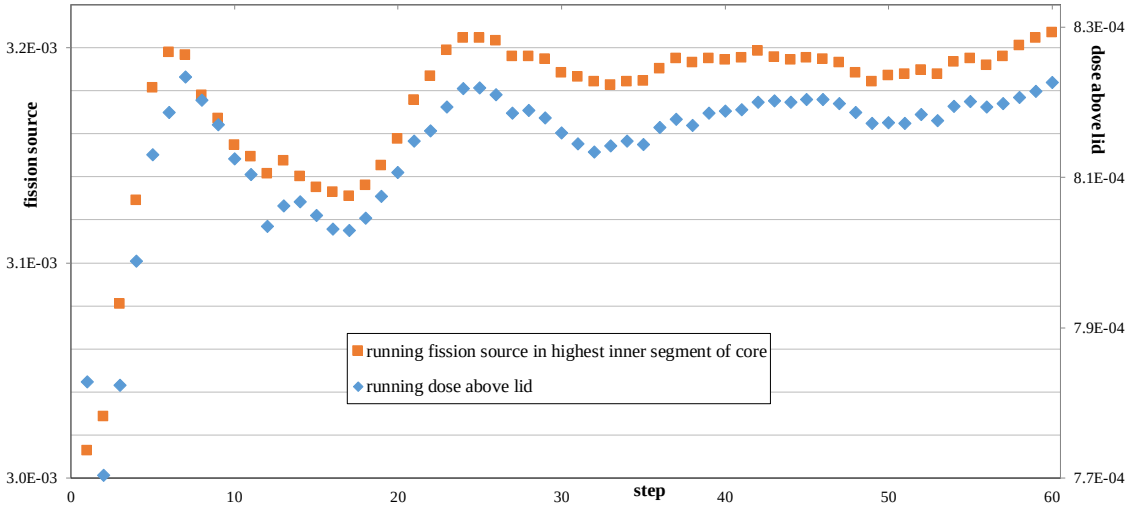

Figure 24. Flooded fuel flask: CMA's of dose above lid (arbitrary units) and fission source in upper 10 cm and inner 25 cm against number of steps (each of size 3.5×10^5 and length 50 superhistories / fission generations) with "analog approach"

Figs. 23 and 24 show firstly that the fission rate in the upper, inner part of the fissile zone is highly correlated with the dose above the lid: nearly all the variance in the dose above the lid comes from the variance in the source. Secondly there looks to be a "sloshing" effect [2,8] that implies that the steps are not independent of one another. That is, 50 fission generations are not a sufficient number to ensure independence between successive fission sources. (This is indeed confirmed in §3.4.)

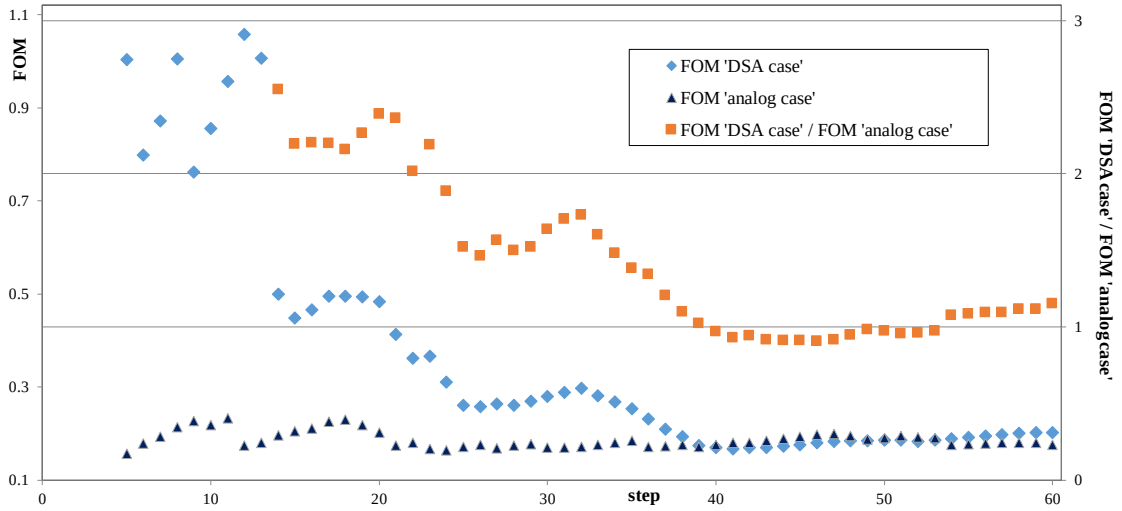

Figure 25. Flooded fuel flask: dose above lid local response FOM's for the two cases in Figs. 23 and 24 and their ratio

Given that apparently 50 fission generations are not a sufficient number to establish independence between the steps, we increased this number to 500 fission generations, with all other parameters remaining unchanged. The results are summarized in Table IV and the fluctuation of the relevant results is shown in Figs. 26 – 28 (analogous to Figs. 23 – 25).

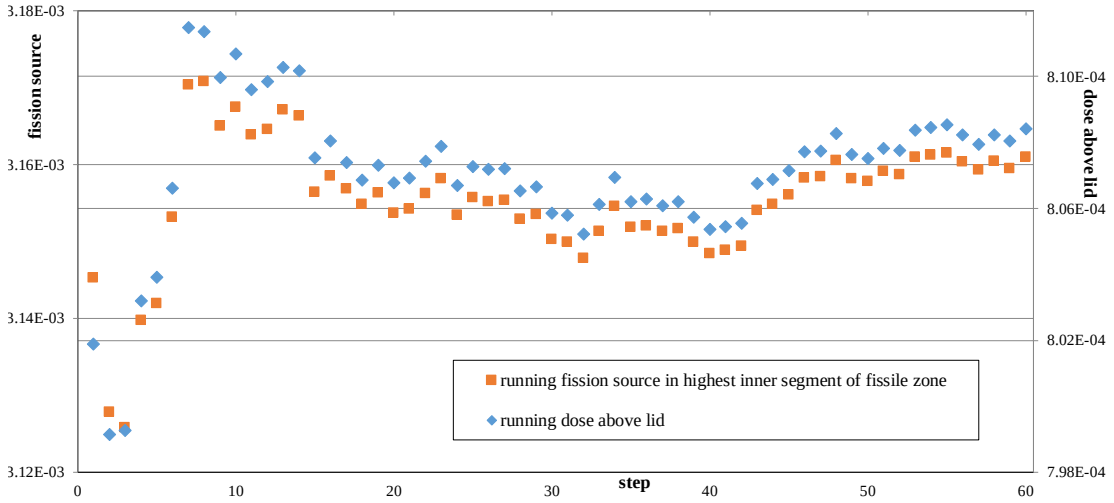

Figure 26. Flooded fuel flask: CMA's of dose above lid (arbitrary units) and fission source in upper 10 cm and inner 25 cm against number of steps (each of size 9×10^6 and length 50 superhistories = 500 fission generations) with "DSA approach"

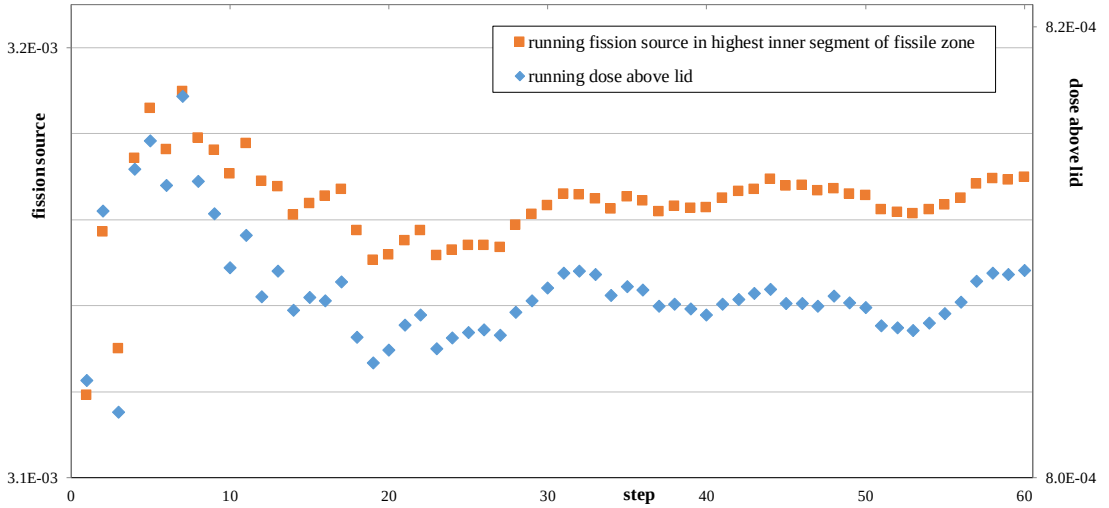

Figure 27. Flooded fuel flask: CMA's of dose above lid (arbitrary units) and fission source in upper 10 cm and inner 25 cm against number of steps (each of size 3.5×10^5 and length 500 superhistories / fission generations) with "analog approach"

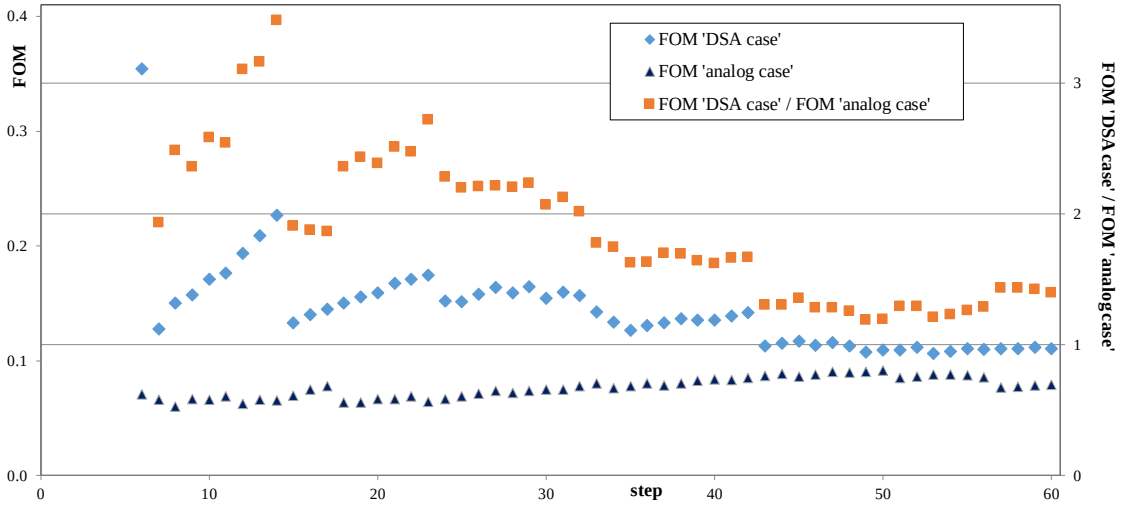

Figure 28. Flooded fuel flask: dose above lid local response FOM's for the two cases in Figs. 26 and 27 and their ratio

In Figs. 26 and 27 we see again a high correlation between the fission rate in the upper, inner part of the fissile zone and the dose above the lid. The "sloshing" effect is now strongly reduced so that each step looks reasonably independent of the previous one (as is seen also in §3.4). We see again in Fig. 28 and Table IV that there is not much gain in *FOM* for the "*DSA* case" compared with the "analog case".

Table IV. Flooded fuel flask: Comparison of the dose above the lid and the fission source in the top, inner, part of the fissile zone for the "analog case" and "DSA case", statistics between 60 steps each of 500 generations

statistics	Details of each individual step	Dose above lid (unnormalized) (1 *fsd*)	*FOM*	*FOM* / *FOM* (shist=1; fiss. *VR* anal.)	Fission neutron tally in top inner part of assemblies (1 *fsd*)	*FOM*	*FOM* / *FOM* (shist=1; fiss. *VR* anal.)	FOM_c (24 fission neutron tallies)	FOM_c / FOM_c (shist=1; fiss. *VR* anal.)
between 60 steps	"analog case" (*NSRCK*=350K; *KCT*=500)	8.0920E-4 (0.0032)	0.0794	1	3.1698E-3 (0.0031)	0.0859	1	0.168	1
between 60 steps	"*DSA* case" (*NSRCK*=9M; *KCT*=50)	8.0841E-4 (0.0027)	0.111	1.40	3.1609E-3 (0.0027)	0.112	1.31	0.147	0.88

In Table IV we note that again that the error in the fission source in the top, inner part of the fissile zone is virtually identical to the error in the dose above the lid – no further variance is introduced by the ex-fissile zone transport. We also note that the FOM_c of the 24 fission neutron tallies is only slightly damaged (88%) in the "*DSA* case" compared with the "analog case". The absolute values of *FOM* and FOM_c are roughly a factor of 2 lower than those in Table III.

3.1.5 Remarks on the Flooded Fuel Flask problem

There look to be two effects at work here:

Firstly, there is the unbalanced fundamental mode discussed at the end of §3.1.1 (illustrated for example in Figs. 19 of [7]) and characterized as collective behaviour or sloshing. This concerns the global responses (i.e. the fission source) and as a consequence the local responses are altered. This occurs with a superhistory of 1 fission generation and is due to the *VR* parameters in the fissile zone. Ways of mitigating this problem are to employ analog *VR* in the fissile zone, to use *FS* cells (which may not be enough by themselves) or to employ superhistories with 10 or so fission generations in the superhistory or a combination of these. Here we employed a superhistory of 10 fission generations with *FS* cells.

Secondly, we saw in §3.1.3 and §3.1.4 that with an empirical approach involving the imposition of analog *VR* in the fission zone, for the same number of fission neutrons the calculation runs about 25 times faster compared with the case of a superhistory of 10 fission generations, fictitious source cells and with *VR* in the fission zone (including the *FS* cells). This is due to RR played on fission neutrons as they are born. Although there is some splitting between the fictitious and real-world source cells in the part of the fissile zone that contributes to the dose, the RR predominates. Thus, with the time saved, we expect to see an improvement in the ex-fissile zone result.

Indeed, in Table II we see an improvement of a factor of around 6 in the quality of the dose response when we employ a superhistory of 10 fission generations with *FS* cells compared with the empirical approach. Such result was obtained with a very limited number of fission generations, but is consistent with results obtained with up to 30000 fission generations (Fig. 22). However, the latter results relied on statistics estimated between superhistories.

When another calculational campaign was made with a total of 3000 fission generations, divided into 60 steps of 50 generations each, we were hardly able to improve the quality of the dose estimate compared with the "analog approach" (with the same ex-core *VR*) (Figs. 23 – 25 and Table III). As the samples looked not to be independent, we ran 10 times more fission generations

in each step making a total of 30000. The results, in Figs. 26 – 28 and Table IV now looked to be independent samples but confirmed the fact that the dose estimate is not greatly improved (just a factor 1.4). The *FOM* value for the fission tally in the upper part of the assemblies in Tables II – IV seems to confirm that it is the variation in the fundamental mode that is driving the variation in the local tally dose. (Under these circumstances when the ex-core detector response is closely correlated with the fission distribution, it is important to ensure that the samples are as independent of each other as possible.)

Although we have contradictory data (a factor of 6 improvement in the *FOM* vs. a factor of 1.4), a tentative conclusion is that the limited number of fission generations employed to generate the *DSA VR* parameters is not sufficient to show up the variation in the fundamental mode over a large number of fission generations. Thus, the gain indicated with the *DSA* during the phase of generating the *VR* parameters does not turn out to be the case. Instead, more calculational effort should be expended within the fissile region and less outside. In any case we can hypothesize that a much greater ex-fissile region penetration should show a gain in efficiency when applying *VR* within the fissile region compared with analog *VR* in the fissile region. In the next problem these hypotheses will be examined.

3.2 EX-FISSILE CONFIGURATION: PWR GEN III WITH THICK STEEL REFLECTOR

We now examine the PWR GEN III model which has already been investigated in [7]. Equilibrium state UOX assembly-wise fuel compositions, distinguishing the rods with and without gadolinium, were employed with no axial variation.

In this problem we pass directly to the comparison of the *DSA*-generated *VR* parameters ex- and in-core [with superhistories of 12 (rather than 10) fission generations and *FS* cells], with the empirical approach of identical *VR* parameters ex-core, analog *VR* in-core and superhistories of 1 fission generation (naming these approaches again the "*DSA* case" and the "analog case" respectively). An identical total number of fission generations was run in each case. As in §3.1 the number of fission generations employed in the final runs with the generated *VR* parameters was much larger than the number employed in the phase of generating the *VR* parameters.

As in §3.1.4 the calculations in the final runs were divided into several steps, each step starting from the fission source written at the end of the previous step, and each step assumed independent. [It will be seen that the number of fission generations per step starts at 144 in §3.2.1, then due to time constraints gradually decreases to 12 in §3.2.6. (Then the effective number of starting fission neutrons per step increases from §3.2.4 to §3.2.6.) The *CMA*'s of the important responses do begin to show worrying correlations when the number of fission generations per step becomes small. However, this is offset when the number of starting fission neutrons per step increases. In §3.4 the correlations are quantified, and it will be seen that the general conclusions do not alter.]

Again, as in §3.1.4 the indicated optimum *VR* parameters in-core in the "*DSA* case" tended to involve more RR than splitting. Although *FOM*'s and FOM_c's, which should be independent of the calculational time, are going to be compared, as in §3.1.4 it was desired to expend roughly the same calculation effort in each case. Given that the same ex-core *VR* parameters were used, this implies the same in-core effort. Thus *NSRCK*, the number of starting fission neutrons in each normalization step or superhistory, was set lower in the "analog case".

We will consider a variety of local ex-core responses (rather than the single one of §3.1). Each collection of responses produced its own set of *VR* parameters, with a differing amount of splitting/RR in the core. Thus, the difference in *NSRCK* between the "*DSA* case" and the "analog case" varied according to the set of responses. In §3.2.1, §3.2.2, §3.2.3 and §3.2.8 the fissile zone was divided into 15 segments for tallying the global responses which in this case were fission heating rates: 5 axial (of roughly equal heights) and 3 radial (the outer assembly ring, the next two assembly rings and the inner assemblies). Instead in §3.2.4, §3.2.5, §3.2.6 and §3.2.7 when the ex-core detector was defined over a limited azimuthal range, two extra segments were added to the fissile zone, making a total of 17. In all problems we employed 7 energy groups but with upper limits slightly different from those in §3.1: 1 eV, 1 keV, 20 keV, 200 keV, 2 MeV, 5 MeV and 20 MeV.

3.2.1 Ex-core mapping of the neutron flux with 48 ex-core responses

The vertical section in Fig. 29 shows the surfaces on which the neutron fluxes were tallied. All tallies are on 360°. There are three zones for the flux tallying:

- Radially in the PV well with 3 axial segments and 6 energy groups (upper limits: 0.2 eV, 20 eV, 2 keV, 200 keV, 2 MeV and 20 MeV);
- On the lower surface of the PV with 2 segments and 3 energy groups (upper limits: 10 eV, 500 keV and 20 MeV);
- In the sacrificial concrete and zirconium oxide basemat at 4 depths, with 2 segments and

3 energy groups (upper limits: 10 eV, 500 keV and 20 MeV).

We divide the 48 ex-core responses into three groups, A (radial in the PV well), B (bottom of the PV well) and C (within the basemat) as illustrated in Fig. 29. A horizontal section at the core mid-plane in Fig, 30 shows the radial tally surface, A.

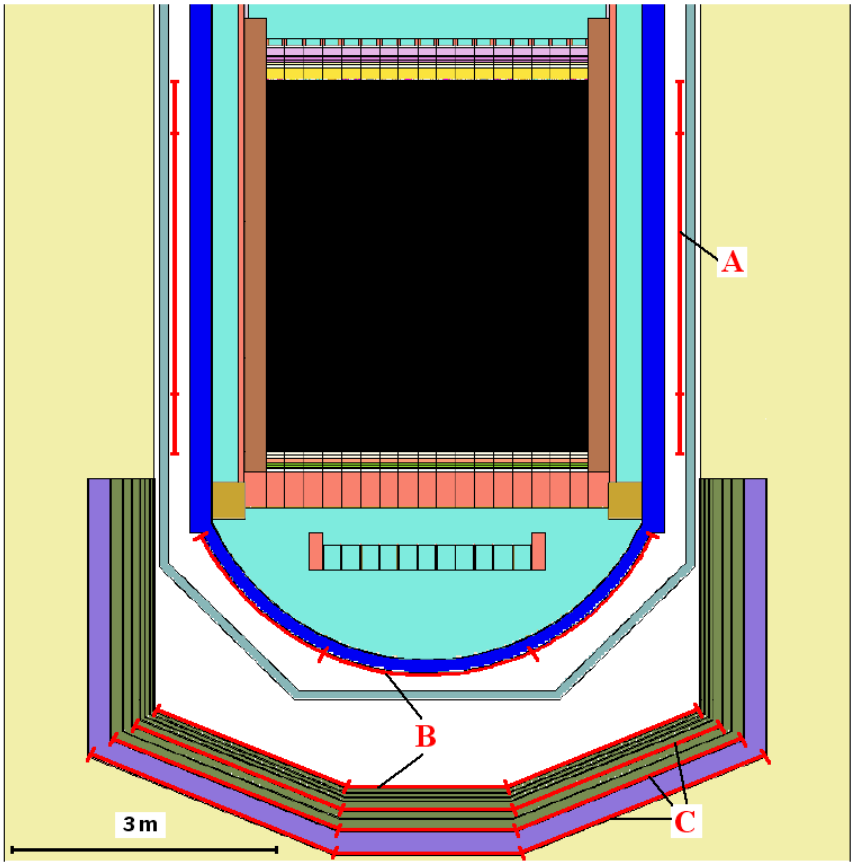

Figure 29. PWR Gen III: ex-core mapping of the neutron flux: vertical section showing surfaces for neutron flux tallying and 3 groups of ex-core tallies

The "*DSA* case" ran only around 240 fission generations at each iteration of the procedure to arrive at the optimum. We employed these optimum importances to run the two cases for 40 steps. In the "*DSA* case" each step had 1.2×10^6 starting neutrons (*NSRCK*), 12 superhistories (*KCT*) and a superhistory length of 12 fission generations.

It is well known that the outer assembly ring is responsible for most of the ex-core response. We therefore expect RR between the fictitious and real-world source cells in the inner and 2nd and 3rd outer rings. Indeed the "analog case" required around 30% of the starting neutrons of the "*DSA* case" for the same computer time. Thus, in the "analog case", *NSRCK* was set as 3.75×10^5 and *KCT* as 144. The total number of fission generations in each case is 144 x 40 = 5760. As already discussed the first superhistory of each step read the fission source written at the end of the previous step, the first step of each case reading the same converged fundamental mode previously generated in an analog calculation.

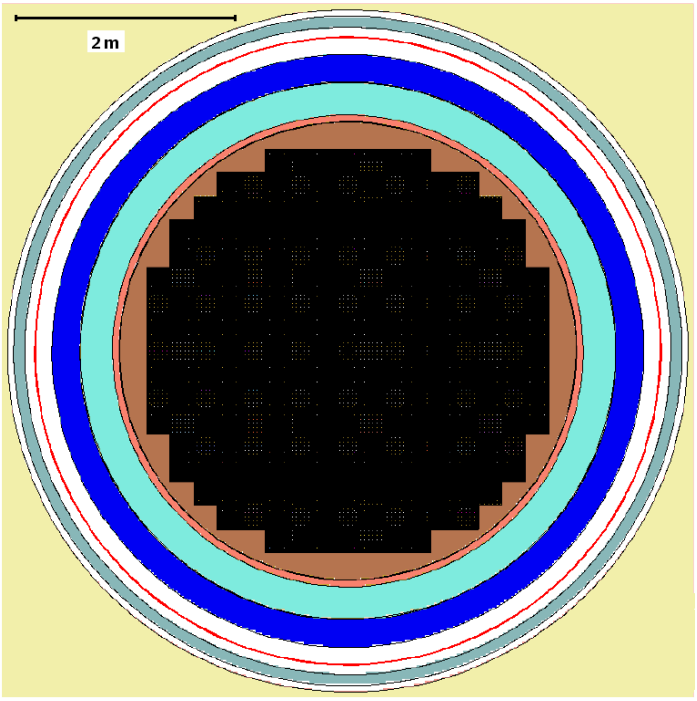

Figure 30. PWR Gen III: ex-core mapping of the neutron flux: horizontal section at core mid-plane showing surface for neutron flux tallying

In Figs. 31 and 32 we show, for the "*DSA* case" and "analog case" respectively, the *CMA*'s of one of the ex-core responses - the flux between 200 keV and 2 MeV in the central tally segment near the core mid-plane in Fig. 29 (part of "A") and the fission heating in the central 3 (out of 5) axial segments of the outer fuel assembly ring. In both cases we see a strong correlation between the ex-core flux and the outer core fission heating.

The running values of the FOM_c's of the two cases ("*DSA*", "analog") and their ratio over the 40 steps for the ex-core response groups A, B and C and for the 15 in-core fission responses are reported in [1]. The final ratios *DSA*/analog after 40 steps were 0.25, 0.44, 0.45 and 0.82 for the 15 in-core fission responses and for the ex-core response groups A, B and C respectively. As expected, this ratio rises as we go further from the core. However, the ratios are disappointingly all less than 1.

From Figs. 31 and 32 and the results for the ratios of the FOM_c's we conclude that the variation in the fundamental mode is more important than the variation in the ex-core transport, even for the responses in the basemat.

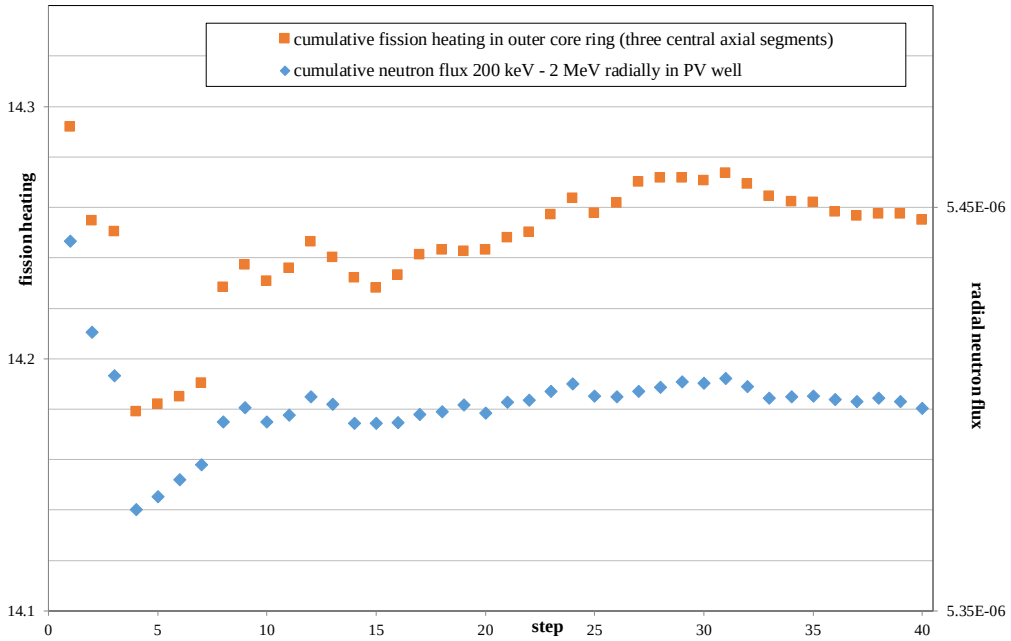

Figure 31. PWR Gen III; ex-core mapping of the neutron flux: CMA's of radial flux (0.2 – 2 MeV) and fission heating in outer fuel assembly ring against number of steps (each of size 1.2×10^6 and length 12 superhistories = 144 fission generations) with "DSA approach"

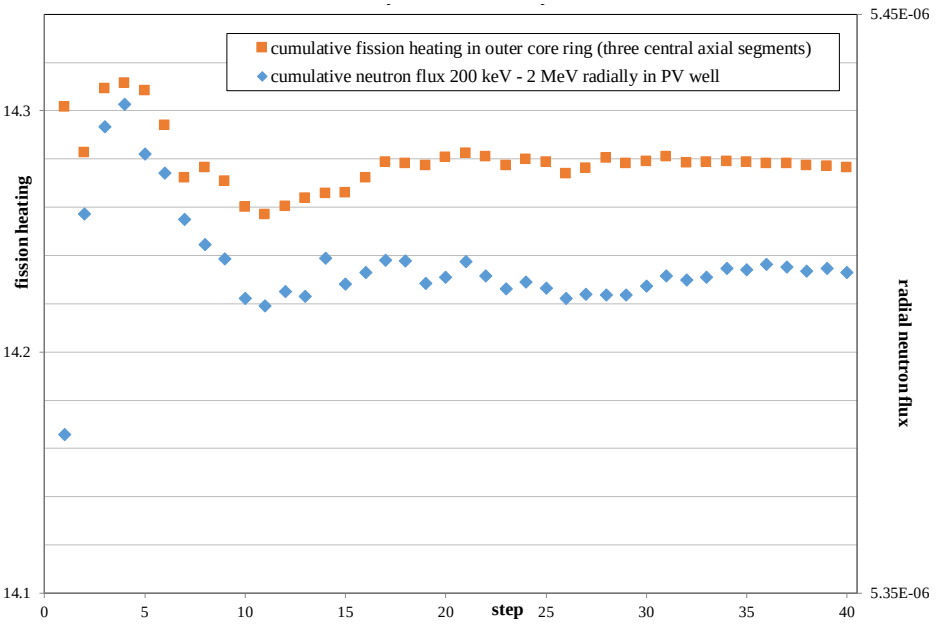

Figure 32. PWR Gen III; ex-core mapping of the neutron flux: CMA's of radial flux (0.2 – 2 MeV) and fission heating in outer fuel assembly ring against number of steps (each of size 3.75×10^5 and length 144 superhistories / fission generations) with "analog approach"

3.2.2 Single ex-core response: neutron flux > 1 MeV on PV at level of core bottom on 360°

The second problem concerns a single ex-core response: the neutron flux above 1 MeV on the inner surface of the PV on 360° at the level of the bottom of the fissile zone. The position is shown in a vertical section in Fig. 33 (the upper pair of the red indicators) and a horizontal section in Fig. 34. The axial extent of the tally was approximately 10 cm.

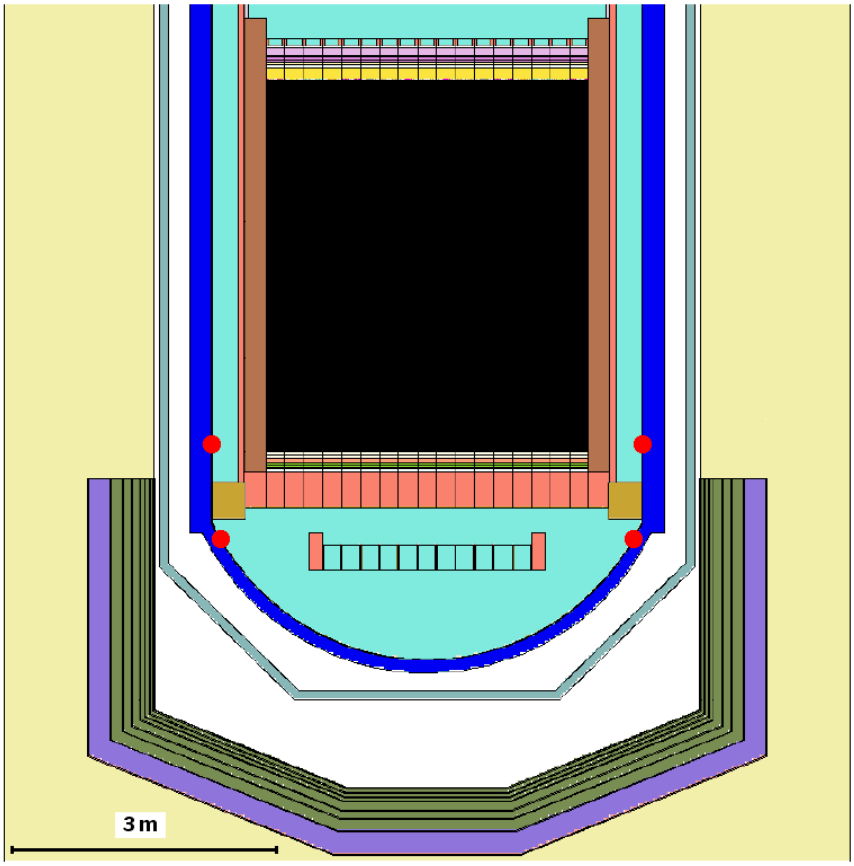

Figure 33. PWR Gen III; fast neutron flux on PV on 360°: tally location at level of bottom of core (upper); below supporting platforms (lower)

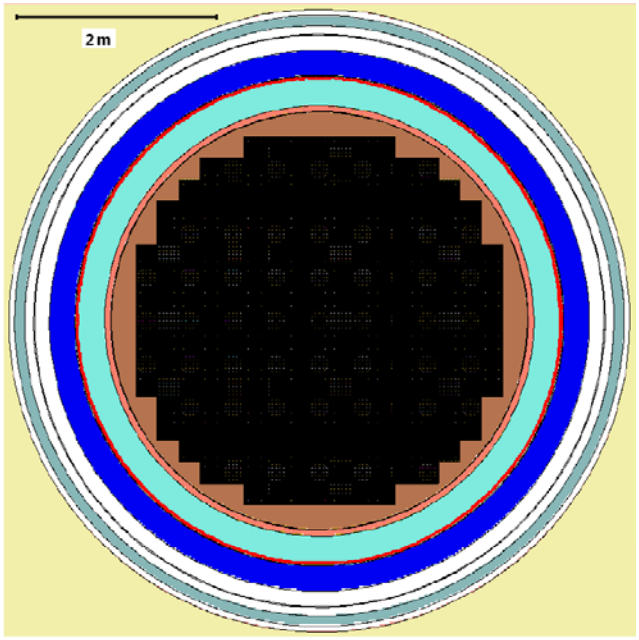

Figure 34. PWR Gen III; fast neutron flux on PV on 360°: tally location at level of bottom of core (horizontal section)

For the "*DSA* case", the superhistory size and fission generation length were the same as previously, that is, 1.2×10^6 and 12 respectively. To achieve a similar calculational effort, the size in the "analog case" was 3×10^5, similar to the previous problem. In both cases, each step consisted of 120 fission generations and the total number of steps was 60. In Figs. 35 and 36 we see, for the "*DSA* case" and "analog case" respectively, the *CMA*'s of the ex-core response and the fission heating in the lowest axial segment of the outer fuel assembly ring. In both cases we see a strong correlation between the in- and ex-core responses.

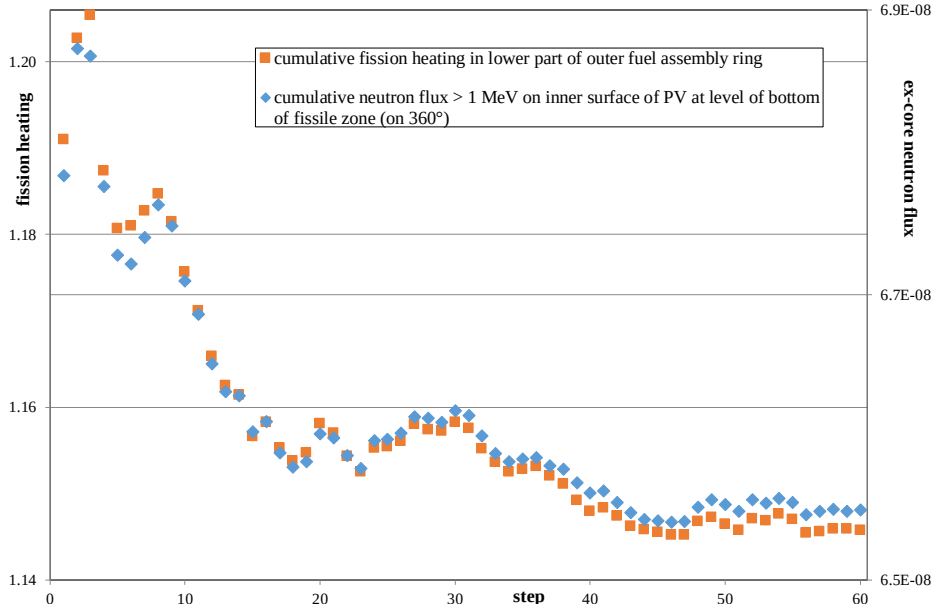

Figure 35. PWR Gen III; fast neutron flux on PV on 360° at level of bottom of core: CMA's of ex-core response and fission heating in lower part of outer fuel assembly ring against number of steps (each of size 1.2×10^6 and length 10 superhistories = 120 fission generations) with "DSA approach"

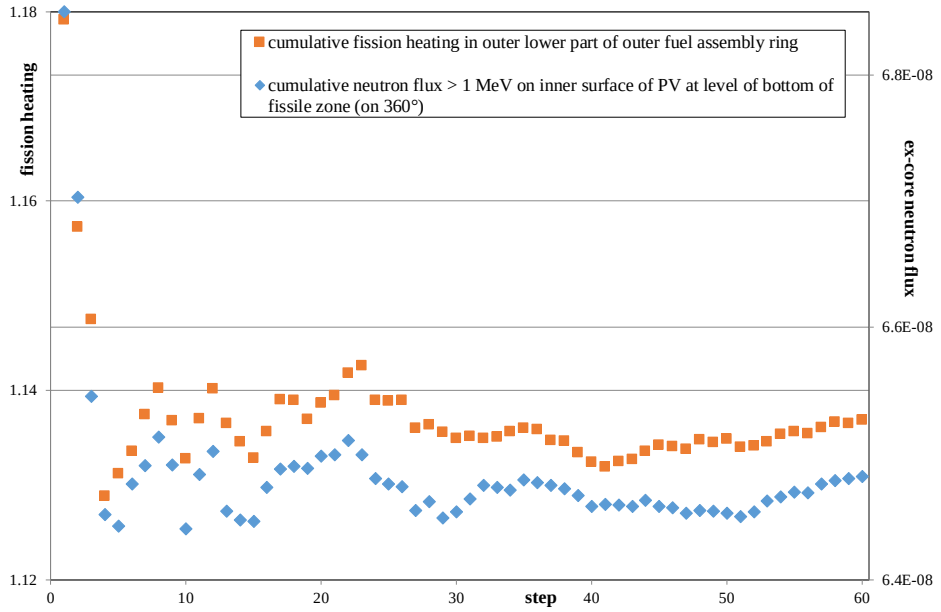

Figure 36. PWR Gen III; fast neutron flux on PV on 360° at level of bottom of core: CMA's of ex-core response and fission heating in lower part of outer fuel assembly ring against number of steps (each of size 3×10^5 and length 120 superhistories / fission generations) with "analog approach"

The *FOM*'s of the two cases ("*DSA*", "analog") and their ratio for the ex-core response are shown in Fig. 37. In Fig. 37 we see that after 60 steps (7200 fission generations) the ratio "*DSA*" / "analog" is only slightly greater than 1. Furthermore, it is degrading (although this is due to the "analog case" *FOM* increasing – the "*DSA* case" *FOM* is reasonably constant over steps 31-60). Thus, again we see that the ex-core penetration is not sufficient to atone for the variation in the fundamental mode.

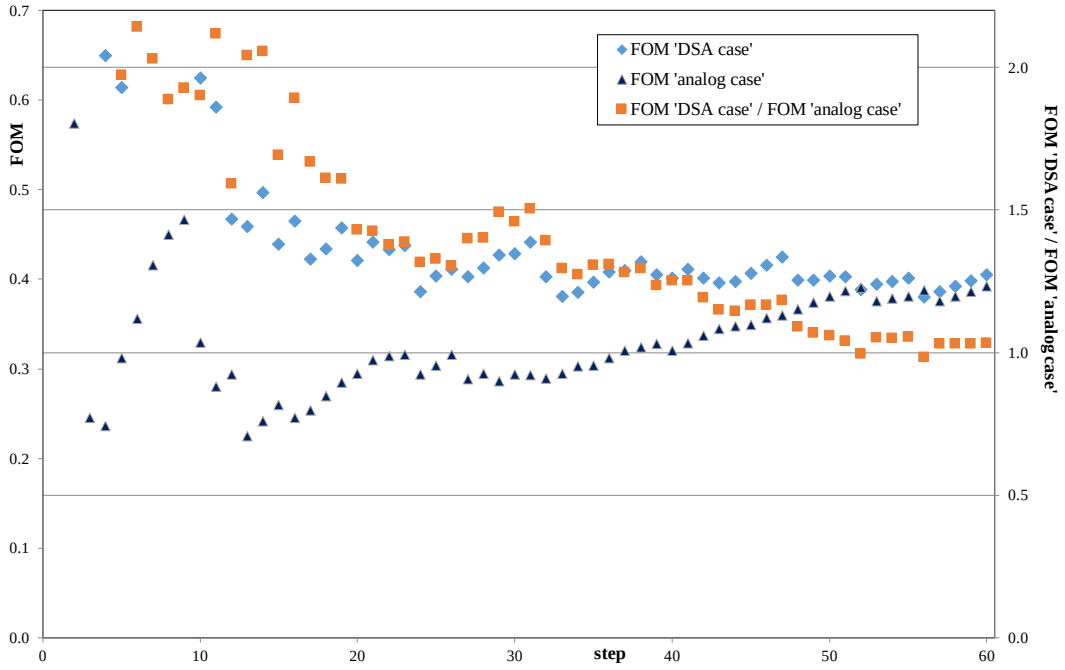

Figure 37. PWR Gen III; fast neutron flux on PV on 360° at level of bottom of core: FOM's of the ex-core response for the two approaches, "DSA" and "analog", and their ratio

The *FOM*$_c$'s of the two cases ("*DSA*", "analog") and their ratio for the 15 global responses are shown in Fig. 38. The ratio of the *FOM*$_c$'s ("*DSA*" / "analog") after 60 steps was 0.59. This is higher than the problem in §3.2.1 (after 40 steps the ratio was 0.25). This may be due to the fact that here there is a single ex-core response whilst in §3.2.1 there were 48, so proportionally more effort is spent here in-core compared with ex-core.

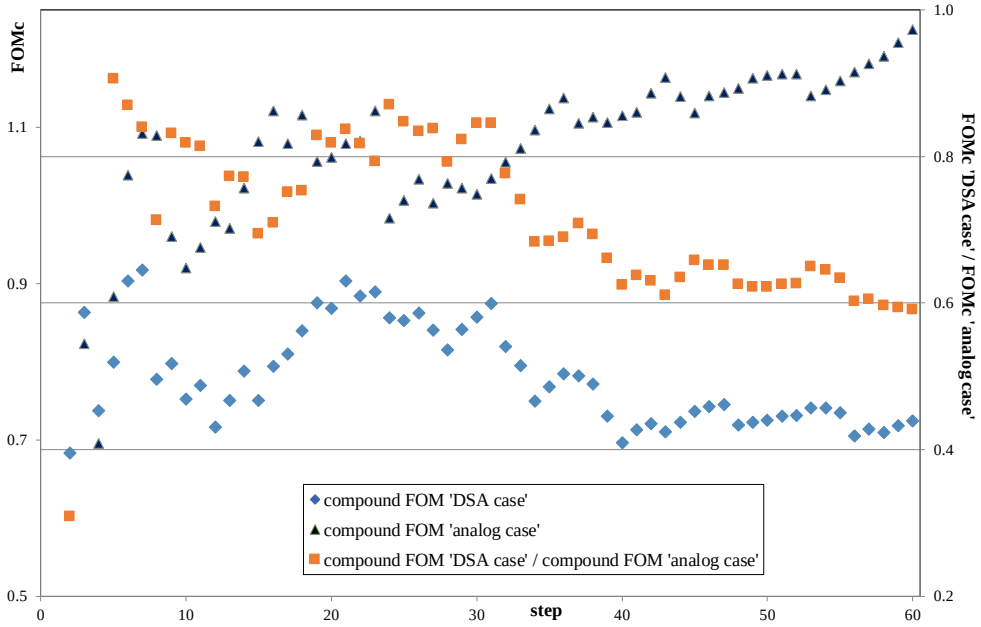

Figure 38. PWR Gen III; fast neutron flux on PV on 360° at level of bottom of core: FOM$_c$'s of the 15 in-core global responses for the two approaches, "DSA" and "analog", and their ratio

3.2.3 Single ex-core response: neutron flux > 1 MeV on PV just below supporting platforms on 360°

The third problem again concerns a single ex-core response: the neutron flux above 1 MeV on the inner surface of the PV just below the supporting platforms. The position is shown in a vertical section in Fig. 33 (the lower pair of the red indicators) and a horizontal section in Fig. 39. The axial extent of the tally was 8.4 cm (vertical). As can be seen from Fig. 33, bearing in mind that the response is > 1 MeV, the penetration is substantially greater than that in §3.2.2.

For the "*DSA* case", the superhistory size and fission generation length were the same as previously, that is, 1.2×10^6 and 12 respectively. To achieve a similar calculational effort, the size in the "analog case" was 2.3×10^5 (compare 3×10^5 in the previous problem). In both cases, each step consisted of 96 fission generations and the total number of steps was 60.

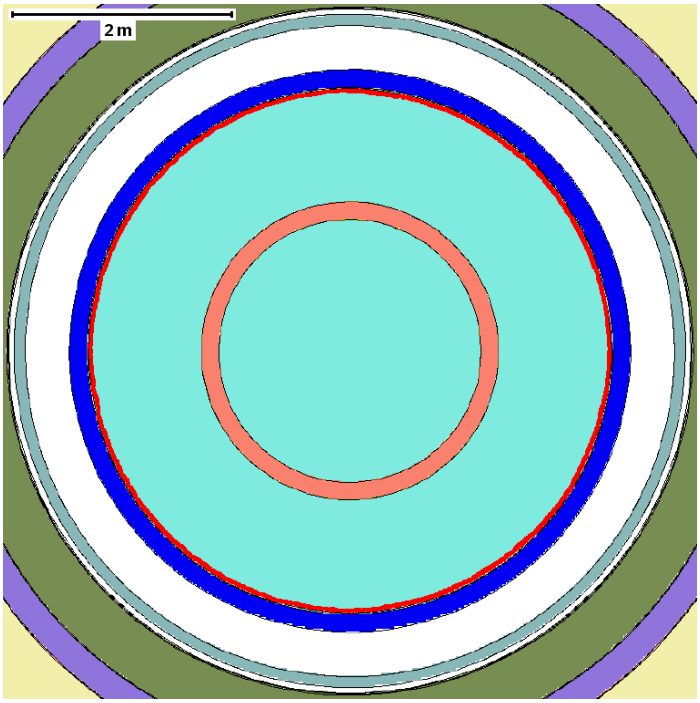

Figure 39. PWR Gen III; fast neutron flux on PV on 360°: tally location below supporting platforms (horizontal section)

In Figs. 40 and 41 we see, for the "*DSA* case" and "analog case" respectively, the *CMA*'s of the ex-core response and the fission heating in the lowest segment of the outer fuel assembly ring. In both cases, we see a weaker correlation between the in- and ex-core responses compared with §3.2.2 (Figs. 35 and 36).

The *FOM*'s of the two cases ("*DSA*", "analog") and their ratio for the ex-core response are shown in Fig. 42. We see that after 60 steps (5760 fission generations) the ratio "*DSA*" / "analog" is around 3.3. Although the ratio is not particularly stable, due to variations in both the "*DSA* case" and "analog case", we see for the first time that the ex-core penetration is sufficient for the extra sampling in the part of the fissile zone that contributes to the ex-core detector together with time saved from RR in the rest of the fissile zone, to more than compensate for the variation in the fundamental mode.

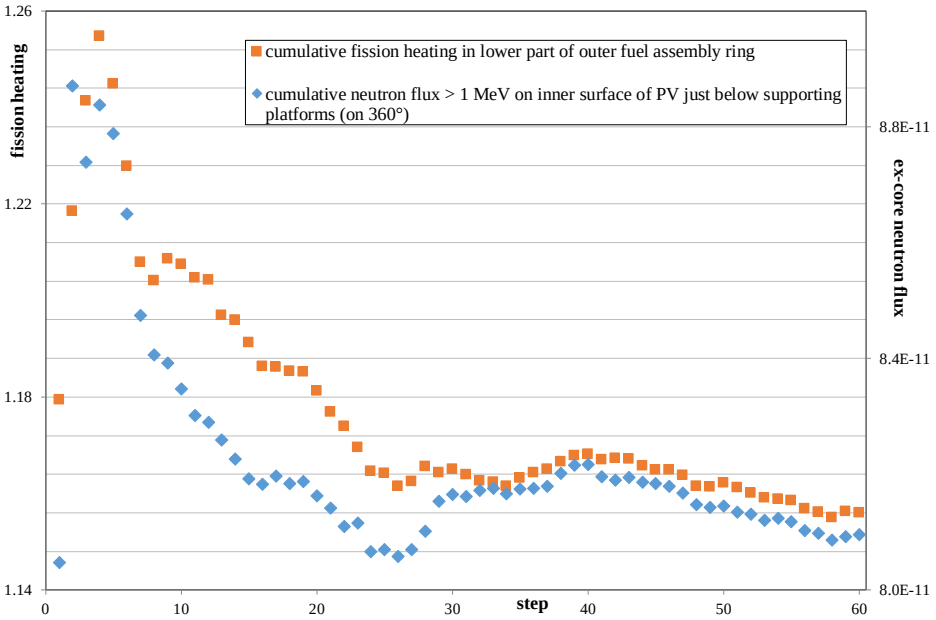

Figure 40. PWR Gen III; fast neutron flux on PV on 360° below supporting platforms: CMA's of ex-core response and fission heating in lower part of outer fuel assembly ring against number of steps (each of size 1.2×10^6 and length 8 superhistories = 96 fission generations) with "DSA approach"

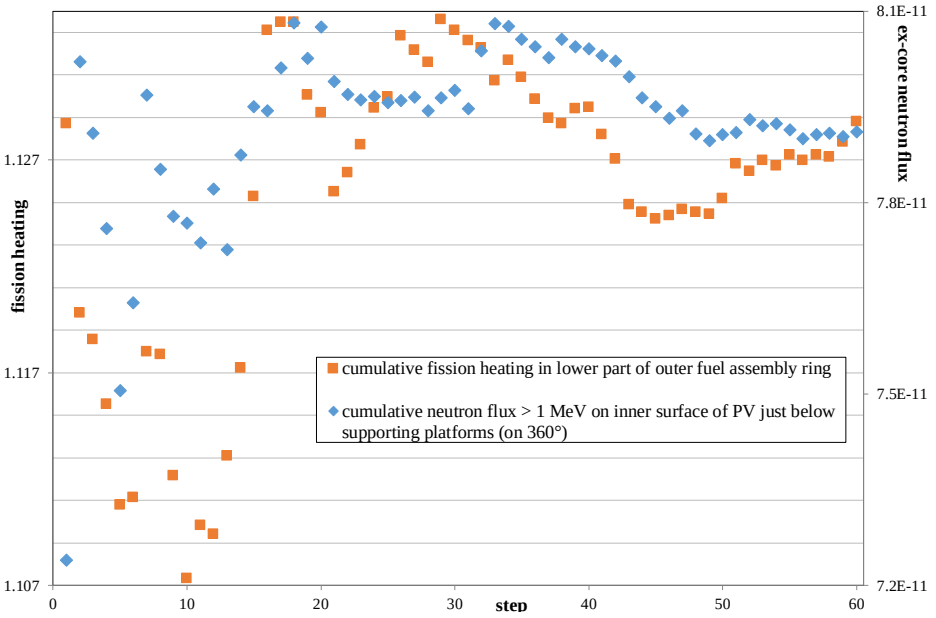

Figure 41. PWR Gen III; fast neutron flux on PV on 360° below supporting platforms: CMA's of ex-core response and fission heating in lower part of outer fuel assembly ring against number of steps (each of size 2.3×10^5 and length 96 superhistories / fission generations) with "analog approach"

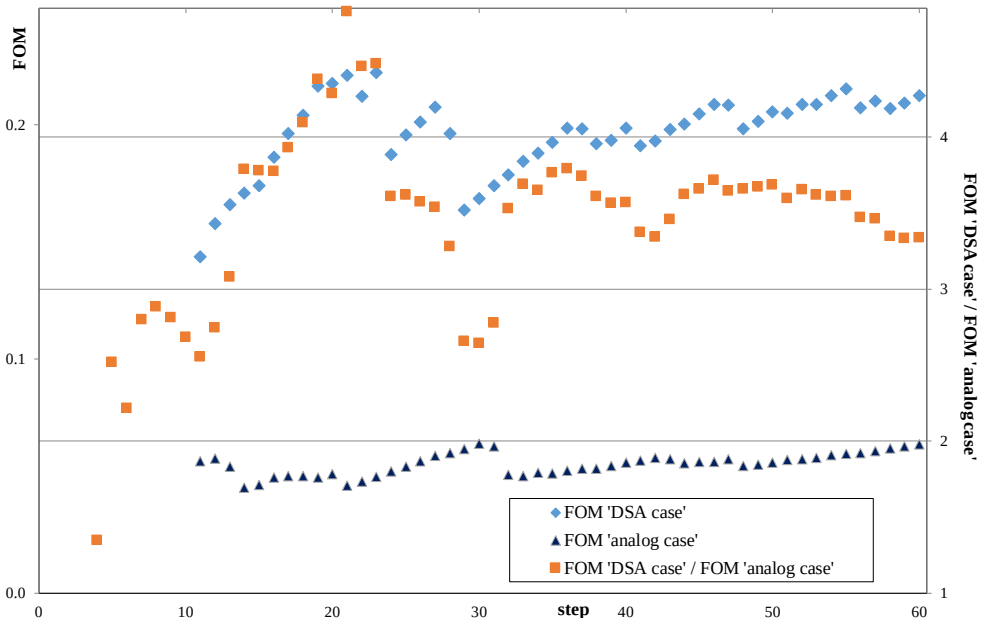

Figure 42. PWR Gen III; fast neutron flux on PV on 360° below supporting platforms: FOM's of the ex-core response for the two approaches, "DSA" and "analog", and their ratio

The *FOM*$_c$'s of the two cases ("*DSA*", "analog") and their ratio for the 15 global responses are shown in Fig. 43. The ratio after 60 steps was 0.58, similar to the value in §3.2.2.

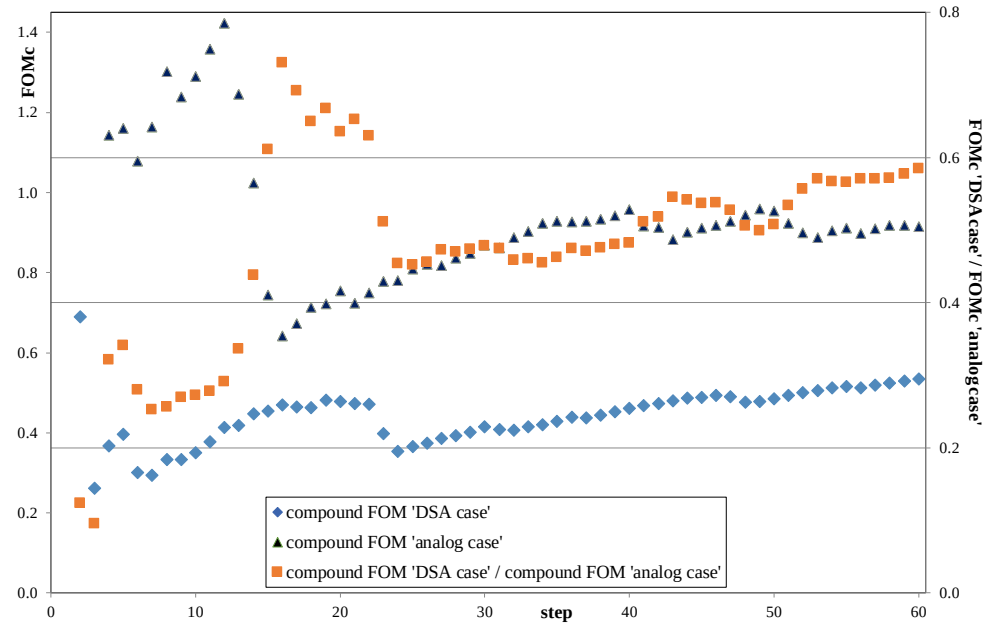

Figure 43. PWR Gen III; fast neutron flux on PV on 360° below supporting platforms: FOM$_c$'s of the 15 in-core global responses for the two approaches, "DSA" and "analog", and their ratio

3.2.4 Single ex-core response: neutron flux > 1 MeV on PV just below supporting platforms subtended by a limited azimuthal angle

The ex-core penetration is further increased by limiting the azimuthal range of the response in §3.2.3: instead of over 360° we limit it to a range of ±2.4° around 0°, that is, directly under a supporting platform (see Figs. 33 and 44). Then to take into account the limited azimuthal range of the ex-core detector, we needed to add extra spatial segments around 0° from the core out to the PV including the lower plenum, bottom plate and the water between the bottom plate and the distribution plate (see Fig. 33).

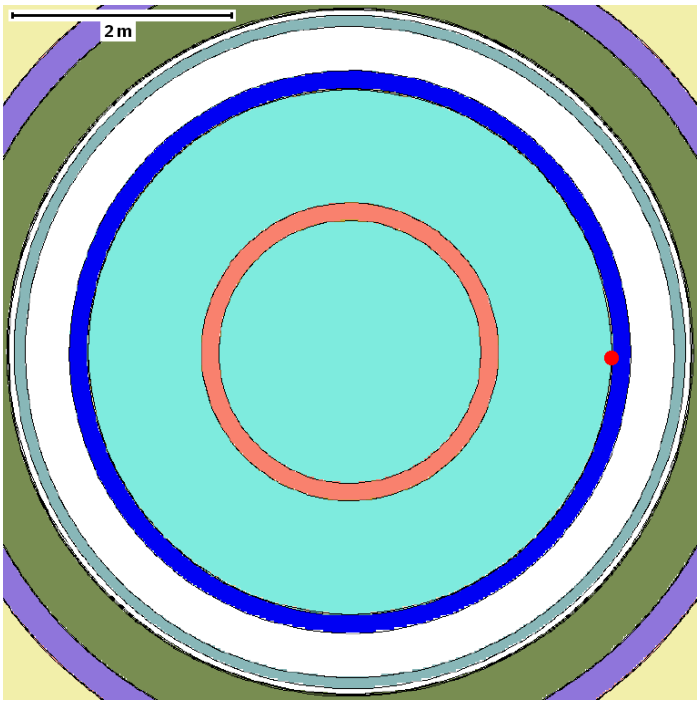

Figure 44. PWR Gen III; fast neutron flux on PV at 0°: tally location below supporting platforms (horizontal section)

It turned out that the greater penetration compared with the previous problem due to the breakdown in azimuthal symmetry, produced a much greater variation in the ratio of importances between the fictitious source cells and their respective real-world cells. This yielded a much smaller fission source size in the "analog case" to engender a similar computer time to the "*DSA* case". As there was concern that the fission source size would result too low, the size of the starting superhistories in the "*DSA* case" was increased to 9×10^6. The fission generation length of each superhistory was maintained at 12. To achieve a similar calculational effort, the size in the "analog case" was then 2.6×10^5. In both cases, each step consisted of 96 fission generations and the total number of steps was 60, as in §3.2.3.

In Figs. 45 and 46 we see, for the "*DSA* case" and "analog case", the *CMA*'s of the ex-core response and fission heating in the lowest axial segment of the outer fuel assembly ring around the 0° azimuth. In both cases the correlation between the in- and ex-core responses looks similar to that in §3.2.3 (Figs. 40 and 41).

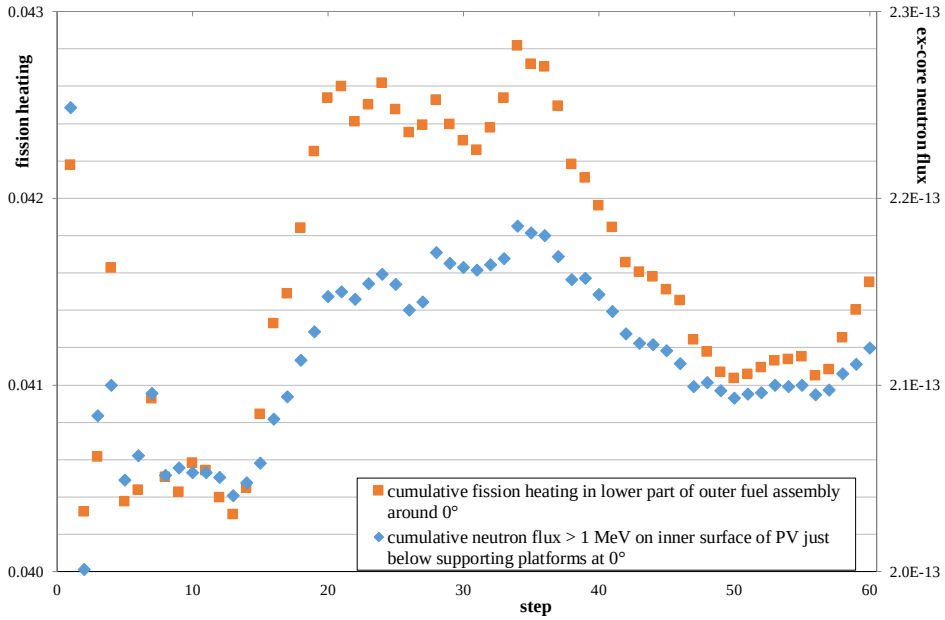

Figure 45. PWR Gen III; fast neutron flux on PV at 0° below supporting platforms: CMA's of ex-core response and fission heating in lower part of outer fuel assembly ring around 0° against number of steps (each of size 9×10^6 and length 8 superhistories = 96 fission generations) with "DSA approach"

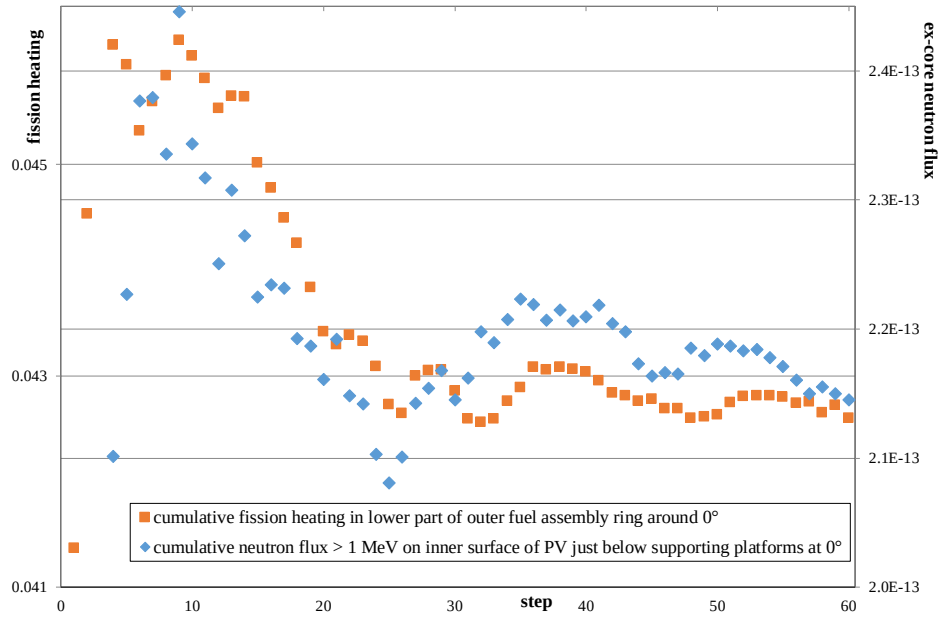

Figure 46. PWR Gen III; fast neutron flux on PV at 0° below supporting platforms: CMA's of ex-core response and fission heating in lower part of outer fuel assembly ring around 0° against number of steps (each of size 2.6×10^5 and length 96 superhistories / fission generations) with "analog approach"

The running values of the FOM_c's of the two cases ("*DSA*", "analog") and their ratio over the 60 steps for the ex-core response and for the 17 in-core fission responses are reported in [1]. The final ratios *DSA*/analog after 60 steps were 0.54 (similar to the values in §3.2.2 and §3.2.3) for the 17 in-core fission responses and 4.1 for the ex-core response. The latter value is not particularly stable and might decrease with further steps.

3.2.5 Revisiting §3.2.4: increasing the number of fission generations in the phase of generating the *VR* parameters

There have been indications both from this PWR GEN III problem and from the previous flooded fuel flask problem that in the "*DSA* case" there are too few fission neutrons entering the real-world source cells from the fictitious source cells. In many of the calculations we have seen a high correlation between the fission rate in the part of the fissile configuration that contributes to the ex-core response and the ex-core response itself: indeed Figs. 26, 31, 35 and 40, which employ *DSA VR* in the fissile zone, show curves that look more correlated compared with those in Figs. 27, 32, 36 and 41 respectively, which employ analog *VR* in the fission zone. (Figs. 45 and 46 seem more marginal.) It looks like the fissile part of the problem is not being sampled enough compared with the transport ex-core. An undersampling of the fissile zone will be more serious for the "*DSA* case" than the "analog case" because of the *VR* performed in the fissile zone in the former case which can unbalance the population. We have two hypotheses as to why our approach is producing this result.

A first hypothesis is that the number of fission generations in the phase of generating the *VR* parameters (here the energy/space cell importances) is not sufficient. The complete "natural" variation of the fission source is not experienced in this phase. The subsequent "optimum" *VR* parameters tend to favour the local ex-core response at the expense of the global in-core responses that model the fundamental mode because the method thinks that the source varies less than it really does, that the global responses are evaluated more accurately than they really are, and time can be saved by doing less work in the fissile zone and more outside. The consequence is that quite strong RR is played when neutrons are born in the majority of the core that does not contribute to the ex-core detector(s). As the calculation that employs these *VR* parameters proceeds, the global responses, including the fission rate (or fission heating) in the part of the core that contributes to the ex-core detector(s), exhibit more variation than predicted.

In §3.2.4 the last iteration in the phase of generating the *VR* parameters employed a superhistory size of 1.2×10^6, a superhistory length of 12 fission generations and a total of 50 superhistories, therefore a total of 50 x 12 = 600 fission generations. We then ran 60 steps each of 96 fission generations (and with a superhistory size of 9×10^6), therefore a total of 60 x 96 = 5760 fission generations. We hypothesize that the number of fission generations in the phase of generating the *DSA VR* parameters is not sufficient and indeed we see that this number is approximately 1/10 of the number of fission generations in the final run employing these *VR* parameters. It is conjectured above that a consequence was the underestimation of the variation of the in-core global responses when generating the *VR* parameters. It seemed that the quite strong Russian roulette between the fictitious and the real-world source cells in much of the core was a result.

Starting from the *VR* parameters employed in §3.2.4 we continued the iterative procedure to generate *VR* parameters, increasing the *KCT* value to 1000. Thus with a superhistory length of 12, this becomes 12000 fission generations. However we had to correspondingly lower the size of each superhistory (*NSRCK*) to 3×10^4 due to CPU time and central memory constraints. (Given the fact that RR is played between fictitious and real-world source cells, the effective size is much smaller.) We then ran the resultant "optimum" *VR* parameters with a superhistory size of 9×10^6 as in §3.2.4. The fission generation length of each superhistory was maintained at 12. To achieve a similar calculational effort, the size in the "analog case" was then 5.65×10^5 (compare 2.6×10^5 in §3.2.4). In both cases, each step consisted of 48 fission generations and the total number of steps was now 80.

In analogy to §3.2.4, Figs. 47 and 48 show the *CMA*'s of the ex-core response and the fission heating in the lowest axial segment of the outer fuel assembly ring, around the 0° azimuth for the "*DSA* case" and "analog case" respectively. Figs. 49 and 50 show the *FOM*'s and FOM_c's of the

two cases and their ratio for the ex-core response and for the 17 global responses respectively.

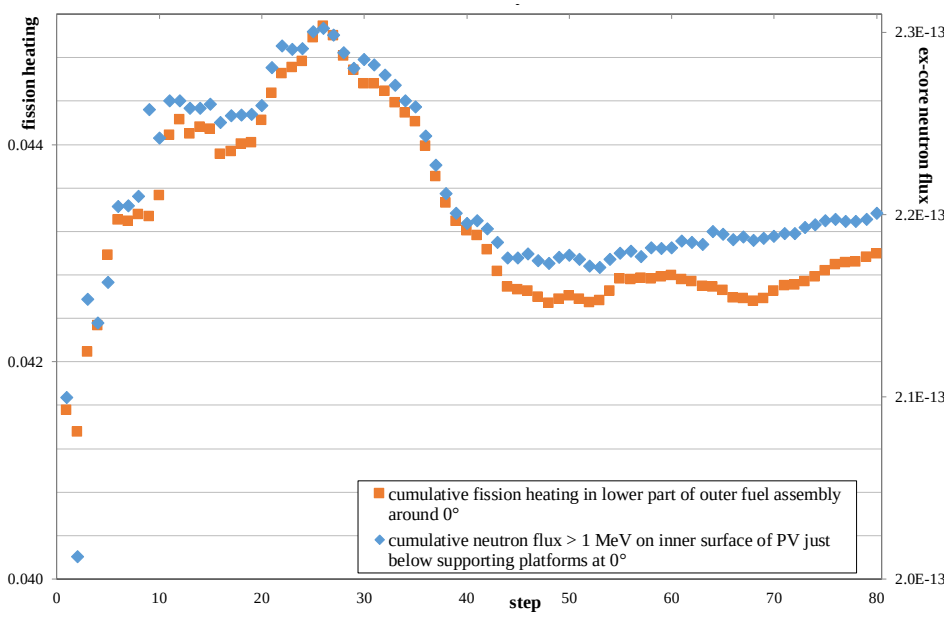

Figure 47. PWR Gen III; fast neutron flux on PV at 0° below supporting platforms (NSRCK=30000, KCT=1000 in the phase of generating the VR parameters): CMA's of ex-core response and fission heating in lower part of outer fuel assembly ring around 0° against number of steps (each of size 9×10^6 and length 4 superhistories = 48 fission generations) with "DSA approach"

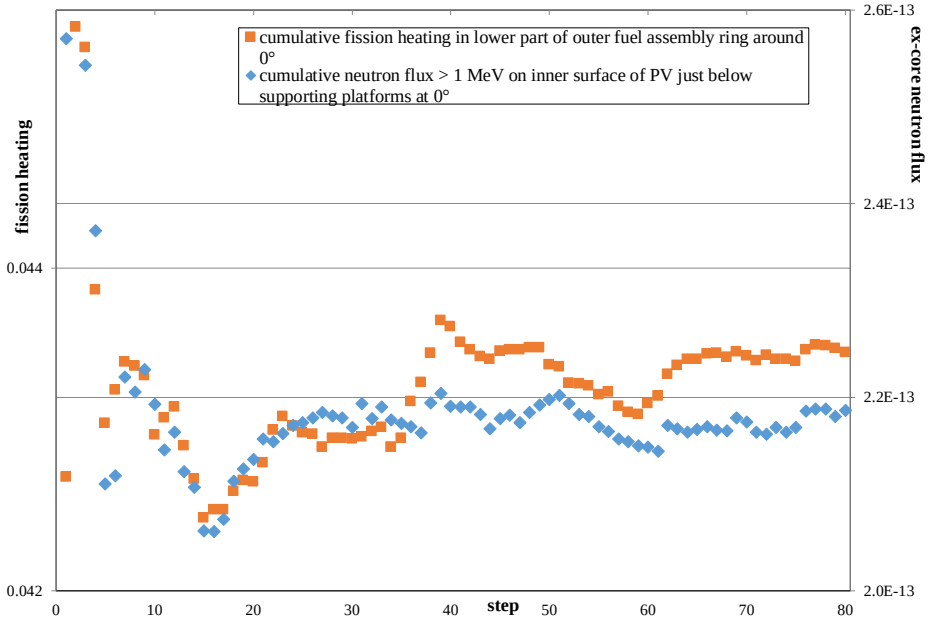

Figure 48. PWR Gen III; fast neutron flux on PV at 0° below supporting platforms (NSRCK=30000, KCT=1000 in the phase of generating the VR parameters): CMA's of ex-core response and fission heating in lower part of outer fuel assembly ring around 0° against number of steps (each of size 5.65×10^5 and length 48 superhistories / fission generations) with "analog approach"

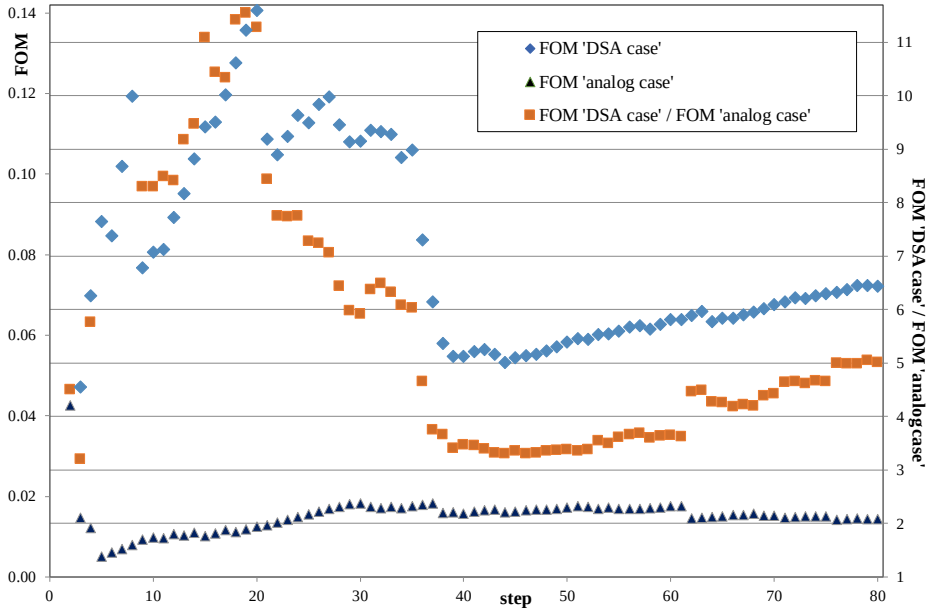

Figure 49. PWR Gen III; fast neutron flux on PV at 0° below supporting platforms (NSRCK=30000, KCT=1000 in the phase of generating the VR parameters): FOM's of the ex-core response for the two approaches, "DSA" and "analog", and their ratio

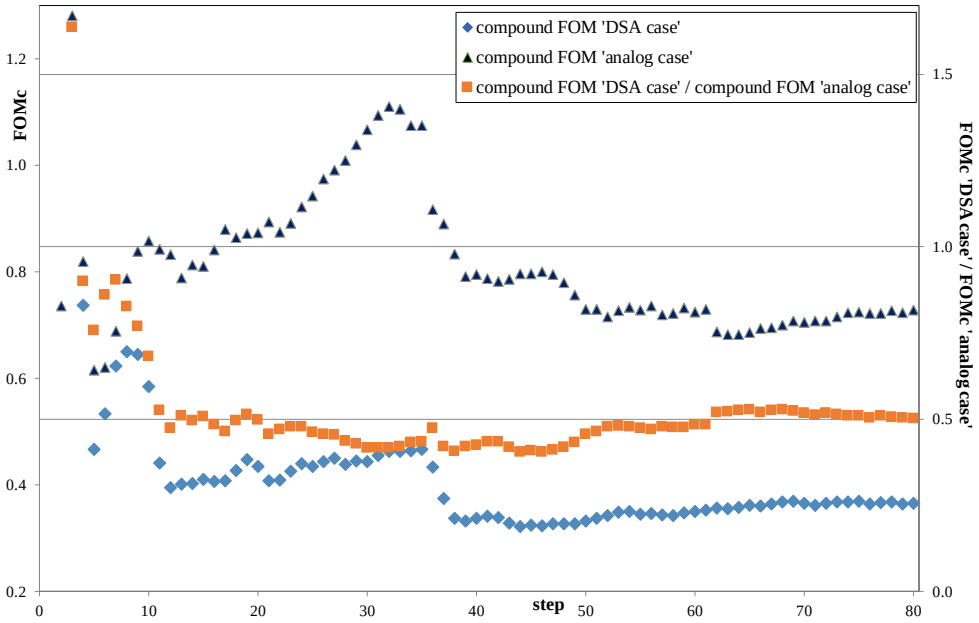

Figure 50. PWR Gen III; fast neutron flux on PV at 0° below supporting platforms (NSRCK=30000, KCT=1000 in the phase of generating the VR parameters): FOM_c's of the 17 in-core global responses for the two approaches, "DSA" and "analog", and their ratio

In Figs. 47 and 48 we see again the correlations between the response of the nearest core segment to the ex-core response and the ex-core response itself, that look possibly higher for the "*DSA* case" compared to the "analog case". In Fig. 49 the ratio of the *FOM*'s of the ex-core response of around 5 is slightly higher than the comparable value in §3.2.4 (which was 4.1 after 60 steps). Instead, the ratios of the FOM_c's of the 17 global responses are comparable to those in §3.2.4.

The results in Figs. 47-50 are not greatly different from those of §3.2.4 notwithstanding the fact that 12000 fission generations were employed in the generating phase in the former case and 600 in the latter case. Although increasing greatly the number of fission generations in the phase of generating the *VR* parameters did not improve matters, it was all the same of interest to further reduce the superhistory size in the generating phase producing thus a still greater variation in the global responses in this phase.

We thus reduced the superhistory size (*NSRCK*) from 3×10^4 to 2×10^3 (to achieve this we needed to put the importances of the fictitious source cells equal to those of the real-world source cells) when generating the *VR* parameters. (We were reasonably relaxed about using such a small size superhistory as we welcomed a greater variation in the global responses, even if artificially induced.) We left the *KCT* value as 1000 (12000 fission generations). We then ran the resulting "optimum" *VR* parameters with a superhistory size of 9×10^6 and a superhistory length of 12 fission generations as previously, and 60 steps, each step consisting of 3 superhistories (36 fission generations). To achieve a similar calculational effort, the size in the "analog case" was then 1.55×10^6 (compare 5.65×10^5 previously and 2.6×10^5 in §3.2.4). Each step in the "analog case" consisted of 36 fission generations and the total number of steps was 60.

Figs. 51-54 are analogous to the previous Figs. 47-50. Comparing these two sets of figures, in Fig. 51 there looks to be slightly less correlation between the ex-core response and the nearest global response compared with Fig. 47. In Fig. 53 the ex-core response looks slightly worse than that in Fig. 49 (in terms of both the absolute value of the *FOM* as well as the gain over the analog case). However, the most interesting result is that the FOM_c of the 17 global responses in Fig. 54 now shows a gain over the analog case (compare Figs. 54, 50 and 17 in [1]). This result was sought having introduced an artificially high variation in the fundamental mode in the phase of generating the *VR* parameters, their employment does indeed hold the fundamental mode particularly steady.

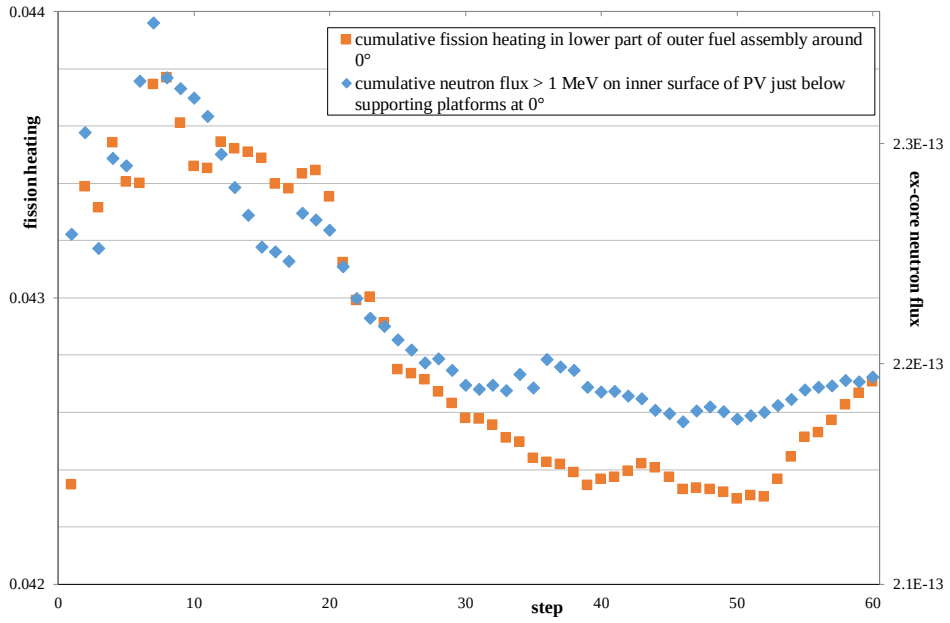

Figure 51. PWR Gen III; fast neutron flux on PV at 0° below supporting platforms (NSRCK=2000, KCT=1000 in the phase of generating the VR parameters): CMA's of ex-core response and fission heating in lower part of outer fuel assembly ring around 0° against number of steps (each of size 9×10^6 and length 3 superhistories = 36 fission generations) with "DSA approach"

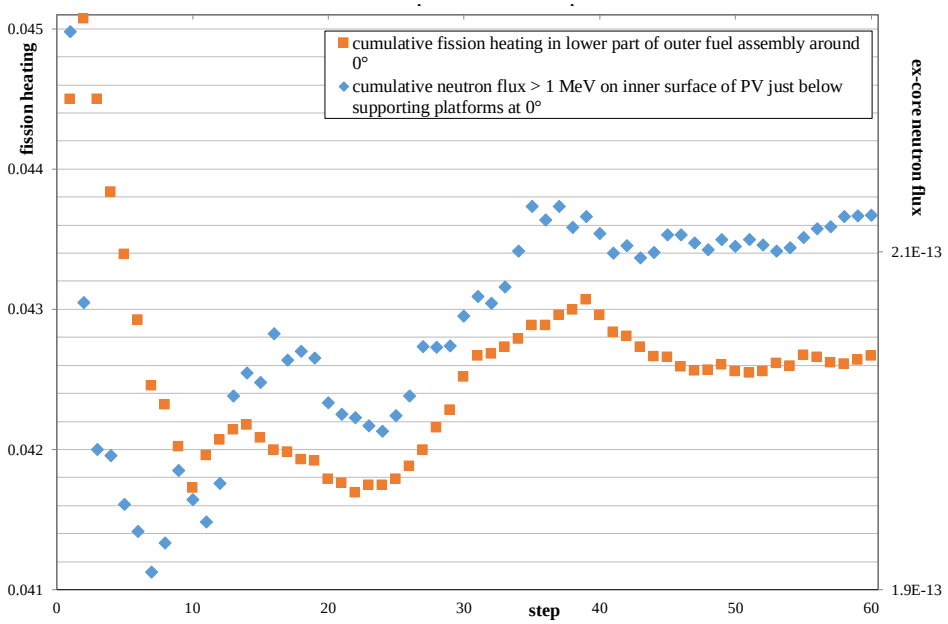

Figure 52. PWR Gen III; fast neutron flux on PV at 0° below supporting platforms (NSRCK=2000, KCT=1000 in the phase of generating the VR parameters): CMA's of ex-core response and fission heating in lower part of outer fuel assembly ring around 0° against number of steps (each of size 1.55×10^6 and length 36 superhistories / fission generations) with "analog approach"

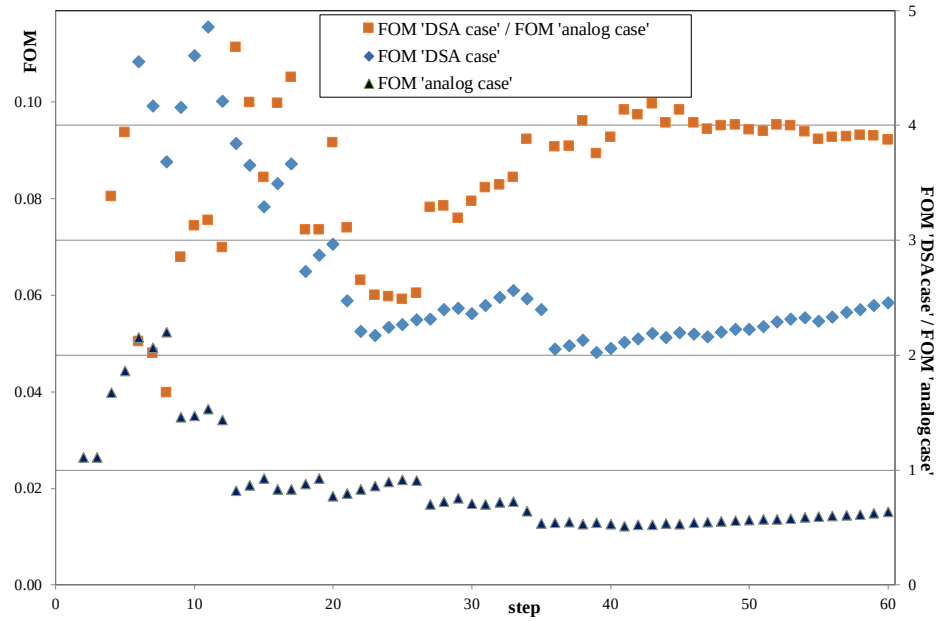

Figure 53. PWR Gen III; fast neutron flux on PV at 0° below supporting platforms (NSRCK=2000, KCT=1000 in the phase of generating the VR parameters): FOM's of the ex-core response for the two approaches, "DSA" and "analog", and their ratio

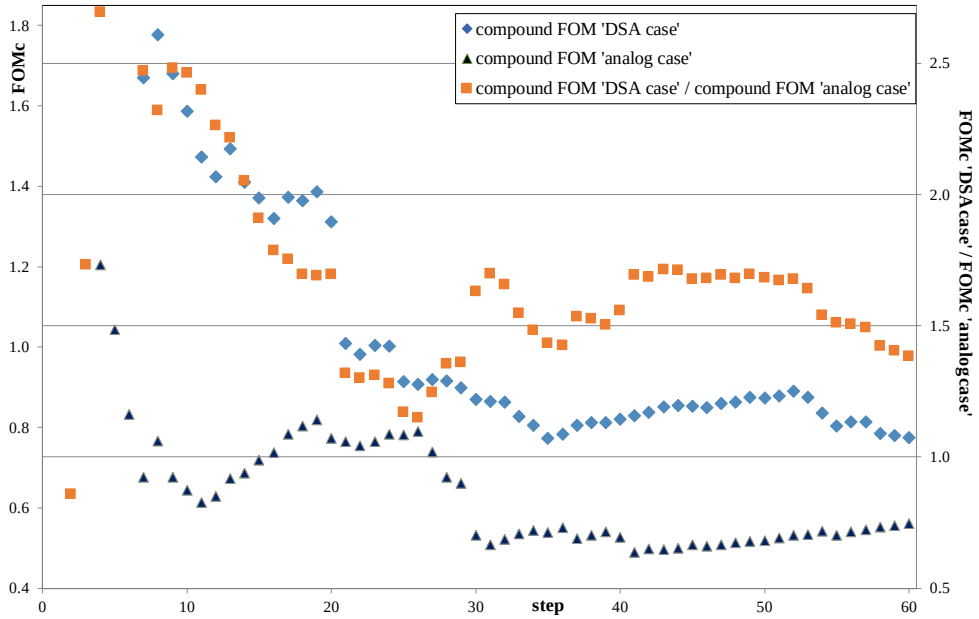

Figure 54. PWR Gen III; fast neutron flux on PV at 0° below supporting platforms (NSRCK=2000, KCT=1000 in the phase of generating the VR parameters): FOM_c's of the 17 in-core global responses for the two approaches, "DSA" and "analog", and their ratio

In conclusion, contrary to what had been hoped for, increasing the number of fission generations in the generating phase of the VR parameters does not seem to appreciably improve the previous results.

3.2.6 Revisiting §3.2.4: increasing the number of fission neutrons passing from the fictitious to the real-world source cells

A second hypothesis as to why our approach is producing too few neutrons in the real-world source cells is discussed in [1]. It concerns the conversion of the *DSA* from fixed source to eigenvalue mode. Here we do not repeat the discussion. We only summarize the necessary elements and the main results.

Before looking at ways of increasing the number of neutrons entering the geometry, it is interesting to see the ratio of the real-world source cell importances to the fictitious source cell importances at the optimum set of cell importances. These ratios are shown in Table V. In Table V the blank spaces are where the data was absent (< 20 keV and 1 – 20 keV in the small segments of the core nearest to the ex-core tally) due to the lack of fission neutrons. As already mentioned, we see Russian roulette in most of the core with splitting only in the part of the core nearest the ex-core detector. The higher the energy, the higher the splitting parameter. Instead, where there is only Russian roulette, the RR parameter does not vary much with energy. The lowest RR survival probability is 0.0039 and the highest splitting is 54-to-1.

Table V. PWR Gen III; fast neutron flux on PV at 0° below supporting platforms (increasing no. fission neutrons passing from fictitious to real-world source cells): Ratio (>1: splitting; < 1: RR) of the real-world source cell importances to the fictitious source cell importances at the optimum (energy: across page, space: down page); *: azimuthal segment nearest to the ex-core tally – see Figs. 33 and 44

assemblies	axial range cm (zero is core mid-plane)	5 – 20 MeV	2 – 5 MeV	0.2 – 2 MeV	20 – 200 keV	1 – 20 keV
inner ring	-210.6 - -147	0.039	0.037	0.042	0.039	0.083
inner ring	-147 - -63	0.017	0.015	0.015	0.015	0.016
inner ring	-63 - +63	0.0070	0.0067	0.0066	0.0068	0.0071
inner ring	+63 - +147	0.016	0.015	0.015	0.015	0.015
inner ring	+147 - +210.6	0.043	0.043	0.043	0.047	0.048
2nd & 3rd outer rings (*)	-210.6 - -180	27	2.3	1.2	0.60	
2nd & 3rd outer rings	-210.6 - -147	1.2	0.103	0.070	0.074	0.047
2nd & 3rd outer rings	-147 - -63	0.0078	0.010	0.0080	0.0080	0.0050
2nd & 3rd outer rings	-63 - +63	0.0045	0.0040	0.0039	0.0043	0.0068
2nd & 3rd outer rings	+63 - +147	0.010	0.010	0.0091	0.010	0.013
2nd & 3rd outer rings	+147 - +210.6	0.028	0.026	0.026	0.030	0.026
outer ring (*)	-210.6 - -180	54	3.0	1.0	1.2	0.21
outer ring	-210.6 - -147	0.22	0.10	0.077	0.063	0.029
outer ring	-147 - -63	0.019	0.010	0.0091	0.0091	0.010
outer ring	-63 - +63	0.0047	0.0045	0.0046	0.0049	
outer ring	+63 - +147	0.011	0.011	0.010	0.010	0.022
outer ring	+147 - +210.6	0.032	0.031	0.031	0.032	0.033

In §3.1.4 (in the footnote) we have introduced the *DSA* functions: the 2nd moment and the (CPU) time functions and the optimum set of *VR* (in this case splitting/RR) parameters that renders their product (the quality function, *q*) a minimum. The 2nd moment function consists of three kinds of terms named “gamma”, “delta” and “branching” [2,16,13,14]. Contributions to the gamma terms occur at every tally score, to the delta terms from correlations at every splitting event at a surface (in space, energy or between fictitious and real-world source cells) and to the branching terms from correlations at every branching that is not a surface splitting event.

We now quantify these ideas. Starting from the set of optimum importances that generated the results in §3.2.4, we varied the importances in all the fictitious source cells (17 spatial x 7 energy groups) by a constant multiplier that ranged from 1/256 to 256 (with a stride of a factor of 2 making 17 sets of importances). Employing the *DSA* 2nd moment and time functions, in Fig. 55 we plot the 2nd moment and time values against each set of importances. (Note that it is the compound 2nd moment function from 17 global and 1 local response.)

In Fig. 55 we see that as the multiplier increases, less splitting and more RR is executed between the fictitious and real-world source cells, the 2nd moment increases, and the CPU time decreases. Vice versa as the multiplier decreases. We see that the branching terms (mainly intra-superhistory fissions) give the major contribution to the 2nd moment. (Note that this is unlike Fig. 7 in [1] where

the same figure is reproduced for the problem in §3.2.1. In that case the delta terms give the major contribution to the 2nd moment.) We also note the reduction in gradient in the delta terms at low multiplier values due to correlations between split particles entering real-world source cells from *FS* cells and raising the 2nd moment. Present although difficult to see is a reduction in gradient in the CPU time at high multiplier values, due to time spent resampling source particles after being rouletted between the fictitious and real-world source cells.

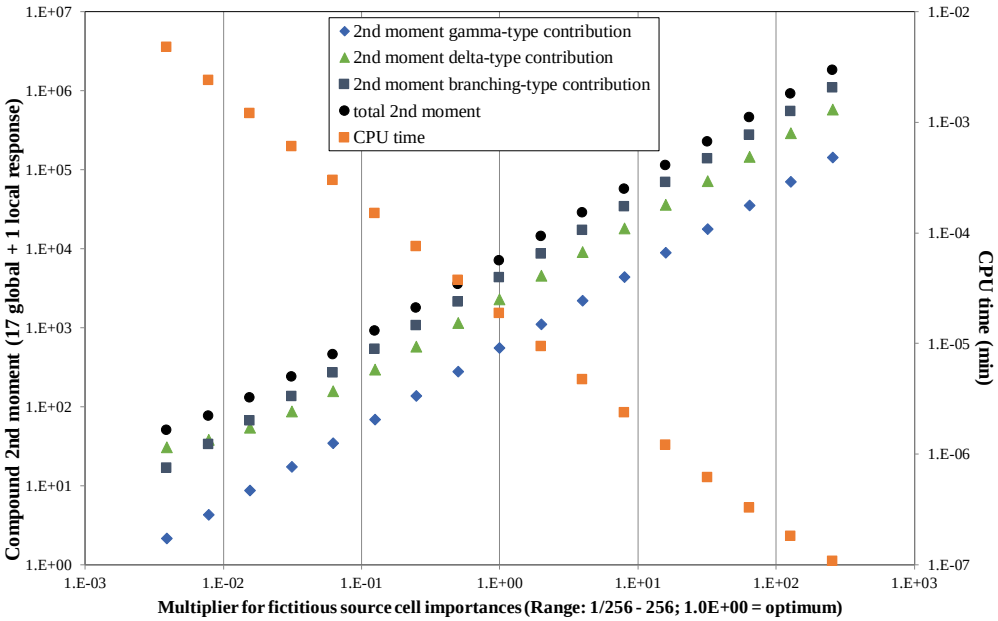

Figure 55. PWR Gen III; fast neutron flux on PV at 0° below supporting platforms (increasing no. fission neutrons passing from fictitious to real-world source cells): 2nd moment and time against multiplier of the fictitious source cell importances

In Fig. 56 (which is identical to Fig. 18 in [1]) the inverse of the quality function (equivalent to FOM_c) is plotted against the multiplier. The main feature of Fig. 56 which we wish to exploit is the wide plateau either side of the optimum. For example, for multiplier values of 16, 8, 1/8 and 1/16, the *1/q* values are 97.5%, 98.8%, 98.7% and 97.0% respectively of the optimum value. This of course is assuming that the source starting each superhistory is fixed.

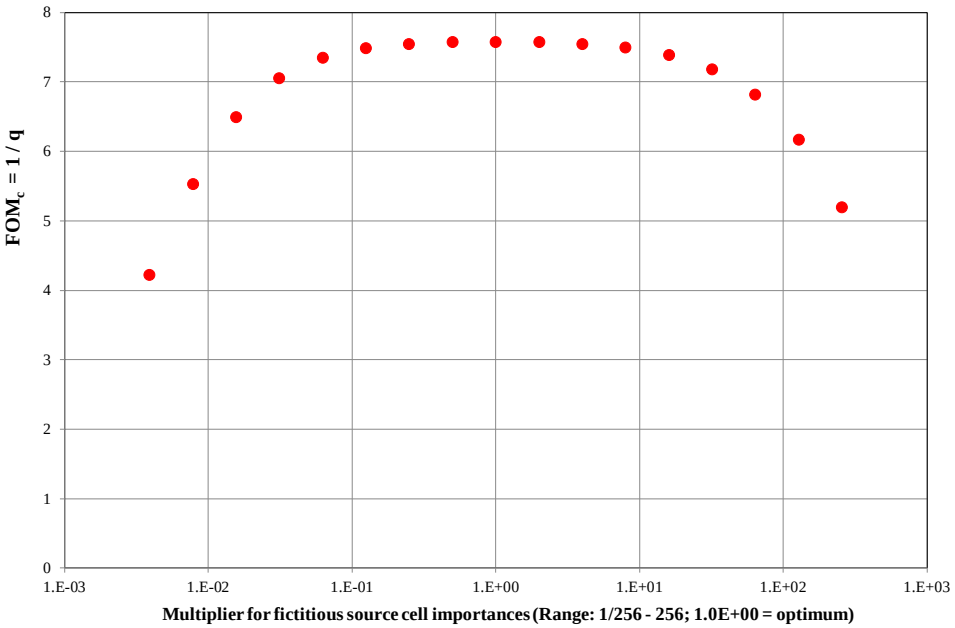

Figure 56. PWR Gen III; fast neutron flux on PV at 0° below supporting platforms (increasing no. fission neutrons passing from fictitious to real-world source cells): inverse of the quality (2nd moment × time) against multiplier of the fictitious source cell importances

In our eigenvalue problem, we wish to increase the fission neutrons in the real-world source cells in the "*DSA* case" without damaging much the quality function so from Fig. 56 we choose a multiplier of 1/8. (We might also have chosen 1/16.) We note that all the parameters in Table V are thus multiplied by 8 so that the highest splitting becomes 430-to-1 and the lowest RR survival probability becomes 0.032. The size of the starting superhistories was kept at 9×10^6. The fission generation length of each superhistory was maintained at 12. To achieve a similar calculational effort, the size in the "analog case" was then made 8 times the value of §3.2.4, or 2.08×10^6. In both cases, each step consisted of just 12 fission generations and the total number of steps was now 80.

In Figs. 57 and 58 we see, for the "*DSA* case" and "analog case" respectively, the *CMA*'s of the ex-core response and the fission heating in the lowest axial segment of the outer fuel assembly ring, around the 0° azimuth. The correlations between the two curves in each figure look similar to those in §3.2.4 (Figs. 45 and 46). Again there looks to be less correlation in the "analog case" compared with the "*DSA* case". Both curves look smoother than those in §3.2.4, especially the "*DSA* case" (compare Figs. 57 and 45 - the computer time per step is very similar).

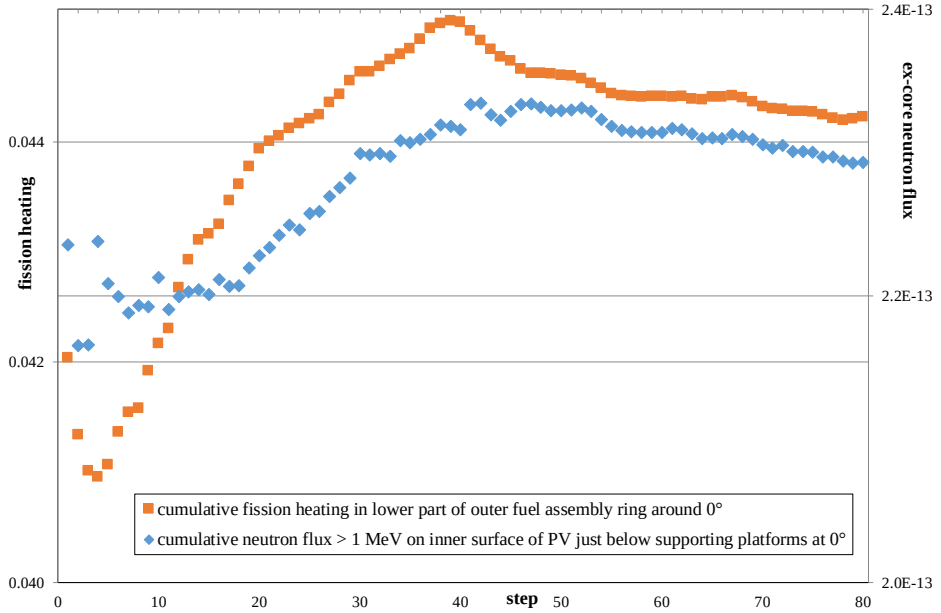

Figure 57. PWR Gen III; fast neutron flux on PV at 0° below supporting platforms (increasing no. fission neutrons passing from fictitious to real-world source cells): CMA's of ex-core response and fission heating in lower part of outer fuel assembly ring around 0° against number of steps (each of size 9×10^6 and length 1 superhistory = 12 fission generations) with "DSA approach"

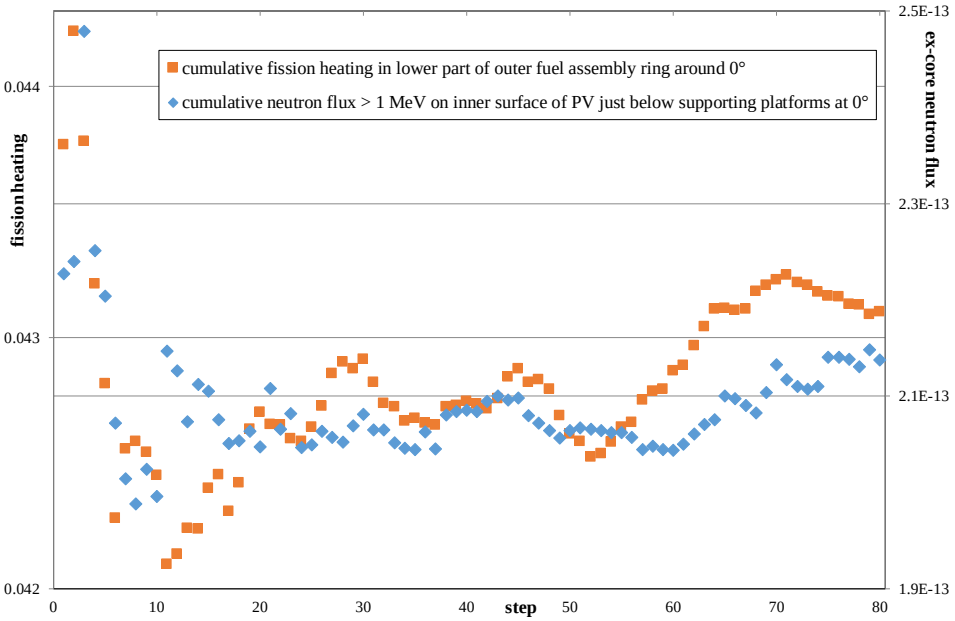

Figure 58. PWR Gen III; fast neutron flux on PV at 0° below supporting platforms (increasing no. fission neutrons passing from fictitious to real-world source cells): CMA's of ex-core response and fission heating in lower part of outer fuel assembly ring around 0° against number of steps (each of size 2.08×10^6 and length 12 superhistories / fission generations) with "analog approach"

The running values of the FOM_c's of the two cases ("*DSA*", "analog") and their ratio over the 80 steps for the ex-core response and for the 17 in-core fission responses are reported in [1]. The final ratios *DSA*/analog after 80 steps were 1.07 for the 17 in-core fission responses and 15.2 for

the ex-core response.

The results in this section begin to look promising and go some way towards supporting the hypothesis outlined at the beginning of this section and in §3.1.2 in [1]. The smoothness of the curves in Fig. 57 and the final FOM_c ratios seem to back the idea that it is important that the size of the fission generation should be adequate, particularly when *VR* is performed in the fissile zone.

We note the different behaviour of the eigenvalue problem compared with the fixed source model that produced the plateau in Fig. 56. The value at the optimum in Fig. 56 is 7.6 (fixed source model). In the eigenvalue problem, for all 17 global responses plus the ex-core response, the comparable value is 0.82 between the 80 steps in this section (which lies between 0.121 for the local response in Fig. 19 in [1] and 1.23 for the 17 global responses in Fig. 20 in [1]). Comparable values in the eigenvalue problem from §3.2.4 before the work-around which improved the results, are 0.16 between the 60 steps (which lies between 0.046 for the local response in Fig. 16 in [1] and 0.19 for the 17 global responses in Fig. 17 in [1]).

Thus, we see that there are large differences in the FOM_c estimate depending on whether it is an eigenvalue or a fixed source model. (Also within the fixed source model there are the approximations implicit in the functional value of *1/q* in Fig. 56.) Furthermore, in the eigenvalue problem that there are large variations in the FOM_c estimate depending on the (real-world) size of the superhistory. There are also variations depending on the way that the error is estimated (between steps of superhistories, between source fission neutrons). Notwithstanding all this, it looks as if the calculational efficiency can be substantially improved in the eigenvalue problem with our approach that derives from the fixed source model.

3.2.7 Revisiting §3.2.4: Empirical adjustment of the “analog case”

We were concerned that the imposition of unity importances in the fissile zone in the “analog case” were not the best values in terms of compatibility with the ex-core importances. We note that the maximum importance value in the fissile zone in the “*DSA* case” in §3.2.4 or §3.2.6 is 23.4 (at 0°, bottom of fission zone). Instead of unity importances in the fissile zone in the “analog case”, it was of interest to raise them to a value near the maximum value of the “*DSA* case”. We chose 20. We also increased *NSRCK* to 9×10^6.

The other parameters were left the same as before (12 fission generations / step, 80 steps). Fig. 59 for this case is analogous to Fig. 58 for the case of §3.2.6. Figs. 60 and 61 compare the *DSA* case FOM_c’s to the new analog case FOM_c’s and are analogous to Figs. 19 and 20 in [1].

In this calculation, by raising the importances in the fission zone in the “analog case”, we tried to emulate the transport out to the ex-core detector of the “*DSA* case”. In particular we tried to ensure that there was not an excessive splitting between the important part of the core in this context and the first ex-core cells. However, there is now a strong RR between the rest of the core and the adjacent ex-core zones.

We firstly note that in Fig. 59 there looks to be a stronger correlation between the fission heating in the lower part of the outer fuel assembly ring around 0° and the ex-core response than is apparent in Fig. 58. Secondly, we see in Fig. 60 that the *FOM* of the ex-core response has degraded by a factor of 6 or so. The reason for this is shown in Fig. 61 where the “analog case” fundamental mode has become so unstable that the “*DSA* case” FOM_c for the fission responses is about 8 times better than the “analog case”.

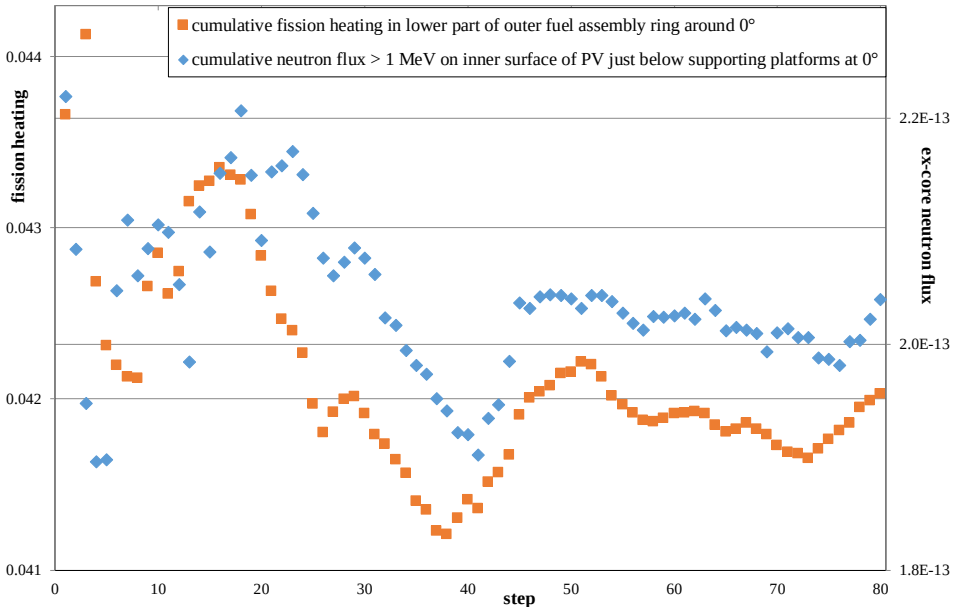

Figure 59. PWR Gen III; fast neutron flux on PV at 0° below supporting platforms: CMA's of ex-core response and fission heating in lower part of outer fuel assembly ring around 0° against number of steps (each of size 9×10^6 and length 12 superhistories / fission generations) with empirically adjusted "analog approach"

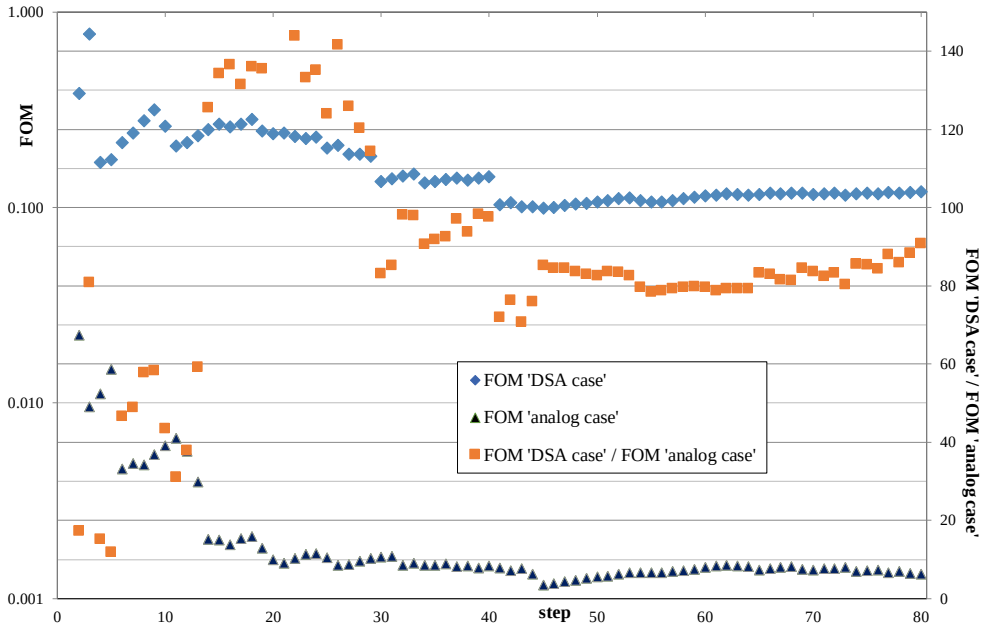

Figure 60. PWR Gen III; fast neutron flux on PV at 0° below supporting platforms: FOM's of the ex-core response for the two approaches, "DSA" (increasing no. fission neutrons passing from the fictitious to the real-world source cells) and "analog" (empirically adjusted), and their ratio

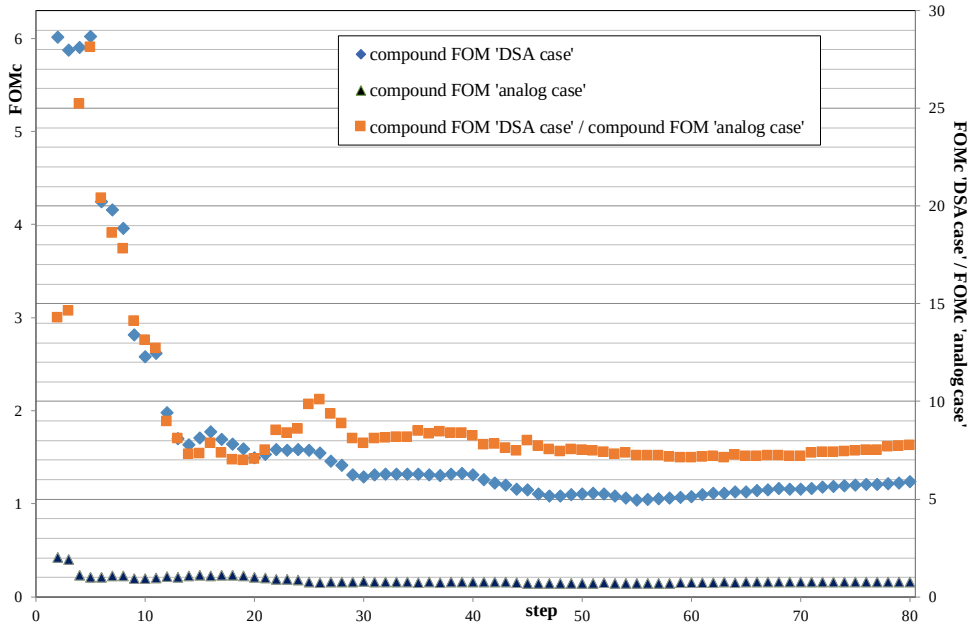

Figure 61. PWR Gen III; fast neutron flux on PV at 0° below supporting platforms: FOM$_c$'s of the 17 in-core global responses for the two approaches, "DSA" (increasing no. fission neutrons passing from the fictitious to the real-world source cells) and "analog" (empirically adjusted), and their ratio

Thus, the instability in the fundamental mode brought about by the strong RR at most of the core boundary causing a variation in the fission source in all the core including the part of the core nearest to the ex-core detector, works through to a variation in the ex-core response. We conclude that it may be difficult to improve the quality of the "analog case" by any empirical adjustment.

3.2.8 Revisiting §3.2.1: increasing the number of fission neutrons passing from the fictitious to the real-world source cells

We apply the same approach as that in §3.2.6 to the problem of §3.2.1. Following §3.2.6 we see in Table VI the ratio of the real-world source cell importances to the fictitious source cell importances at the optimum set of cell importances. In Table VI we note that there is no data below 20 keV due to the lack of fission neutrons. We see Russian roulette in most of the core with splitting only in the outer assembly ring in the highest energy group. Where there is only Russian roulette, the RR parameter does not vary much with energy. The lowest RR survival probability is 0.035 and the highest splitting is 9.0-to-1.

Again following §3.2.6 we varied the importances in all the fictitious source cells (15 spatial x 7 energy groups) by a constant multiplier. When we plotted the inverse of the quality function against the multiplier, we saw a similar curve to Fig. 56 (see Fig. 8 in [1]).

We therefore adopt the multiplication factor 1/8 as in §3.2.6 for the importances of the *FS* cells. (This means that all the parameters in Table VI are multiplied by 8 so that the highest splitting becomes 72-to-1 and the lowest RR survival probability becomes 0.28.) Then for the reasons discussed in [1], in the "*DSA* case" we employed a *NSRCK* value of 3.5×10^6 with 3 superhistories (and as usual 12 fission generations per superhistory) and in the "analog case" a *NSRCK* value of 9×10^6 and 36 superhistories. We ran 60 steps in each case under the usual conditions.

Table VI. PWR Gen III; ex-core mapping of the neutron flux (increasing no. fission neutrons passing from fictitious to real-world source cells): Ratio (>1: splitting; < 1: RR) of the real-world source cell importances to the fictitious source cell importances at the optimum (energy: across page, space: down page)

assemblies	axial range cm (zero is core mid-plane)	5 – 20 MeV	2 – 5 MeV	0.2 – 2 MeV	20 – 200 keV	1 – 20 keV
inner ring	-210.6 - -147	0.23	0.22	0.21	0.24	0.31
inner ring	-147 - -63	0.10	0.073	0.075	0.081	0.057
inner ring	-63 - +63	0.043	0.040	0.039	0.042	0.062
inner ring	+63 - +147	0.086	0.079	0.079	0.083	0.051
inner ring	+147 - +210.6	0.21	0.20	0.20	0.23	0.22
2nd & 3rd outer rings	-210.6 - -147	0.86	0.23	0.22	0.35	0.26
2nd & 3rd outer rings	-147 - -63	0.25	0.10	0.10	0.080	0.29
2nd & 3rd outer rings	-63 - +63	0.086	0.043	0.040	0.035	0.10
2nd & 3rd outer rings	+63 - +147	0.077	0.059	0.056	0.059	0.072
2nd & 3rd outer rings	+147 - +210.6	0.17	0.15	0.15	0.16	0.11
outer ring	-210.6 - -147	9.0	1.0	0.47	0.62	0.29
outer ring	-147 - -63	3.6	0.43	0.22	0.22	0.24
outer ring	-63 - +63	1.2	0.17	0.091	0.11	0.047
outer ring	+63 - +147	1.4	0.24	0.13	0.12	0.12
outer ring	+147 - +210.6	3.2	0.55	0.17	0.19	0.053

Figs. 62 and 63 are analogous to Figs. 31 and 32 of §3.2.1. In Figs. 62 and 63 there looks to be less correlation between the ex-core flux and the outer core fission heating compared with Figs. 31 and 32.

The running values over the 60 steps of the FOM_c's of the three response groups A, B and C and of the 15 in-core fission responses, are reported in [1]. We see in [1] that the FOM_c ratios "*DSA* case" / "analog case" have all increased by around a factor of 2. This means that now the group C tallies have nearly twice the efficiency with the *DSA* parameters in-core compared with the analog parameters, but the groups A and B tallies still have ratios < 1, as have also of course the 15 in-core tallies. These results are illustrated in Fig. 64. There is further discussion in [1] as to how to further improve the results of the "*DSA* case".

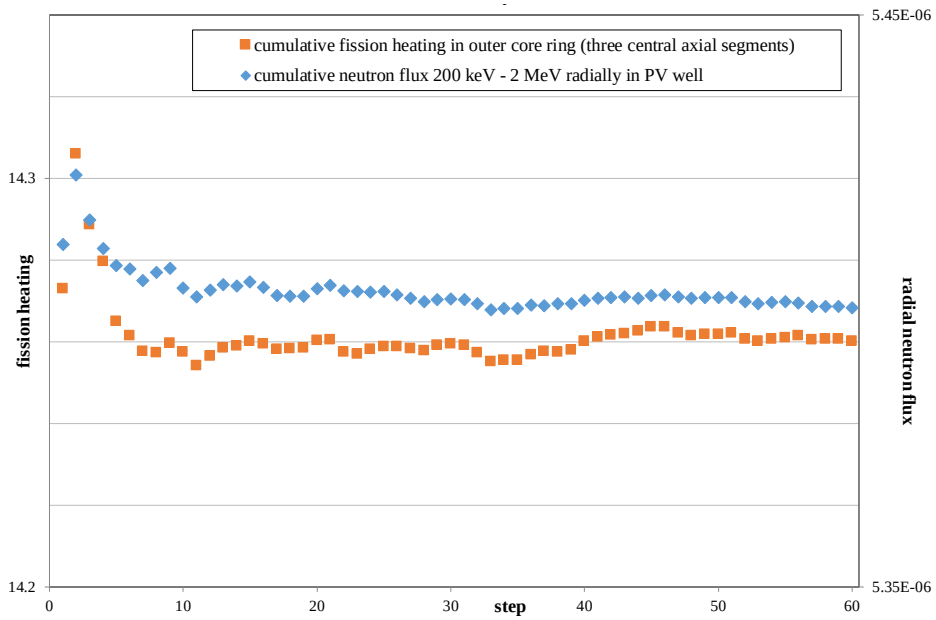

Figure 62. PWR Gen III; ex-core mapping of the neutron flux (increasing no. fission neutrons passing from fictitious to real-world source cells): CMA's of radial flux (0.2 – 2 MeV) and fission heating in outer fuel assembly ring against number of steps (each of size 3.5×10^6 and length 3 superhistories = 36 fission generations) with "DSA approach"

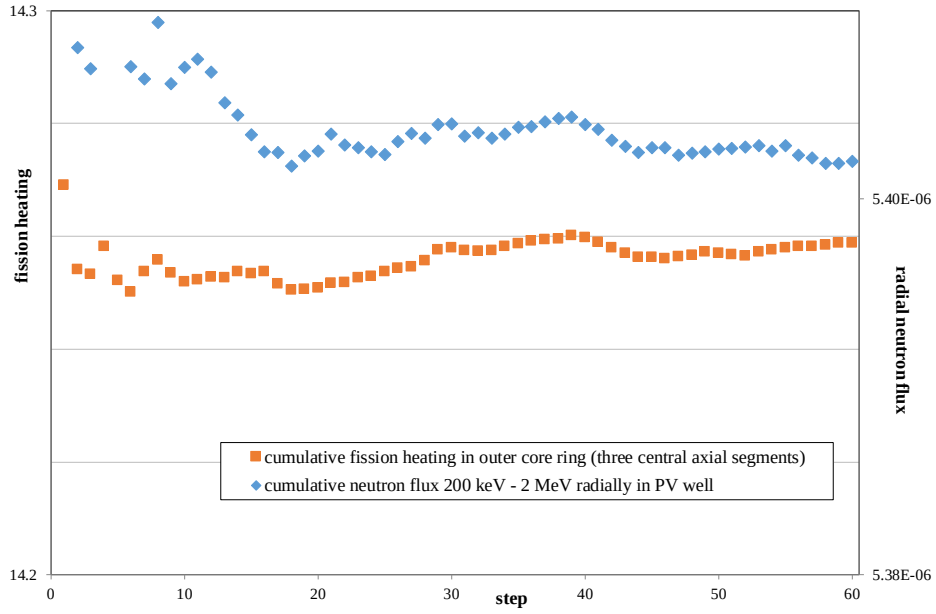

Figure 63. PWR Gen III; ex-core mapping of the neutron flux (increasing no. fission neutrons passing from fictitious to real-world source cells): CMA's of radial flux (0.2 – 2 MeV) and fission heating in outer fuel assembly ring against number of steps (each of size 9×10^6 and length 36 superhistories / fission generations) with "analog approach"

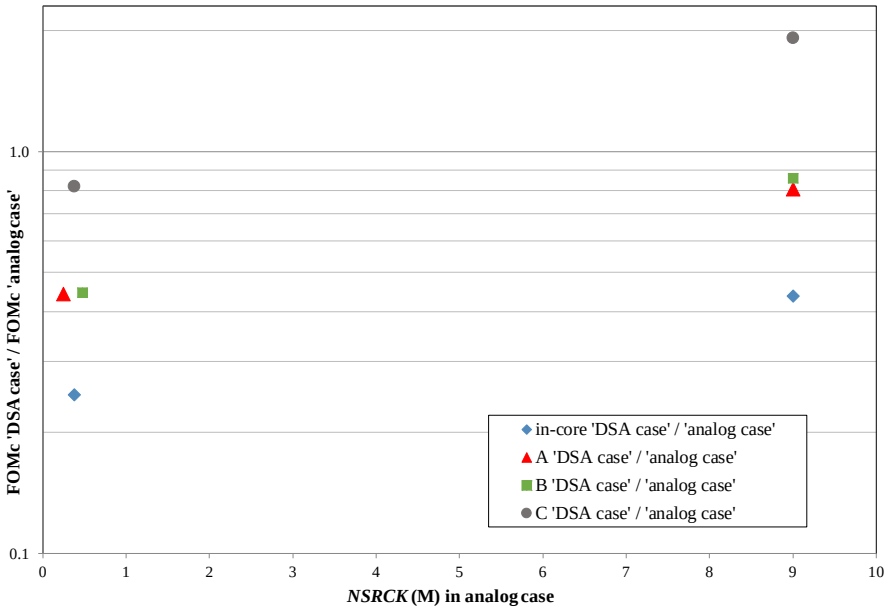

Figure 64. PWR Gen III; ex-core mapping of the neutron flux: final FOM_c ratios of the two approaches, "DSA" and "analog", for the 15 in-core global responses and the three groups of local ex-core responses for the results in §3.2.1 and in this section

3.2.9 Remarks on the PWR GEN III with Thick Steel Reflector problems

In §3.2.1 we saw that for a range of neutron responses in and below the PV well, the empirical, analog approach was better than the *DSA* approach. This was the case even for neutron responses in the basemat of the PV well which are at quite deep penetration (Fig. 29).

We then looked at a fast neutron response nearer the core that is "seen" by only a limited axial portion of the core. The response was the flux > 1 MeV on the inner surface of the PV. In §3.2.2 the response was at the level of the bottom of the fission zone on 360°, in §3.2.3 it was below the supporting platforms, again on 360° and in §3.2.4 it was below the supporting platforms but subtended by an azimuthal angle of ±2.4°. The ex-core penetration substantially increases going from §3.2.2 to §3.2.4.

In §3.2.2 the benefit of playing *VR* in the core looked marginal. In §3.2.3 instead a factor of just over 3 was obtained in the *FOM* of the fast neutron response (that is, in inverse proportion to the computer time) and in §3.2.4 such factor was around 4. In all three cases neither the *FOM*'s nor the *FOM* ratio "*DSA* case" to "analog case" were particularly stable. Furthermore, the size of each superhistory *NSRCK* was not the same between §3.2.3 and §3.2.4 (and even if the size were the same, the presence of fictitious source cells means that the number of neutrons entering the real-world source cells varies). Notwithstanding, these *caveats*, we believe there to be a signal here and the ratio of the *FOM*'s *DSA* / analog is increasing.

The reason that the results in §3.2.1 - §3.2.4 were poorer than expected was suspected to be that too few fission neutrons were entering the real-world source cells from the fictitious source cells. In §3.2.5 we tested the first of two hypotheses that might explain why our approach produced this result. This was that the number of fission generations in the phase of generating the *VR* parameters was not sufficient. Increasing this number did indeed firstly double and then sextuple the number of fission neutrons entering the real-world source cells from the fictitious source cells. However, this was at the expense of the quality of the calculation as determined by the size of each superhistory and the results obtained when running with the resultant *VR* parameters were

not much improved.

The second of the two hypotheses was that a basic assumption of the *DSA* approach (its fixed source nature) broke down in the eigenvalue case and this was responsible for the lack of fission neutrons. A work-around was made that did not involve any empiricism which was tested in §3.2.6. Now we saw a definite improvement in the results of the "*DSA* approach", with a substantial gain over the "analog approach" in the ex-core result.

A *caveat* might be attached to the results in §3.2.6: the step size of 12 fission generations was rather small and some correlations between steps may be present. Such correlations will probably be greater in the "*DSA* case" compared to the "analog case". It will be seen in §3.4 that these correlations are in fact rather small.

In §3.2.7 an attempt to empirically improve the "analog approach" in §3.2.4 came to nothing.

In §3.2.8 we employed the same reasoning to the problem of §3.2.1 that we applied in §3.2.6 to the problem of §3.2.4. The results looked consistent with those of §3.2.6 although the improvement was less. It looks useful to search empirically for further improvement through the size of the superhistory and by altering the *VR* parameters in the *FS* cells. An analytic effort might well be helpful here.

3.3 IN-CORE CONFIGURATION: NEUTRON FLUX AND RESPONSE AT CONTROL ROD SURFACE

Concerning in-core responses, we test the technique firstly on a single assembly model (work in [17] prompted this analysis), then a full-core model of the VERA (Virtual Environment for Reactor Applications) computational benchmark [18].

3.3.1 Assembly in infinite lattice

The neutron flux crossing the lower surface of a single control rod (CR) in an assembly in an infinite lattice is evaluated. The enrichment of the fuel is 2.619%. The CR's, occupying all the guide tube positions apart from the central one, are assumed to be composed of AIC (Ag-In-Cd) along all their length and are nearly totally inserted (~90% in). Fig. 65 shows a vertical cross-section of the assembly and Fig. 66 shows horizontal cross-sections above and below the lower surface of the CR.

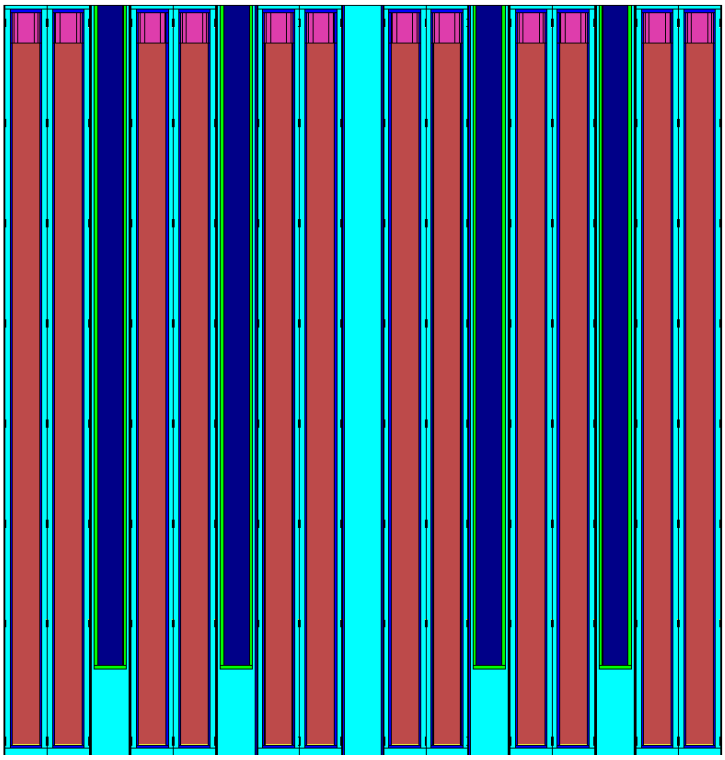

Figure 65. VERA assembly in an infinite lattice: vertical cross-section with CR's ~90% in (scale: vertical 391.5 cm; horizontal 21.5 cm)

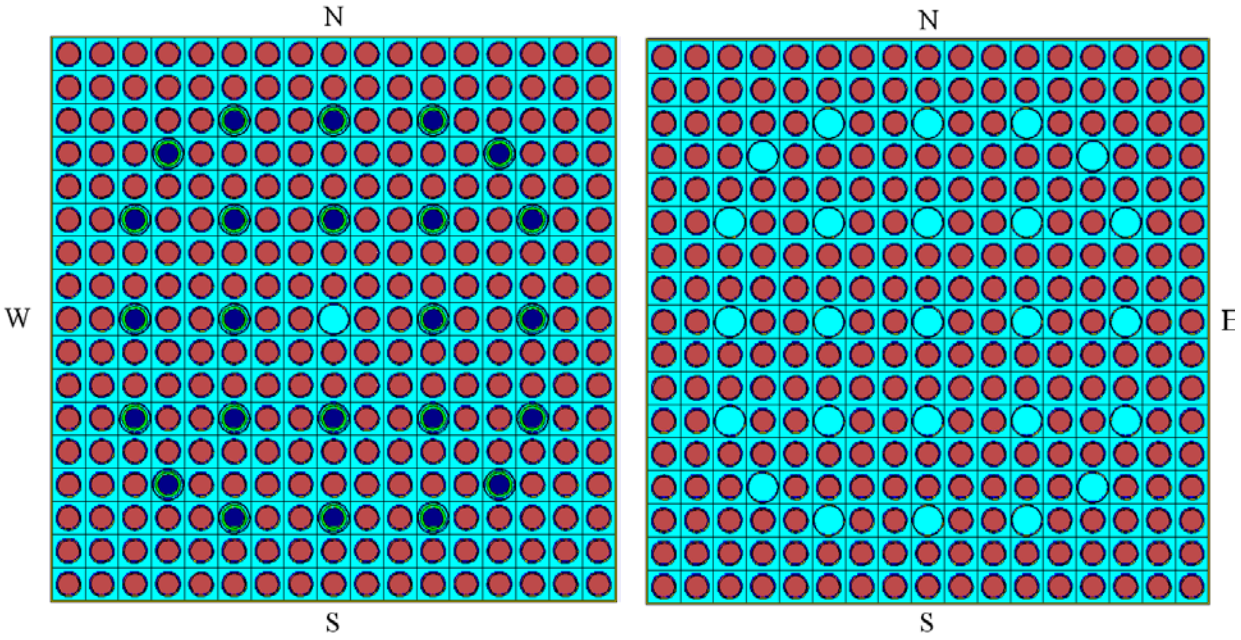

Figure 66. VERA assembly horizontal cross-section, above (left), below (right) CR lower surface (scale: vertical, horizontal 21.5 cm)

The total neutron flux at the lower surface of the single CR at position [6 0] in Fig. 66 was the "local" tally-of-interest. There were 10 "global" fission responses along the length of the assembly whose role is to hold the fundamental mode steady. These were chosen as fission heating responses (type 7 MCNP tallies). Both radial and axial *VR* was employed with 6 energy groups with upper limits: 1 eV, 1 keV, 200 keV, 2 MeV, 5 MeV and 20 MeV. Superhistories of 10 fission generations were employed without *FS* cells.

Estimating statistical errors between superhistories, the optimum space/energy importances provided a gain of close to 2.5 in the FOM_c over analog. Note that the gain in the *FOM* of the local response and in the FOM_c (that of the combined local response and the 10 global responses) over analog were similar.

3.3.2 Assembly in a reactor core

An assembly like that of the first problem but with a fuel enrichment of 2.11% and with the CR's in the nearly-out position (~11% in – see Fig. 67) is placed in a full core (see Fig. 68) with all the other assemblies having all 25 guide tube positions empty (i.e. without Pyrex burnable neutron absorber rods, just with water). The assemblies have three different enrichments: 2.11, 2.619 and 3.1% as shown in Fig. 69.

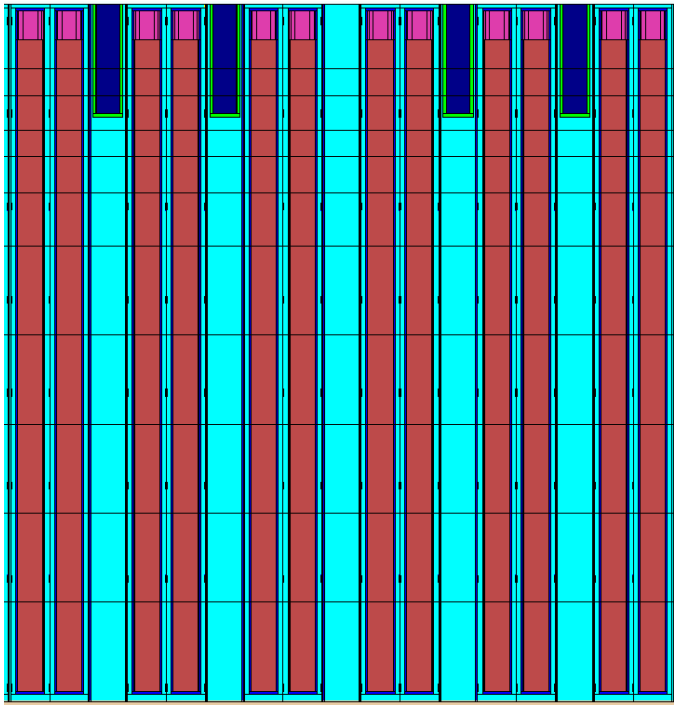

Figure 67. VERA assembly in whole core: vertical cross-section with CR's ~11% in (scale: vertical 391.5 cm; horizontal 21.5 cm)

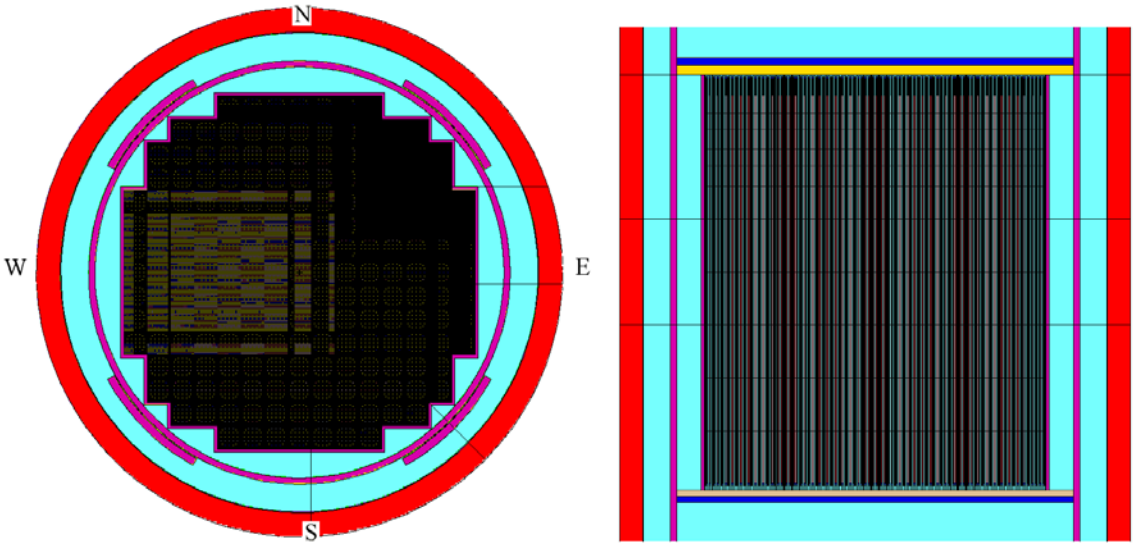

Figure 68. VERA full core horizontal (left) and vertical (right) cross-sections

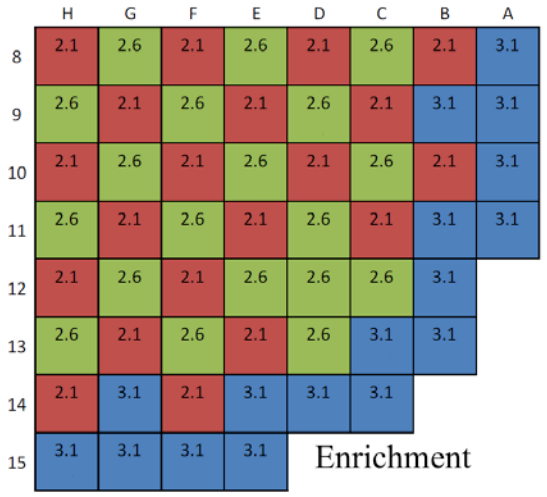

Figure 69. VERA core assembly configuration (from Fig. 9 of [18]) (1/4 core, 1/8 core symmetry)

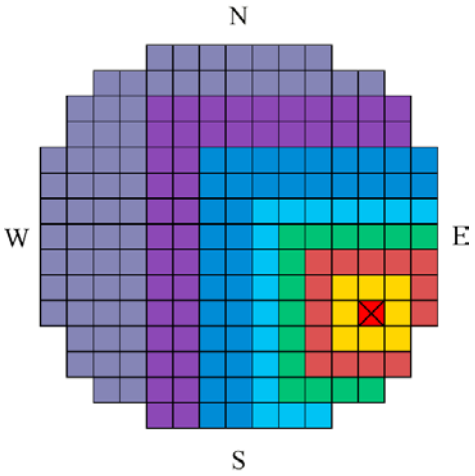

Figure 70. VERA core: assembly containing the tally-of-interest and radial VR division

The tally-of-interest was the total neutron flux crossing the lower surface of the single CR in Fig. 66 at position [3 -6] in the assembly that is at position [5 -3]. This assembly is shown in Fig. 70 together with the 8 radial *VR* subdivisions. The same radial division was employed to create the global fission heating responses in the core. Instead, the axial divisions were different for the global response definition and for *VR*: there were 11 axial sub-divisions for the global responses making a total of 11×8=88 global responses and 7 axial sub-divisions for *VR* making a total of 7×8=56 core cells for *VR*. 6 energy groups were again used with the same upper limits. A superhistory length of 10 fission generations was employed again without *FS* cells. These 10 generations were divided into 5 sub-groups with different *VR* in each sub-group.

The results again with statistical errors estimated between superhistories are summarized in Table VII. The subscript *an* denotes analog. As usual the analog run had a superhistory of 1 fission generation.

Table VII. VERA full core: Results for neutron flux at lower surface of a single control rod

Run	*CTM* min	*NSRCK*(M) **KCT*	Φ_n (unnormalized) at lower surface of CR (*fsd*)	*FOM*	*FOM* / FOM_{an}	FOM_c (89 responses)	FOM_c / $FOM_{c,an}$
analog	230814	2*3500	3.90E-7 (0.0385)	0.00292	1	0.265	1
VR	348884	2*1000	3.99E-7 (0.0045)	0.142	48.4	5.55	20.9

We note that as expected the gain over analog is substantially higher than the gain for the assembly in an infinite lattice. (The CR's are at opposite positions in the two cases: if anything, the gain might be higher in the full core case with the CR's in the "nearly down" position.) Here it may be remarked that for a PWR design similar to that in §3.2 (PWR GEN III), the fission heating in a 8 cm length of a single pin was calculated with a factor of 80 gain over analog with the same *VR* parameters in the 10 fission generations of a superhistory [2]. Varying the *VR* over the fission generations gave a further factor of approximately 2. A factor that may account for the difference

in gain between ~50 here and ~160 previously is as follows:

> Here we are optimizing to 1 local response and 88 "global" responses that cover the core and mock-up the fundamental mode. In [2] the single local response was accompanied by 16 "global" responses. It is probable that 88 is too many, indeed the difference in gain-over-analog between *FOM* of only the local response (gain 48) and FOM_c of all the responses (gain 21) implies that too much work is being expended on the global responses. Reducing this number could improve the quality of the local response (and if the global responses are too few, this will appear in the variance of the local response).

3.3.3 Assembly in a reactor core with a ^{96}Zr(n,γ) response

Now we take the problem of §3.3.2 and add a ^{96}Zr(n,γ) response function at the lower surface of the CR in question. (This was inspired by an earlier attempt to calculate the same response in a wire in the core of a WWRSM–type research reactor [19].)

For this problem we employed a superhistory of 10 fission generations and 5 fission generation sub-groups with different *VR* in each sub-group (as before) and included *FS* cells. In contrast to the problem of §3.2.2, the global fission heating responses in the core were defined as identical to the *VR* cells, thus 56 global responses. Further details are given in [1].

A summary of the results with statistics estimated between superhistories is shown in Table I in [1]. We see there that the analog result for the total flux *FOM* has a value of 0.00148 which is roughly ½ that in Table VII. Presumably this is due to the different time taken in this problem (for example due to the added ^{96}Zr(n,γ) reaction rate). Furthermore the number of fission generations is a factor of 7 greater. (Under ideal conditions *FOM* and FOM_c should not depend on the length of the calculation, in practice these rarely obtain.)

In [1] the error was then estimated in a similar fashion to what was done in §3.1 (from Table III onwards) and §3.2. That is, a calculation was run over a relatively large number of fission generations, splitting it into a number of steps. The fundamental mode, written at the end of a step is used as source for the subsequent step. Each step consisted of 800 fission generations and is assumed independent of the previous step (again, this assumption is examined in §3.4). Results after 36 steps are shown in Table II in [1].

The results with statistics calculated between steps in Table II in [1] are reasonably consistent with those calculated between superhistories in Table I in [1].

The running values of the *FOM's* of the total flux at the lower surface of the CR and their ratio over the 36 steps for the two cases (shist=10 with *VR* and shist=1 analog) are shown in [1]. In Fig. 71 is shown the *FOM* for the ^{96}Zr(n,γ) rate at the lower surface of the CR for the case: shist=10 with *VR*. In the last two thirds of the problem we see a "saw tooth" effect, that is however small. Finally in Fig. 72 we see the FOM_c*'s* of the 56 global fission responses for the two cases and their ratio. We see that the FOM_c of the case: shist=10 with *VR* is reasonably constant and the analog case, although having a higher FOM_c, actually exhibits a greater variation.

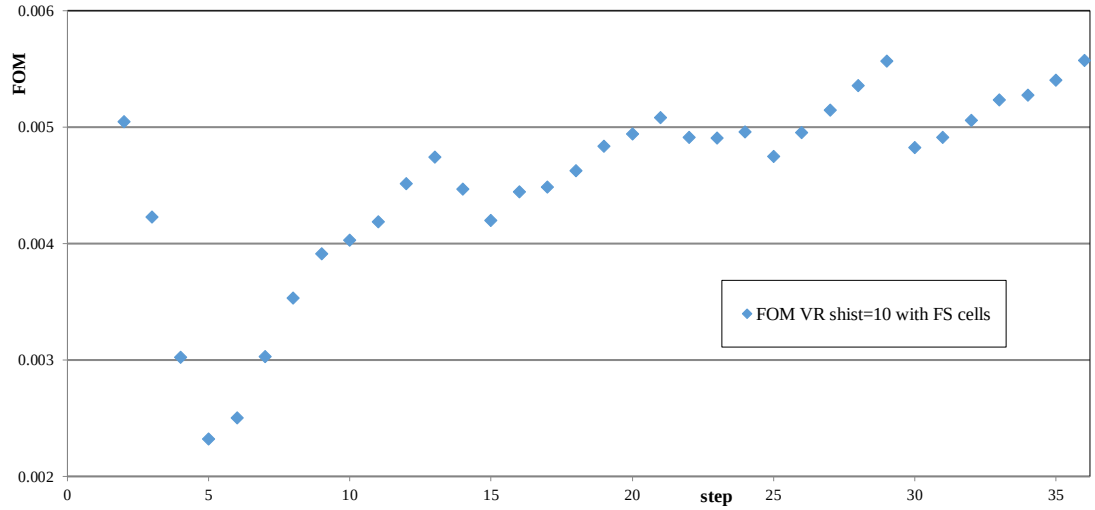

Figure 71. VERA full core with ^{96}Zr(n,γ) response: ^{96}Zr(n,γ) rate at lower surface of CR; FOM

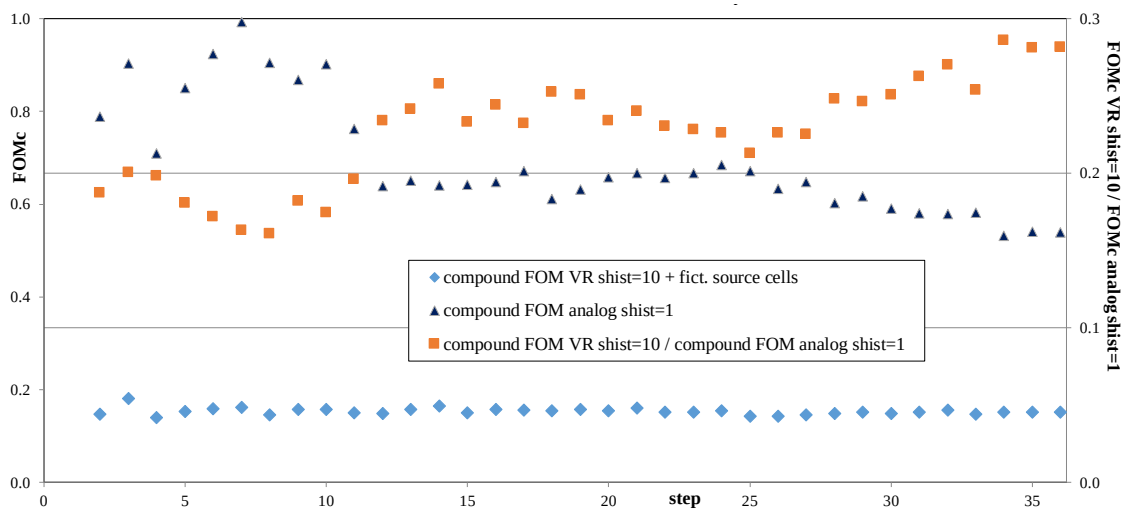

Figure 72. VERA full core with ^{96}Zr(n,γ) response: 56 global fission responses; FOM$_c$'s for the two approaches and their ratio

3.3.4 Remarks on the VERA problems

We saw a progressive gain in the calculational efficiency over analog moving from a single CR in an infinite lattice to a full core, and then with the addition of a ^{96}Zr(n,γ) reaction rate (although the first two cases did not employ *FS* cells whilst the third case did). Full results for the full core case with ^{96}Zr(n,γ) are in [1].

The gains in the full core case with the ^{96}Zr(n,γ) reaction rate were verified by both calculating the error between superhistories (of 1 and 10 fission generations) and between batches of superhistories (each batch made up of 800 fission generations).

3.4 INDEPENDENCE BETWEEN STEPS IN SELECTED PROBLEMS IN §3.1, §3.2 AND §3.3

We have mentioned two kinds of correlations in the discussion of the test problems: that between

the nearest part of the fissile configuration and the ex-core response (for example between the fission heating in the lower, outer part of the core and the fast neutron flux on the lower part of the PV in Fig. 35) and that between successive individual steps of the same long calculation. Here we consider the latter.

We have assumed the steps to be independent so as to be able to generate confidence intervals and quantify possible gains of the *DSA* over other approaches. So far, our only handle on this assumption has been to observe the fluctuation of some responses over the steps. Thus, for example in Fig. 23 we inferred that the steps are not independent of one another and we increased the number of fission generations in each step so that in Fig. 26 the steps were assumed to be independent.

Here we take a more quantitative approach and follow the standard procedure of grouping the steps into batches and evaluating the error assuming that successive batches of steps are independent of one another. This is identical to what is done in MCNP [20]. Following [20] we adopt the same yardstick of an increase of 30% in the standard deviation as an indication of too much correlation between steps. We also bear in mind that we need a large enough sample of batches of steps - the recommendation in [20] is at least 30. (As we have a total of only between 36 and 80 steps depending on the problem, this constraint is easily broken.)

Tables VIII and IX show the *fsd*'s and the *fsd*'s normalized to the *fsd* of 1 step/batch respectively for selected test problems and between 1 and 5 steps per batch. In these tables the number of batches are in brackets. Also "*NSRCK* of equivalent analog case" is the starting number of fission neutrons in the "analog case" that takes approximately the same CPU time as the "*DSA* case". Therefore, in both cases it is approximately the effective number of fission neutrons entering the real-world source cells in each superhistory.

In these tables most of the results have been presented previously. Exceptions are the 5^{th} and 6^{th} rows which are for one of the ex-core tallies in group C (below the central part of the basemat in Fig. 29). Also, the last and penultimate rows are presented as *FOM's* in Fig. 27 in [1]. In Table IX following [20] we have highlighted values > 1.30.

We see from Table IX, that as suspected from the behavior of Figs. 23 and 24, indeed 50 fission generations per step was not sufficient. Instead, 500 was sufficient. We also see that in general the "analog case" tends to have less correlations than the "*DSA* case". As expected, the more fission generations per step, the lower the correlations between steps. Also, the larger the effective number of neutrons entering the real-world source cells, the lower are the correlations between steps. The ex-core response in §3.2.1 and §3.2.8 differs from the other responses in §3.2 in that the whole external part of the core can contribute to it, and not just a limited axial and/or azimuthal part. Therefore, one would expect the *VR* parameters not to produce the correlations between steps that are more apparent in §3.2.3, §3.2.4, §3.2.5 and §3.2.6. Whilst this is the case for §3.2.1, for §3.2.8 it is not necessarily so, at least at 4 and 5 steps per batch. The principal *caveat* here is that, as previously mentioned, the number of batches becomes very low, especially at 4 and 5 steps per batch.

However, the main conclusion is that the "*DSA* case" results in both §3.2.6 and §3.3.3 do not show great step-to-step correlations. Thus, the gains reported in the PWR GEN III and VERA problems are not invalidated.

Table VIII. Examination of the assumption of independence between steps: fsd's (no. batches) of selected problems with statistics between batches of between 1 and 5 steps per batch

			Steps per batch:				
problem	Fission generations / step	*NSRCK* of equivalent analog case	1	2	3	4	5
§3.1.4; Fig. 23; dose	50	3.5×10^5	0.0065 (60)	0.0088 (30)	0.0104 (20)	0.0124 (15)	0.0130 (12)
§3.1.4; Fig. 24; dose	50	3.5×10^5	0.0079 (60)	0.0091 (30)	0.0104 (20)	0.0097 (15)	0.0096 (12)
§3.1.4; Fig. 26; dose	500	3.5×10^5	0.0027 (60)	0.0028 (30)	0.0026 (20)	0.0028 (15)	0.0027 (12)
§3.1.4; Fig. 27; dose	500	3.5×10^5	0.0032 (60)	0.0031 (30)	0.0034 (20)	0.0036 (15)	0.0032 (12)
§3.2.1; $\Phi_n(10 - 5\times10^5$ eV)[1]	144	3.75×10^5	0.0049 (40)	0.0050 (20)		0.0049 (10)	0.0020 (8)
§3.2.1; $\Phi_n(10 - 5\times10^5$ eV)[2]	144	3.75×10^5	0.0049 (40)	0.0052 (20)		0.0028 (10)	0.0052 (8)
§3.2.2; Fig. 35; Φ_n(ex-core)	120	3×10^5	0.0048 (60)	0.0052 (30)	0.0059 (20)	0.0054 (15)	0.0060 (12)
§3.2.2; Fig. 36; Φ_n(ex-core)	120	3×10^5	0.0048 (60)	0.0056 (30)	0.0050 (20)	0.0046 (15)	0.0054 (12)
§3.2.3; Fig. 40; Φ_n(ex-core)	96	2.3×10^5	0.0084 (60)	0.0096 (30)	0.0109 (20)	0.0116 (15)	0.0129 (12)
§3.2.3; Fig. 41; Φ_n(ex-core)	96	2.3×10^5	0.0151 (60)	0.0132 (30)	0.0140 (20)	0.0145 (15)	0.0150 (12)
§3.2.4; Fig. 45; Φ_n(ex-core)	96	2.6×10^5	0.0164 (60)	0.0197 (30)	0.0211 (20)	0.0228 (15)	0.0245 (12)
§3.2.4; Fig. 46; Φ_n(ex-core)	96	2.6×10^5	0.0338 (60)	0.0321 (30)	0.0408 (20)	0.0309 (15)	0.0406 (12)
§3.2.5; Fig. 47; Φ_n(ex-core)	48	5.65×10^5	0.0106 (80)	0.0129 (40)		0.0159 (20)	0.0178 (16)
§3.2.5; Fig. 48; Φ_n(ex-core)	48	5.65×10^5	0.0244 (80)	0.0238 (40)		0.0230 (20)	0.0222 (16)
§3.2.5; Fig. 51; Φ_n(ex-core)	36	1.55×10^6	0.0098 (60)	0.0108 (30)	0.0121 (20)	0.0132 (15)	0.0139 (12)
§3.2.5; Fig. 52; Φ_n(ex-core)	36	1.55×10^6	0.0191 (60)	0.0183 (30)	0.0213 (20)	0.0234 (15)	0.0245 (12)
§3.2.6; Fig. 57; Φ_n(ex-core)	12	2.08×10^6	0.0089 (80)	0.0103 (40)		0.0102 (20)	0.0105 (16)
§3.2.6; Fig. 58; Φ_n(ex-core)	12	2.08×10^6	0.0346 (80)	0.0344 (40)		0.0280 (20)	0.0337 (16)
§3.2.8; $\Phi_n(10 - 5\times10^5$ eV)[1]	36	9×10^6	0.0013 (60)	0.0014 (30)	0.0015 (20)	0.0018 (15)	0.0018 (12)
§3.2.8; $\Phi_n(10 - 5\times10^5$ eV)[2]	36	9×10^6	0.0019 (60)	0.0020 (30)	0.0020 (20)	0.0014 (15)	0.0017 (12)
§3.2.8; $\Phi_n(10 - 5\times10^5$ eV)[1]	12	23.143×10^6	0.0016 (60)	0.0017 (30)	0.0019 (20)	0.0021 (15)	0.0022 (12)
§3.3.3; [1], Fig. 27; Φ_n(in-core)[3]	800	2×10^5	0.0074 (36)	0.0077 (18)		0.0075 (9)	
§3.3.3; [1]. Fig. 27; Φ_n(in-core)[4]	800	2×10^5	0.0452 (36)	0.0392 (18)		0.0278 (9)	

[1]: flux between 10 eV and 500 keV; lowest tally in central part of basemat (part of group C responses, see Fig. 29), "*VR* case" (superhistory of 12 fission generations)

[2]: flux between 10 eV and 500 keV; lowest tally in central part of basemat (part of group C responses, see Fig. 29), "analog case" (superhistory of 1 fission generation)

[3]: total flux at lower surface of CR in VERA, "*VR* case" (superhistory of 10 fission generations)

[4]: total flux at lower surface of CR in VERA, "analog case" (superhistory of 1 fission generation)

Table IX. Examination of the assumption of independence between steps: fsd's normalized to the fsd of 1 step/batch (no. batches) of selected problems with statistics between batches of between 1 and 5 steps per batch

			Steps per batch:				
problem	Fission generations / step	*NSRCK* of equivalent analog case	1	2	3	4	5
§3.1.4; Fig. 23; dose	50	3.5×10^5	1 (60)	1.36 (30)	1.61 (20)	1.92 (15)	2.01 (12)
§3.1.4; Fig. 24; dose	50	3.5×10^5	1 (60)	1.15 (30)	1.33 (20)	1.42 (15)	1.40 (12)
§3.1.4; Fig. 26; dose	500	3.5×10^5	1 (60)	1.05 (30)	0.98 (20)	1.03 (15)	1.00 (12)
§3.1.4; Fig. 27; dose	500	3.5×10^5	1 (60)	0.96 (30)	1.08 (20)	1.13 (15)	1.00 (12)
§3.2.1; $\Phi_n(10 - 5\times10^5$ eV)[1]	144	3.75×10^5	1 (40)	1.04 (20)		1.00 (10)	0.42 (8)
§3.2.1; $\Phi_n(10 - 5\times10^5$ eV)[2]	144	3.75×10^5	1 (40)	1.06 (20)		0.56 (10)	1.06 (8)
§3.2.2; Fig. 35; Φ_n(ex-core)	120	3×10^5	1 (60)	1.09 (30)	1.24 (20)	1.13 (15)	1.26 (12)
§3.2.2; Fig. 36; Φ_n(ex-core)	120	3×10^5	1 (60)	1.17 (30)	1.04 (20)	0.95 (15)	1.13 (12)
§3.2.3; Fig. 40; Φ_n(ex-core)	96	2.3×10^5	1 (60)	1.15 (30)	1.30 (20)	1.39 (15)	1.55 (12)
§3.2.3; Fig. 41; Φ_n(ex-core)	96	2.3×10^5	1 (60)	0.87 (30)	0.93 (20)	0.97 (15)	1.00 (12)
§3.2.4; Fig. 45; Φ_n(ex-core)	96	2.6×10^5	1 (60)	1.20 (30)	1.29 (20)	1.39 (15)	1.49 (12)
§3.2.4; Fig. 46; Φ_n(ex-core)	96	2.6×10^5	1 (60)	0.95 (30)	1.21 (20)	0.91 (15)	1.20 (12)
§3.2.5; Fig. 47; Φ_n(ex-core)	48	5.65×10^5	1 (80)	1.21 (40)		1.50 (20)	1.67 (16)
§3.2.5; Fig. 48; Φ_n(ex-core)	48	5.65×10^5	1 (80)	0.98 (40)		0.95 (20)	0.91 (16)
§3.2.5; Fig. 51; Φ_n(ex-core)	36	1.55×10^6	1 (60)	1.10 (30)	1.23 (20)	1.34 (15)	1.42 (12)
§3.2.5; Fig. 52; Φ_n(ex-core)	36	1.55×10^6	1 (60)	0.96 (30)	1.11 (20)	1.22 (15)	1.28 (12)
§3.2.6; Fig. 57; Φ_n(ex-core)	12	2.08×10^6	1 (80)	1.16 (40)		1.14 (20)	1.18 (16)
§3.2.6; Fig. 58; Φ_n(ex-core)	12	2.08×10^6	1 (80)	0.99 (40)		0.81 (20)	0.97 (16)
§3.2.8; $\Phi_n(10 - 5\times10^5$ eV)[1]	36	9×10^6	1 (60)	1.13 (30)	1.14 (20)	1.41 (15)	1.42 (12)
§3.2.8; $\Phi_n(10 - 5\times10^5$ eV)[2]	36	9×10^6	1 (60)	1.06 (30)	1.04 (20)	0.71 (15)	0.88 (12)
§3.2.8; $\Phi_n(10 - 5\times10^5$ eV)[1]	12	23.143×10^6	1 (60)	1.06 (30)	1.19 (20)	1.31 (15)	1.39 (12)
§3.3.3; [1], Fig. 27; Φ_n(in-core)[3]	800	2×10^5	1 (36)	1.03 (18)		1.00 (9)	
§3.3.3; [1]. Fig. 27; Φ_n(in-core)[4]	800	2×10^5	1 (36)	0.87 (18)		0.62 (9)	

[1]: flux between 10 eV and 500 keV; lowest tally in central part of basemat (part of group C responses, see Fig. 29), "*VR* case" (superhistory of 12 fission generations)

[2]: flux between 10 eV and 500 keV; lowest tally in central part of basemat (part of group C responses, see Fig. 29), "analog case" (superhistory of 1 fission generation)

[3]: total flux at lower surface of CR in VERA, "*VR* case" (superhistory of 10 fission generations)

[4]: total flux at lower surface of CR in VERA, "analog case" (superhistory of 1 fission generation)

4. CONCLUDING REMARKS

This report has provided support to an external paper [1] that contains the main discussion and results. The support includes:

- an expansion of the methodology including an illustration of fictitious source cells;
- an additional set of “ex-core” test problems involving a flooded spent fuel transport flask;
- cumulative moving averages (*CMA*’s) of selected local and global responses in the ex-core test problems that primarily allow a qualitative idea of the correlations between in- and ex-core responses (and to a lesser extent allow some idea of step-to-step correlations);
- §3.4 that gives a more quantitative estimate of step-to-step correlations of selected ex-core responses in the ex-core problems in §3.1 and §3.2 and an in-core response in the in-core problem in §3.3.

The *CMA*’s provided a handle into an understanding of the reason for the underperformance of the *DSA* technique in some standard ex-core configurations. Essentially this was that too much effort was spent ex-core and not enough in-core. There followed a way to, at least partially, solve this problem.

Notwithstanding this work-around, many responses in the PV well of a GEN III PWR remain more easily solved with a simple empirical approach. Only at some optical distance outside the PV well does this cease to be the case. Instead, some very localized responses on the PV below the core contain features that cause their calculation with the *DSA* to exhibit at least an order of magnitude improvement in efficiency over the empirical approach. This improvement is accentuated when moving to localized responses within the core.

In [1] areas of further analytical study are indicated.

ACKNOWLEDGMENTS

Dr. Hao Li of the Dept. of Engineering Physics, Tsinghua University, Beijing, China, suggested the VERA single assembly problem and provided the MCNP input deck.

The computing resources and the related technical support used for this work have been provided by CRESCO/ENEAGRID High Performance Computing infrastructure and its staff. CRESCO/ENEAGRID High Performance Computing infrastructure is funded by ENEA, the Italian National Agency for New Technologies, Energy and Sustainable Economic Development and by Italian and European research programmes, see http://www.cresco.enea.it/english for information.

Dedication

This paper is dedicated to the memory of Arie Dubi (1944–2015), the originator of the *DSA* and a pioneering Monte-Carlo developer.

REFERENCES

1. M. Brovchenko, K.W. Burn, P. Console Camprini "On Integrating Monte-Carlo Calculations in and around Near-Critical Configurations – I. Methodology," submitted to *Ann. Nucl. Energy* (2021)
2. K.W. Burn, "Optimizing variance reduction in Monte Carlo eigenvalue calculations that employ the source iteration approach," *Ann. Nucl. Energy*, **73**, pp. 218–240 (2014)
3. K.W. Burn, "A correction and a clarification to 'Optimizing variance reduction in Monte Carlo eigenvalue calculations that employ the source iteration approach'," *Ann. Nucl. Energy*, **85**, pp. 776–777 (2015)
4. K.W. Burn, "Estimating Local In- and Ex-Core Responses within Monte Carlo Source Iteration Eigenvalue Calculations," *Proceedings of PHYSOR-2014*, Kyoto, Sept. 28 – Oct. 3, 2014, JAEA-Conf 2014-003 paper no. 1228305 (2014)
5. Denise B. Pelowitz (Ed.), "MCNP6™ User's Manual – Version 1.0", Los Alamos National Laboratory, LA-CP-13-00634, Rev. 0 (2013)
6. R.J. Brissenden and A.R. Garlick, "Biases in the Estimation of Keff and Its Error by Monte Carlo Methods," *Ann. Nucl. Energy* **13**(2), pp. 63–83 (1986)
7. K.W. Burn and P. Console Camprini, "Radiation transport out from the reactor core: to decouple or not to decouple," *Proceedings of the ICRS-13*, Paris, Oct. 3–6, 2016, EPJ Web of Conferences **153**, 05007 (2017)
8. K.W. Burn and P. Console Camprini, "A Consistent Monte Carlo Treatment of Radiation Responses in and around Critical Configurations," *Proceedings of PHYSOR-2018*, Cancun, April 22 – 26, pp. 576–586 (2018)
9. K. W. Burn, "Optimizing Monte Carlo to Multiple Responses: the Direct Statistical Approach, 10 Years On," *Nucl. Technol.* **175**, pp.138–145 (2011)
10. T. E. Booth and K. W. Burn, "Some Sample Problem Comparisons Between the DSA Cell Model and the Quasi–Deterministic Method," *Ann. nucl. Energy* **20–11** 733 (1993)
11. R. von Mises and H. Pollaczek-Geiringer, "Praktische Verfahren der Gleichungsauflösung," *ZAMM - Zeitschrift für Angewandte Mathematik und Mechanik*, **9**, pp. 152–164 (1929)
12. J. Lieberoth, "A Monte Carlo Technique to Solve the Static Eigenvalue Problem of the Boltzmann Transport Equation," *Nukleonik* **11**, pp. 213–219 (1968)
13. K. W. Burn, "Extending the Direct Statistical Approach to Include Particle Bifurcation between the Splitting Surfaces," *Nucl. Sci. Eng.*, **119**, 44 (1995)
14. K. W. Burn, "A New Weight–Dependent DSA Model," *Nucl. Sci. Eng.*, **125**, 128 (1997)
15. T. E. Booth, "Genesis of the Weight Window and the Weight Window Generator in MCNP – A Personal History," LA-UR-06-5807, Los Alamos National Laboratory (2006)
16. K.W. Burn, "Complete Optimization of Space/Energy Cell Importances with the DSA Cell Importance Model," *Ann. Nucl. Energy*, **19**–**2**, 65 (1992)
17. Hao Li, Ganglin Yu, Shanfang Huang, Gang Wang and Kan Wang, "Mathematics Derivation of the Adjoint-Weighted Tally Value for Geometric Perturbation of K-Eigenvalue based on Continuous-Energy Monte Carlo Method," *Proceedings of PHYSOR-2018*, Cancun, April 22–26, pp. 3938–3947 (2018)
18. A.T. Godfrey, "VERA Core Physics Benchmark Progression Problem Specifications," Consortium for Advanced Simulation of LWRs, CASL-U-2012-0131-004, Revision 4, Aug. 29, 2014
19. K. W. Burn, "Learning Aspects of the Direct Statistical Approach to the Optimization of Monte Carlo Radiation Transport Calculation," Workshop on Adaptive Monte Carlo Methods, Los Alamos, Aug. 1996, ENEA-IRIS Open Archive: http://hdl.handle.net/20.500.12079/3659
20. X-5 Monte Carlo Team, "MCNP – A General Monte Carlo N-Particle Transport Code, Version 5 Volume II: User's Guide", Los Alamos National Laboratory, LA-CP-03-0245, pp. 5-74 – 5-78, 5-107 (2003)

DISTRIBUTION LIST

M. Tarantino	FSN – PROIN	mariano.tarantino@enea.it
D. Giusti	FSN – PROIN	davide.giusti@enea.it
P. Meloni	FSN - SICNUC	paride.meloni@enea.it
F. Rocchi	FSN – SICNUC – SIN	federico.rocchi@enea.it
A. Guglielmelli	FSN – SICNUC - SIN	antonio.guglielmelli@enea.it
G. Grasso	FSN – SICNUC - PSSN	giacomo.grasso@enea.it
R. Pergreffi	FSN – SICNUC – PSSN	roberto.pregreffi@enea.it

ARCHIVIO FSN – PROIN